SYNTHESIS AND TRIBOLOGICAL CHARACTERIZATION OF *IN-SITU* SPARK PLASMA SINTERED Ti_3SiC_2 AND Ti_3SIC_2-TiC COMPOSITES.

By

NIDUL CHANDRA GHOSH

Bachelor of Science in Mechanical Engineering

Bangladesh University of Engineering and Technology

Dhaka, Bangladesh

October 2009

Submitted to the Faculty of the
Graduate College of the
Oklahoma State University
in partial fulfillment of
the requirements for
the Degree of
MASTER OF SCIENCE
December, 2012

SYNTHESIS AND TRIBOLOGICAL

CHARACTERIZATION OF *IN-SITU* SPARK PLASMA

SINTERED Ti_3SiC_2 AND Ti_3SIC_2-TiC COMPOSITES.

Thesis Approved:

Dr. Sandip P. Harimkar

Thesis Adviser

Dr. Kaan Kalkan

Dr. Raman Singh

Dr. Sheryl A. Tucker

Dean of the Graduate College

TABLE OF CONTENTS

Chapter Page

LIST OF TABLES

Table Page

LIST OF FIGURES

Figure Page

CHAPTER I

INTRODUCTION

1.1 Introduction:

Metallic materials are usually ductile, tough, thermally and electrically conductive, and easily machinable. However, the use of metallic materials for load bearing application at a high temperature is often limited due to their lower melting point and degradation of strength. On the other hand, ceramics are strong, high temperature resistant, and elastically stiff. However, these excellent properties of ceramics are also accompanied with inherent brittleness and poor machinability and thermal shock resistance. The materials that possess optimum combination of strength, ductility, toughness, and machinability have been unavailable until serendipitous rediscovery of family of layered ternary Carbide and Nitrides, MAX phase materials [1]. This class of solids was first discovered by Nowotny's group in Vienna [2-3] but the interest renewed only after Barsoum and El-Raghy synthesized single phase Ti_3SiC_2 and were able to characterize mechanical properties which was anomalous to conventional ceramics [4]. MAX phase materials, sometimes reported as "ductile ceramics", exhibit combinations of properties of metallic materials and ceramics such as- excellent electrical and thermal conductivity, machinability, thermal shock resistance, damage tolerance, elastic stiffness, strength, and sometimes fatigue, creep and high temperature oxidation resistance [5-8].

Processing of MAX phases is often accompanied by secondary binary carbides, nitrides which deteriorate some of the exclusive properties of these materials. Difficulties in processing of monolithic MAX phase and their poor wear resistance because of lower hardness limits their application in advanced structure.

In this chapter an overview of Ti_3SiC_2 including properties and potential applications followed by its processing mechanism is given. Along with that, previous research studies on processing of Ti_3SiC_2 and their composites through Spark Plasma Sintering are reviewed.

1.2 MAX Phase Materials:

The MAX phases are polycrystalline nanolaminates of ternary carbides and nitrides, named from their general formula of $M_{n+1}AX_n$ (where *M* is a transition metal, *A* is an A group (mostly IIIA and IVA) element, and, *X* is C and/or N and n=1 to 3) [5]. Until now, over 60 MAX phases have been found. According to the value of n, different MAX phase stoichiometries are usually referred as- M_2AX or 211 phases, M_3AX_2 or 312 phases, and M_4AX_3 or 413 phases. The MAX phase's exhibit layered hexagonal structure, where M layers are separated by layers of A group element and X atoms fitting into octahedral sites of M layers. The basic difference in the crystal structure of these three groups is the number of M layers separating A layers. There are two, three and four M layers in between two A layers in 211, 312, 413 phases respectively. In place of A group element Cd was reported to form MAX phase with Ti and C. Existence of higher order MAX phases such as Ti_5SiC_4 [9], Ta_6AlC_5 [10], Ti_7SnC_6 [11] have been proposed based on TEM studies and theoretical calculation.

1.3 Titanium Silicon Carbide, Ti_3SiC_2:

Ti_3SiC_2 is one of the representative members of the MAX phase family. Ti_3SiC_2 has hexagonal crystal structure with P63/mmc space group having lattice parameters of a=0.3068 nm and c=1.7669 nm [12] as shown on fig. 1.1. The unit cell of Ti_3SiC_2 consists of double layers of Ti-C blocks, made up by filling Ti_6C octahedral sites of Ti with C atoms and these Ti-C blocks are interleaved by hexagonal nets of Si layers. Ti_3SiC_2 has close crystal structure relationship with TiC and the structure is described as periodic Si embolism into the twin boundary of Ti_3C_2 [13]. Intercalation of Si into Ti_3C_2 leads to formation of Ti_3SiC_2 and similarly Si evaporation from Ti_3SiC_2 results in reverse transformation into Ti_3C_2. Strong crystallographic relationship between Ti_3SiC_2 and TiC is the reason for existence of TiC as main impurity phase in Ti_3SiC_2 processing and hence very important in finding processing route to synthesize monolithic Ti_3SiC_2.

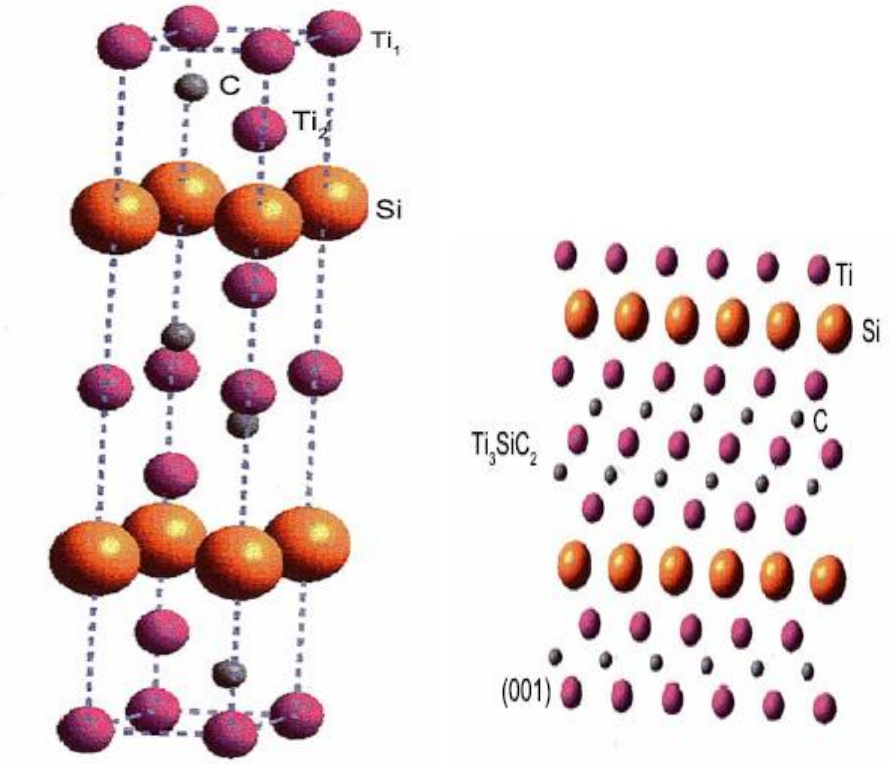

Fig. 1.1 Crystal structure of Ti_3SiC_2 [14].

1.3.1 Crystal structure & properties of Ti_3SiC_2:

Unexpected combinational properties embodied in Ti_3SiC_2 are contributed to the presence of three different type chemical bonding. In Ti_3SiC_2 every two Ti-C-Ti-C-Ti chains are bonded together with Si atom and periodic repetition of Ti-C-Ti-C-Ti-Si chain has been reported [15]. These chains are connected through inhomogeneous metallic bonding to configure Ti_3SiC_2. The bonding between Ti-C and Ti-Si are covalent in nature and the interatomic distance between Ti and C and Ti and Si are 2.13 Å and 2.67 Å respectively. Demonstration of polar characteristic by Ti-C and Ti-Si bonding indicates presence of ionic bonding along with covalent bonding. The vibration amplification of Si atoms was reported to be significantly higher compared to Ti and C atoms suggesting Ti-Si bonds are relatively weaker than Ti-C bond [15]. The interatomic distance between Si-Si in Ti_3SiC_2 is reported as 3.068 Å in high temperature neutron diffraction studies which is greater than Si-Si distance in elemental powder indicating no in-plane Si-Si bonding. Raman spectra of Ti_3SiC_2 showed six sharp peaks at 159, 228, 281, 312, 631, 678 cm^{-1} [16]. Low energy modes (<312 cm^{-1}) related to (along a axis) related to the weak C-Ti-Si bonds and High energy modes (along c axis) related to strong C-Ti-C bonds. Amer at al.[16] also compared Raman peaks between Ti_3SiC_2 and $TiC_{0.67,}$ peak at 150 cm^{-1} was found for Ti_3SiC_2 and ascribed to the vibrational shear modes between Ti-C sheets and Si planes which is absent on the corresponding binary carbide $TiC_{0.67}$. This low energy shear mode demonstrates relative weakness of Ti-Si bonding against shear leading to higher friction coefficient and wear loss in polycrystalline $Ti_3SiC_{2.}$ Special crystal chain structure and unique combination of metallic-covalent-ionic chemical bonding determines the combinational properties of both metal and ceramics in $Ti_3SiC_{2.}$ Ceramic like properties of Ti_3SiC_2 such as high melting point and higher modulus of elasticity are derived from strong Ti-C-Ti-C-Ti bonding unit. Metallic properties such as higher electrical conductivity are attributed to the metallic bonding in-between adjacent Ti-C-Ti-C-Ti chains.

Ti_3SiC_2 shares many of the properties of their corresponding binary carbide, TiC because of their similar bonding environment as both of them share Ti-C covalent bond. Like TiC, Ti_3SiC_2 is elastically stiff, electrically and thermally conductive, are resistant to high temperature oxidation and chemical attack and have low density and low thermal expansion coefficients [5]. However their mechanical properties are incredibly different having low hardness value, machinability like graphite, excellent damage tolerance and non-susceptibility to thermal shock. Typical values for mechanical and electrical properties are summarized in table 1.1.

Table 1.1 Fundamental Properties of Titanium Silicon Carbide. [17-21]

Property	Value
Density ($g.cm^{-3}$)	4.52
Shear modulus (Gpa)	139
Young modulus (GPa)	343-339
Poisson's ratio	0.20
Bulk modulus (GPa)	190-206
Vickers hardness (Gpa)	4
Fracture toughness ($MPa.m^{1/2}$)	7
Flexural strength (MPa)	260±20
Compressive strength (MPa)	900(25 °C), 300 (1300 °C)
Tensile Strength (MPa)	200(25 °C), 12 (1300 °C)
Thermal conductivity (W/m.K)	37
Thermal Expansion Coefficient (k^{-1})	$9.2*10^{-6}$
Electrical conductivity ($\Omega^{-1}.m^{-1}$)	$9.6*10^{6}$
Heat Capacity (J/mol.K)	110

Unusual characteristic mechanical properties of Ti_3SiC_2 were ascribed to the following facts:

(1) In Ti_3SiC_2 basal slip is the only dislocation mechanism and basal plane dislocations are operative at all temperature (as low as 77 K) [22-24]. Thus Ti_3SiC_2 lies on the middle ground between typical ceramics and ductile materials as they have more independent slip system than ceramics (no operative slip system on ceramics) but less than required for ductility i.e. five independent slip system. Highly oriented, large grained Ti_3SiC_2 under restrained deformation demonstrates ductile behavior like damage tolerance, thermal shock resistance at higher temperature [25]. At room temperature and unconstrained deformation randomly oriented polycrystalline sample behaves more like a brittle material.

(2) As the dislocations are contained to the basal planes, they arrange themselves either in arrays parallel to the basal planes on identical slip plane or in walls perpendicular to the basal planes (similar to high or low angle grain boundaries). Hence, Dislocations interaction would not occur except for the orthogonal direction. Reversible back and forth movement ability of the dislocations contributes to the fully reversible pseudo-plasticity behavior of ternary carbide, Ti_3SiC_2.

(3) On account of the high c/a ratio (5.76) twining is unlikely to occur in Ti_3SiC_2. Similarly, nonbasal dislocations have never been reported as effective deformation mechanism as basal interatomic vectors are the shortest full translational vector in the structure. Deformation takes place in Ti_3SiC_2 by a combination of glide and the formation of dislocation based incipient kink bands (IKB) within the grains as shown on fig. 1.2 [26-27].

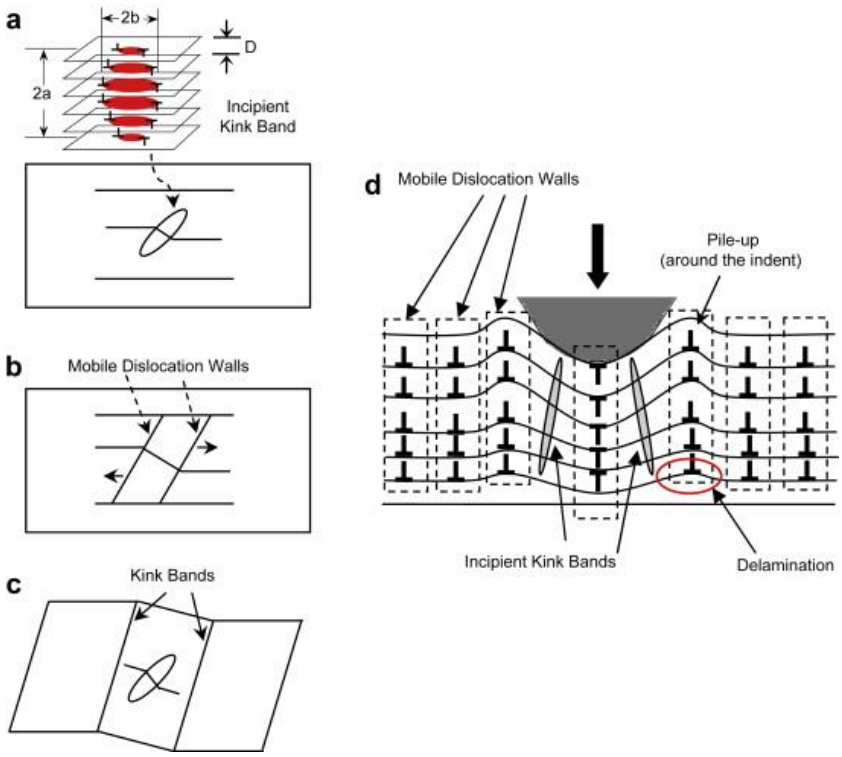

Fig. 1.2 a) incipient kink band (IKB) formation b) At higher stress condition Mobile Dislocation Walls forms. c) At very high stress condition (more than b) IKB converts to permanent kink bands (KBs). (d) Formation of Nested MDWs under a spherical indention during hardness testing [28].

Kink bands are common in layered materials where the layers are able to glide against each other and formed when loaded parallel to the slip or weak share planes. IKB formed by edge dislocations on the crystal and framed as near parallel dislocation walls of opposite polarity. As they are of opposite polarity upon removal of applied load that attract each other and allows the IKB to collapse. With increasing load levels and/or temperature IKBs decouple into mobile walls and form regular or immobile kink bands (KBs) [29]. These mobile walls move in two opposite direction and arranged themselves into the wall defining the kink boundaries. Cracks cannot propagate beyond the kink boundaries as to pass through it has to move all the dislocations present on the boundaries. Resultantly Kink boundaries act as container or reflector of damages

and locally harden the area instead of weakening [1]. Confinement of damage plays an important role in the damage tolerant properties of the layered ternary carbides.

Due to their hexagonal layered structure, mechanical properties of Ti_3SiC_2 were reported to be strongly anisotropic in the literature. For example, hardness of the crystal was found to be nearly 4-5 GPa when measured parallel to the basal plane whereas varies from 12-15 GPa normal to the basal planes [30-31]. In contrast to their strong mechanical anisotropy, Ti_3SiC_2 demonstrates nearly thermally isotropic properties. Along C axis of Ti_3SiC_2, Ti-C-Ti-C-Ti-Si chain is periodically repeated. Among the C-Ti-C, C-Ti-Si, and Ti-Si-Ti bonds C-Ti-C are stronger and Ti-Si-Ti bonds are reported to be weaker than the average Ti-C bonds [32]. Along the C axis corresponding thermal expansion of C-Ti-C, C-Ti-Si, and Ti-Si-Ti bonds were found to be 5.5, 8.8 and 13 $*10^{-6}$ K^{-1}, respectively. Bulk thermal expansion of Ti_3SiC_2 is reported to be $9.2*10^{-6}$ K^{-} [33] which are almost identical to the average expansion of these three bonds. Thermal expansion is almost isotropic as along c axis C-Ti-C bond is stronger and Ti-Si-Ti bond is weaker compared to average Ti-C bond thus averaging the effect.

Ease of machinability is the furthermost important characteristic of Ti_3SiC_2 from the application point of view. Other high temperature structural materials i.e. ceramics and super alloys are very difficult and expensive to machining. Ti_3SiC_2 can be easily machined using regular high speed tools without any lubrication or cooling even just with manual hacksaw. Easy machinability of Ti_3SiC_2 allows fabrication of machine parts meeting required tolerances. Similarly, prototypes useful for testing cane be processed precisely and economically using Ti_3SiC_2. This material can also be machined using electron discharge as it has excellent electrical conductivity like metals.

1.3.2 Application of Ti_3SiC_2:

- The most potential use of Ti_3SiC_2 could be on the high temperature applications like, engine cylinders and jet engines. Nickel or cobalt based super alloys are currently being used on this sector as they can operate at higher temperature and high stress condition without breakage. Ti_3SiC_2 has half of the density of the Ni based super alloys; whereas they have similar strength and exceeds all super alloys in corrosion resistance. (fig. 1.3)

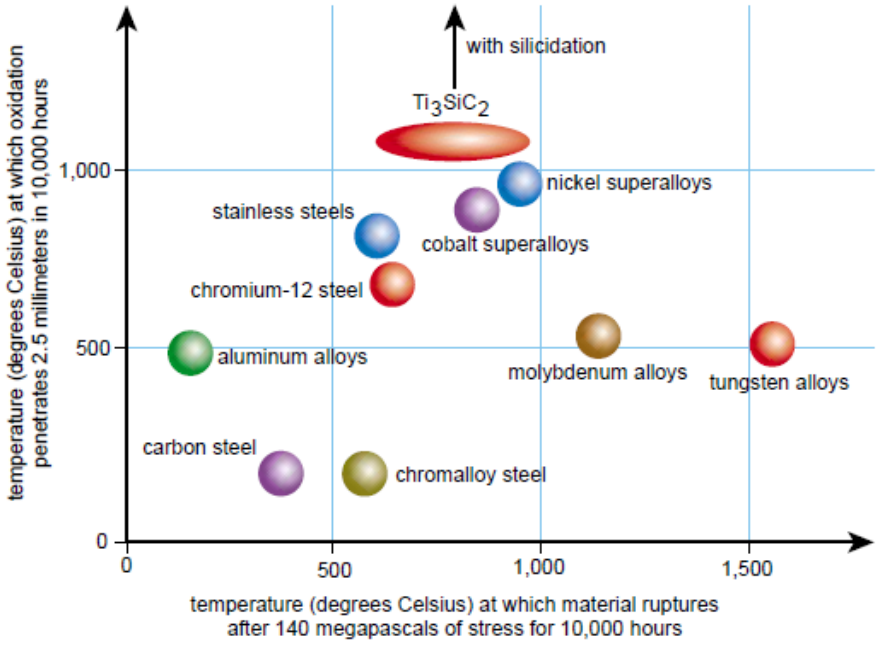

Fig. 1.3 Comparison of high temperature strength and oxidation resistance between Ti_3SiC_2 and other commonly used superalloys [1].

Most importantly the high temperature applicability of the Ti_3SiC_2 could be easily improved by silicidation or carburization. Surface of the Ti_3SiC_2 could also be modified in such a way that at higher temperature layer of SiO_2 formed which further could improve the oxidation resistance of Ti_3SiC_2.

- Very high electrical conductivity along with is excellent thermal conductivity made Ti_3SiC_2 as potential material for many electronic devices where rapid dissipation of heat is required to keep the temperature below a certain range.
- Ti_3SiC_2 can be used in electrical contacts because of its good thermal conduction, high temperature and corrosive environment sustainability, plasticity and thermal shock resistance ability. Normally electrical contacts are made off gold but it has very poor mechanical properties and susceptible to wear. Ti_3SiC_2 can overcome these shortcomings of gold with its excellent mechanical properties and low cost of production. The wear resistance of Ti_3SiC_2 could also be easily improved by addition of other binary carbides. Wear resistant Ti_3SiC_2 composites also have applications where rotating parts are used, such as brushes in electrical motors.
- Ti_3SiC_2 has found application in turbine blades because of its exclusive damage tolerance properties, and high temperature sustainability. Because of its damage tolerance properties cracks are confined into a certain zone which increases the lifetime of the coatings as well as the turbine blades.
- Unique properties of Ti_3SiC_2 such as, high strength at very high temperature; thermal shock resistance; thermal, radiation and erosion resistance along with its very low density made it potential material for use in Severe environment like in spacecrafts [33].
- Very good corrosion resistance properties of Ti_3SiC_2 in acids and alkalis environment made it a promising material for use in gas pipes for fuel transportation, gas burner nozzles and in thermally sprayed corrosion coatings.
- Electronic Industry is looking for new Electromagnetic Interference shielding (EMI) materials which has high electrical conductivity, low density better mechanical properties and corrosion resistant. Metals were previously used for EMI application but their lower density and corrosion susceptibility limits their application. Ceramics have lower density

but their low electrical conductivity act as a constraint to be used as EMI material. Addition of Ti_3SiC_2 into ceramics (Al_2O_3) greatly improves their electrical conductivity resultantly shielding effectiveness of EMI and could be a potential material in this field [34].

- Because of the excellent thermal conductivity and thermal shock resistance of Ti_3SiC_2, It could be possibly be used in Heat exchanger application. Even Ti_3SiC_2 could be reinforced by several other ceramics like TiC or SiC to be used on heat exchanger application without compromising their thermal conductivity.
- Recently, Ti_3SiC_2 was found to be very promising material for using in primary circuit of lead cooled fast reactor, such as pump impeller and bearing which works on high temperature and high velocity lead. Ti_3SiC_2 showed very high corrosion resistance in presence of lead and no lead penetration inside Ti_3SiC_2 was found at 500 °C fluent lead at about 1 m/s for 2000 h [35].
- Excellent mechanical properties at high temperature along with its easy machiniablity made Ti_3SiC_2 good candidate material for advanced nuclear reactor application [36].

1.4 Synthesis of Ti_3SiC_2:

Ti_3SiC_2 was first discovered by by Nowotny's group in 1967, while they had been working on synthesizing groups of carbides and nitrides later known as Hagg phases [2, 12]. Ti_3SiC_2 was synthesized through the reaction between TiH_2, Grahite and Silicon but the mechanical properties were still unrevealed because of lack of density and purity of the sample. Nickl et al. [37] employed chemical vapor deposition (CVD) from $TiCl_4$, $SiCl_4$, CCl_4 and H_2 and were able to deposit thin films of Ti_3SiC_2 along with $Ti_5Si_3C_x$ auxiliary phase. They were the first to report the anomalously soft behavior for the carbide. Later on, Recault et al. [38] attempted synthesis of Ti_3SiC_2 through reactive sintering but they were unable to attain single phase. Over the years

from 1967 to present, many methods, including Magnetron Sputtering (MS), [39, 40] arc melting and post annealing, [41] Self-propagating High temperature Synthesis (SHS), [42] Pulsed Laser Deposition (PLD), [43] Mechanical Alloying (MA), [44-46] combustion synthesis with hot isostatic pressing, [47] were employed for Ti_3SiC_2 synthesis. However, these processes almost always result in formation of Ti_3SiC_2 with ancillary phases such as TiC, SiC, Ti_5Si_3 and $TiSi_2$. TiC is the most common secondary phase among them and it has been proved to be really difficult to completely remove TiC because of their close structural relationship with Ti_3SiC_2 [13]. Even the best sample contains nearly 10-20% of impurity phase which deteriorate some of the exclusive properties of Ti_3SiC_2. Barsoum et al. synthesized almost single phase Ti_3SiC_2 from Ti, graphite, and SiC powders by employing hot isostatic pressing (HIP) [4]. HIP process was also successfully employed to synthesize other MAX phases such as M_2SnC (M=Ti, Zr, Hf and Nb), [48] Ti_4AlN_3,[49] Ti_3GeC_2, M_2AlC (M=Ti, V, Ta, Nb) [50] by the same group.

In recent years, spark plasma sintering (SPS) process has been introduced for the synthesis of bulk MAX phases. The SPS presents tremendous potential for processing of single phase fully dense samples in relatively shorter time, at lower temperature, and with improved mechanical properties compared to conventional hot isostatic pressing and other densification processes. In this section, A short introduction SPS is followed by reviewing previous work on synthesizing Ti_3SiC_2 with emphasis on effect of initial compositions and SPS processing parameters on microstructures and properties of sintered materials.

1.5 Spark Plasma Sintering:

1.5.1 Spark Plasma Sintering Mechanism:

The SPS is a solid state consolidation process where uniaxial compaction pressure is applied to powder along with pulse direct current for rapid heating and activation of sintering process. The idea of using electric current as the sintering aid could be traced in patents issued in 1933. These

patents discussed the use of electric current supplied through the powders for heating during welding processing and sintering of hard metal compositions [51, 52]. The SPS equipment for sintering metals and ceramics was patented in the United States by Inoue et al. in 1960s and 1970s, [53-55] and most of these equipment's were sold in the US and Japan. The commercial application of SPS method was initiated in Japan with third generation equipment's. Currently, Japan has largest number of SPS installations. Because of superiority of SPS process over the other conventional sintering processes, an exponential increase is noticed in recent years in the number of published papers on SPS. The SPS process is also referred by several names, such as Pulsed Electric Current Sintering (PECS), Pulse Discharge Sintering (PDS), Plasma Activated Sintering (PAS), Resistance Sintering (RS), Pulse Current Sintering (PCS), Plasma Pressure Compaction (P^2C), and Field Activated Sintering Technique (FAST). The SPS was named by believing the presence of "spark" and/or "plasma" during the sintering process but the existence of spark or plasma has not yet been unambiguously proved for lack of experimental evidence [56, 57]. Thus, in recent publications authors mostly use the term Pulsed Electric Current Sintering (PECS) to avoid the controversy. In this review paper, SPS designation will be employed as its mostly used rubric by the investigators (nearly 66.2%) [58].

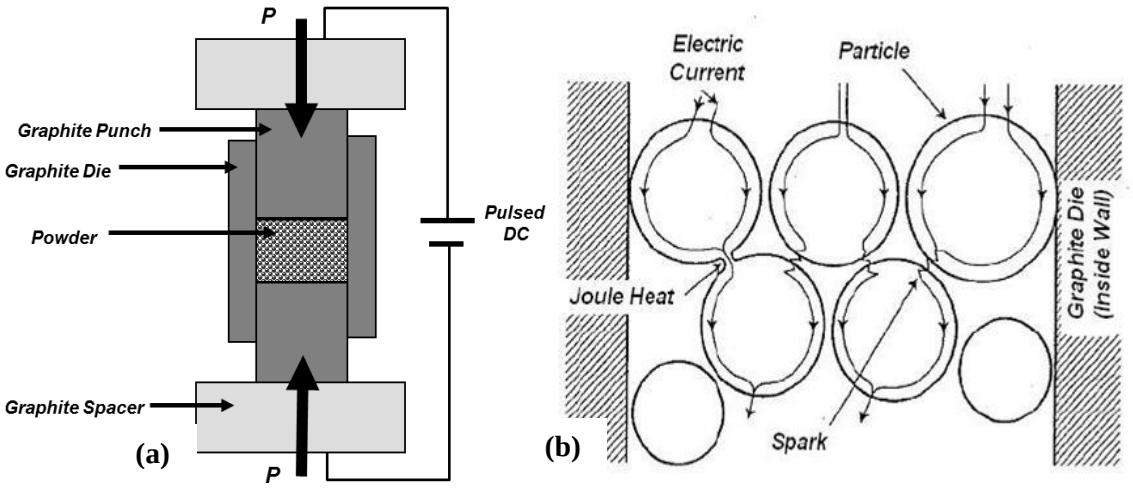

Fig. 1.4 Schematic of (a) spark plasma sintering set-up, and (b) mechanisms of sintering [59].

The SPS process utilizes pulsed high DC current and uniaxial pressure for rapid sintering of powder. A typical set-up of the SPS process is shown in Fig. 1.4. The starting powders which could be electrically conductive or insulating, are loaded into graphite or metallic die. The powders are initially activated by pulsed current; and after attaining a certain activation level, pressure is applied to consolidate the powder. The mechanical effect of the applied pressure rearranges the particles and breaks some forms of agglomeration. The driving force for sintering also increases because of the intrinsic role of external pressure. The major difference between hot pressing and SPS is the application of current. Powders are heated through joule effect and by heat transfer from dies and punches. Higher heating rates (as high as 1000°C/min) in SPS process provide an additional driving force due to large thermal gradients which helps to bypass the low temperature stages where surface diffusion (non-densifying mechanism) dominates mass transport [60]. In SPS, because of the prominent grain boundary and volume diffusion (densifying mechanism) grain size reduces. Moreover very short sintering time retards grain coarsening and increases sinterability of the powder. The application of current during SPS also enhances mass transport by increasing point defect concentration or enhancing defect mobility [61]. Unselmi et al. [62] conducted experiments on the reaction between Mo and Si with and without current to determine the effects of current on mass transport; and they reported significant influence of current on the reaction during SPS. Application of Pulse DC current instead of constant DC current is reported to enhance densification of Al_2O_3 [63]. Pulsed Dc current pass through the contact points between particles as the current always choose the path with less resistance. Because of the oxide layer on particle surfaces small capacitors are formed across the contact points and electrical discharge is caused in between the capacitor gaps. Generation of electrical discharge clean the surfaces from absorbed CO_2, H_2O and OH^- and increase point defect concentration which later favors densification process increasing grain boundary diffusion. Simultaneous application of Pressure along with current decreases the distance between the particles i.e. increases mass transfer between particles. The agglomeration present on the

precursor powder is destroyed because of with increase of mechanical pressure. Combined effect of these two factors accelerates densification on final product.

In conventional solid state synthesis of ternary phases like Ti_3SiC_2, when constituent elements were pressed together intermediate phases forms through the diffusion of powder at contact points. This process continues till all the powders have been converted into corresponding intermediate phases. Final product i.e. ternary phases form through the reaction between the intermediate phases. But these intermediate phases are thermodynamically more stable requiring higher energy for the decomposition. So, the ternary phase always accompanied by undesirable intermediate phases. These retained intermediate phases are isolated by the growing final phase and act as diffusion barrier for further conversion of intermediate phases into product phase. To overcome this shortcoming, conventional sintering requires higher temperature leading to evaporative loss of constituent phases. In SPS, along with homogeneous distribution in macroscopic scale, the heating power is dissipated on the contact points between the particles. Thus, powder particle surface becomes more active than in conventional sintering leading to higher material transfer rate in both macro and microscopic level. Because of this phenomena, high purity sintered compact of ternary phases is obtained from the dissolution of intermediate phases at lower sintering temperature.

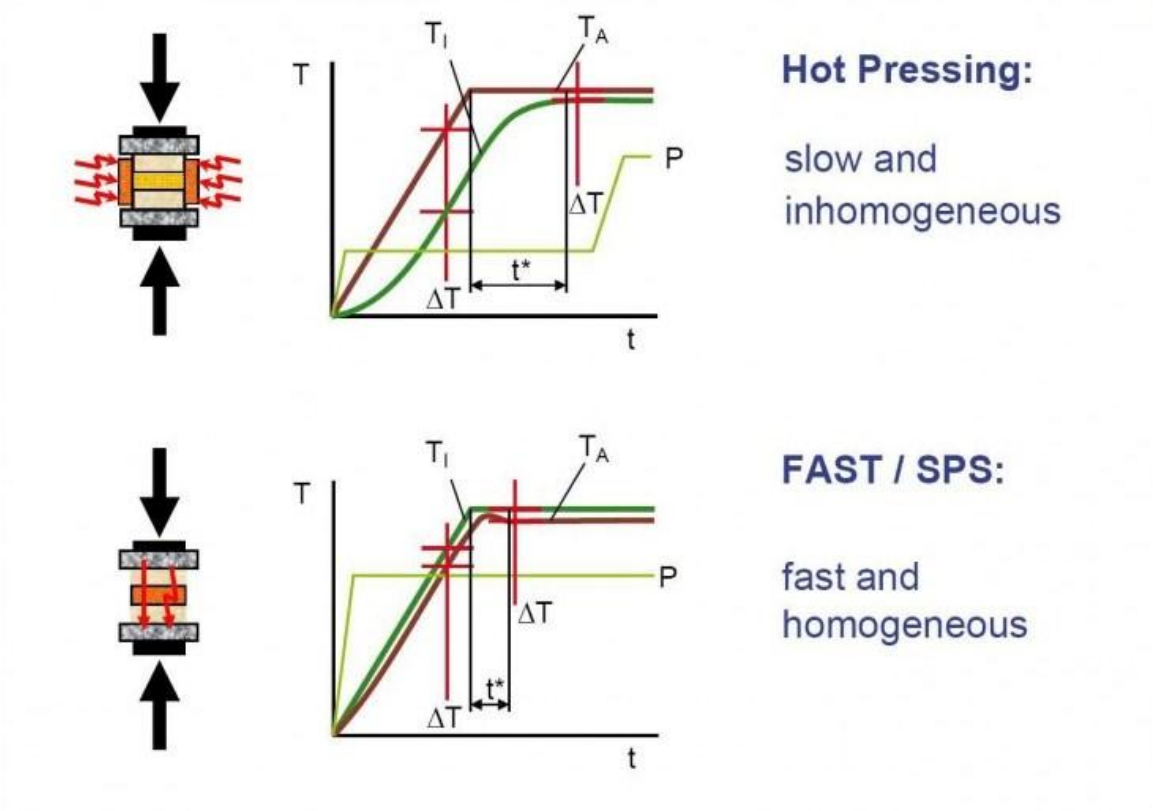

Fig. 1.5: Comparison between SPS and Convention hot pressing [64].

A comparison between hot pressing and SPS is represented on fig. 1.5 wherein T_I and T_A represent temperature of the center and edge of powder compact respectively. The SPS process is characterized by various technological and economic advantages over conventional sintering processes, such as, shorter sintering time, lower sintering temperature and pressure, no need of cold compaction, finer and homogeneous microstructure, higher density and densification rate, less sensitivity to initial powder composition, and synthesis of difficult to sinter materials. In addition, due to shorter processing time, SPS processing allows sintering without undesirable phase changes and provides comparatively cleaner grain boundaries marked with significant improvement in properties of synthesized material.

1.5.2 Application of Spark Plasma Sintering:

SPS process demonstrates immense possibilities for the sintering of material which are difficult to sinter by conventional sintering. Through SPS ceramic materials can be compacted within few minutes of at significantly lower temperature compared to HP or HIP. Fully dense carbides, nitrides, borides and oxides were reported to process employing SPS. Fabrication of nonocrystalline materials with special microstructure has been enabled by SPS as grain growth is minimal in this process and it requires lower consolidation time and temperature. Employing SPS on processing opens the door of using nanomaterials in industrial application and many of the commonly used structural materials with finer and homogenous microstructure i.e. better mechanical characteristics will find exclusive application.

SPS is effective in in situ processing of monolithic materials and composites. For example, Ti_3SiC_2 is processed from commercially available Ti, Si and TiC powders through in situ Spark Plasma Sintering process. Composites processed through in situ sintering process demonstrate more homogenous distribution of phases. TiN/Al_2O_3 nanocomposites were reported to process from Ti, AlN and TiO_2 powders and manifests grain size below 400 nm as SPS ensures molecular level mixing between the constituent powders. Similarly, uniform dispersion of reinforcing particles in metals and ceramics, for example CNT reinforced Aluminium [65] and SiC reinforced ZrB_2 [66] with has also been reported through SPS. Since SPS requires less time for complete densification thus, voids the possibility of reaction between material components and avoids structural damage of the reinforcement particles contributing better mechanical properties. Cross section of Al_2O_3/Cr_2O_3 interface presented only 4 μm of interference because of the shorter sintering time required in SPS [67].

SPS is being used to Near-net-shape production in recent publication which decreases the overall cost as very minor machining is required in this process. Using SPS, Al_2O_3 spheres has processed

in only single step from Al_2O_3 powder by galy et al. [67]. SPS allows sintering ceramics and other difficult to consolidate materials without the use of binders. Binders used in processing are vulnerable to chemical reaction, increase grain growth and degrade the mechanical properties such as hardness, strength and oxidation resistance. Also, removing binders from the processed product increase the cost of production. This particular advantage is very useful in numerous applications such as, diamond tungsten carbide composites, [68] binder less WC, [69] and ceramic fuel cells. These refractory carbides are being tremendously used in machining and drilling industries and also have application in preparing dies for optical applications.

1.6 Review of Spark Plasma Sintering of Ti_3SiC_2:

Based on commercial accessibility of initial powders and Ti-Si-C ternary phase diagram, following possible reaction paths are found for ternary polycrystalline Ti_3SiC_2 synthesis by SPS:

(1) $Ti + Si + C \rightarrow Ti_3SiC_2$;

(2) $Ti + Si + TiC \rightarrow Ti_3SiC_2$;

(3) $Ti + SiC + C \rightarrow Ti_3SiC_2$;

(4) $Ti + SiC + TiC \rightarrow Ti_3SiC_2$;

(5) $Ti + TiSi_2 + TiC \rightarrow Ti_3SiC_2$; and

(6) $TiH_2 + SiC + C \rightarrow Ti_3SiC_2$.

Consolidation of Ti_3SiC_2 starting from different compositions at different processing parameters by SPS is summarized in table 1.2.

Table 2.2 An overview of the previous works on Spark Plasma Sintering of Ti_3SiC_2.

Compound powders	Molar ratio of compound powders	Preparation before sintering	Sintering parameters (Temperature, pressure, heating rate, soaking time)	Products (Ti_3SiC_2) wt.%
Ti/Si/C [70]	3:(1/1.05/1.1/1.15): 2 5:2:3 3:1.5:2	Mixed in turbula mixer for 24 h	1200-1500 °C, 50 MPa , 50-60 °C/min, 15-60 min	< 65.4 % 91 % 93.6 %
Ti/Si/TiC	1:1:2 [71-72] 2:2:3	Mixed and ball milled for 24 h	1200-1400 °C, 50 MPa, 50-60 °C/min, 8-240 min	96-97 % 99 %
	1:1:2 [73]	Mixed and ball milled in ethanol.	1125-1400 °C, 20-60 MPa, 100°C/min, 10 min	98 %
	2:2:3 [74]	Mixed in turbula shaker for 24 h	1300 °C, 50 MPa, 50 °C/min, 15 min	99 %
	1: (1/1.05/1.1/1.15):2 [75]		1250-1300 °C, 50 MPa, 50 °C/min, 30 min	97.5 %
Ti/SiC/C	3:(1/1.1):1 [76]	Mixed in	1200-1400 °C, 50	50 %

	5:2:1 3:1.5:0.5	turbula shaker for 24 h	MPa, 50-60 °C/min, 15-60 min	93 % < 80 %
	3:1:1 [77]		1250-1400 °C	< 50 %
Ti/SiC/TiC [78]	4:2:1	Mixed in turbula shaker for 24 h	1250-1450 °C, 50 MPa, 50-60 °C/min, 15-120 min	92 %
Ti/$TiSi_2$/TiC [79]	1:1:4 1:1:3		1100-1325 °C, 50 MPa, 50-60 °C/min, 0-60 min	93 % 95 %
TiH_2/SiC/C [80]	1:1:1.8	Mixed in turbula shaker	900-1450 °C, 50 MPa, 50 °C/min, 0-20 min	99 %
Effect of Al Addition				
Ti/Si/Al/C [81-83]	3:1.2:0:2 3:1:0.2:2	Mixed in ethanol for 24h	1250 °C, 30 MPa, 80 °C/min, 10 min	Nearly 85 % ≥99 %
Ti/Si/C/Al [84]	3:1:2: (0/.1/.2/.3)	High energy MA for 10h	800-1100 °C, 30 MPa, 100 °C/min, 5 min	99 %

1.6.1: Ti/Si/C powder mixture:

For Stoichiometric ratio of Ti/Si/C the percentage of Ti_3SiC_2 present in the final product decreased with sintering temperature and soaking time. Maximum of 65.4% Ti_3SiC_2 was achieved for powder mixture Ti:Si:C (3:1:2) sintered at 1250°C for 15 min [70]. To compensate the evaporation of Si, excess of Si was added; but, no effect was observed on amount of Ti_3SiC_2 with up to 15% of excess Si addition. For powder ratio of 5:2:3, which is slightly off-stoichiometric, the auxiliary TiC content decreased to 6.4% (i.e. about 93.6% pure Ti_3SiC_2) and density increased to about 99% with SPS processing at 1300°C for 15 min of soaking time. With further increase in Si content, the new auxiliary phase $TiSi_2$ appeared in final products.

1.6.2 Ti/Si/TiC powder mixture:

Using starting powder of Ti/Si/TiC, the phase content of Ti_3SiC_2 was increased from 97% to 99% by adjusting the composition from 1:1:2 to the off-stoichiometric ratio of 2:2:3 [71-74]. In both the cases, the relative density was observed to be higher than 99%. Fig. 1.6 shows contents of TiC which is main auxiliary phase in both stoichiometric and off-stoichiometric compositions under different processing conditions. The microstructure of Ti_3SiC_2 samples SPS sintered with various combinations of sintering temperatures and times are presented in Fig. 1.7. At lower temperatures (1250-1300°C), densely packed microstructure with fine plate-like grains was observed. The percentage of plate-like grains increased with soaking time. At higher sintering temperature (1400°C), plate-like grains continued to expand and reached about 80-100 μm in length and 30-50 μm in width. At optimum sintering temperature of 1300°C, duplex microstructure comprises of fine (5 to 10μm) and plate-like (30 to 50μm) grains were typical.

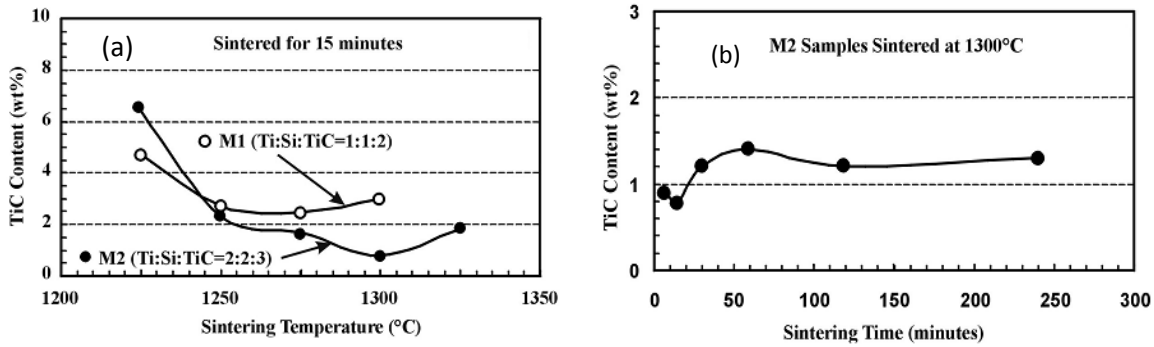

Fig. 1.6 TiC content in the samples sintered (a) at temperature range of 1225°C-1325°C for 15 min. and (b) at 1300°C for 8-240 min [71].

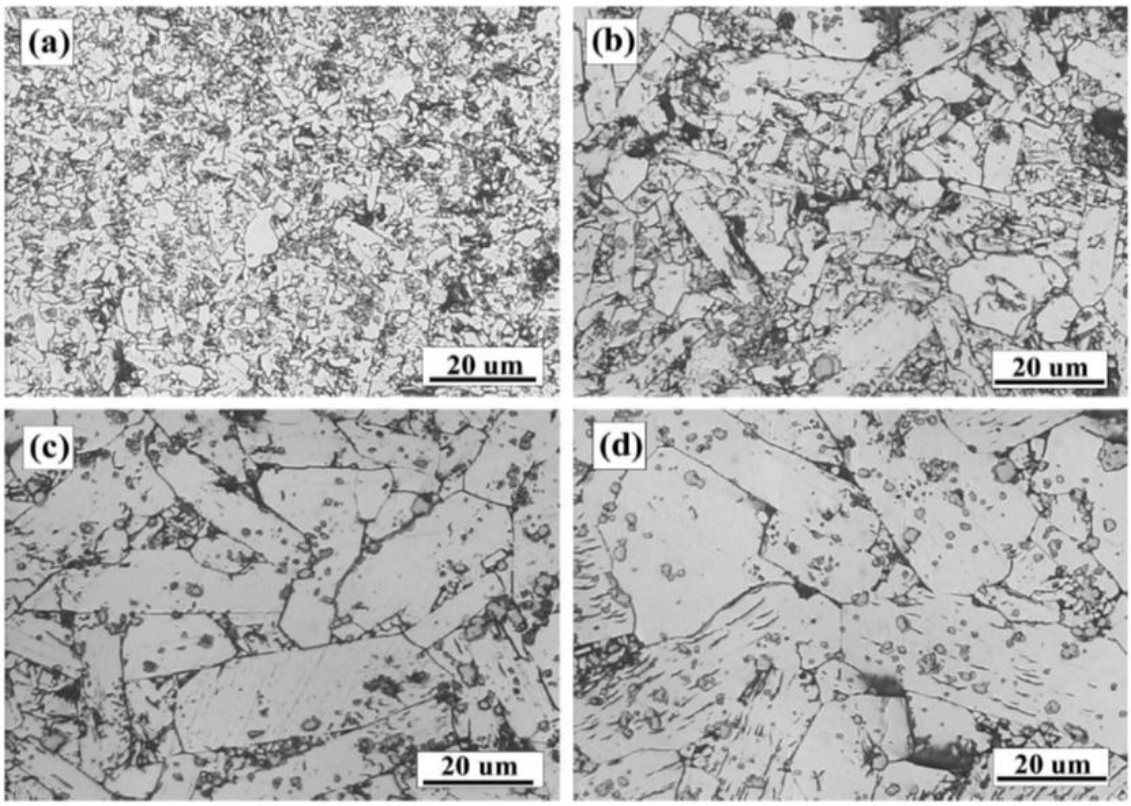

Fig. 1.7 Microstructures of samples SPS sintered at different combinations of temperatures and soaking times: (a) 1250°C, 30min; (b) 1300°C, 30min ; (c) 1300°C, 120min and (d) 1400°C, 30min [71].

1.6.3 Ti/SiC/C powder mixture:

The optimum composition of starting powders is important for achieving higher percentage of Ti_3SiC_2 in the final product from Ti/SiC/C reactants. Using the stoichiometric ratio (3:1:1), only low purity products like 50% pure Ti_3SiC_2 were possible over wide ranges of sintering temperatures and times. When off-stoichiometric powders with molar ratio of 5:2:1 were sintered at 1250°C to 1300°C, the amount of principal auxiliary phase TiC reduced to 7-8% with about 99% relative density. Increasing content of SiC resulted in decreasing purity of Ti_3SiC_2 phase in terminal products [76-77].

1.6.4 Ti/SiC/TiC powder mixture:

The molar ratio of Ti/SiC/TiC was chosen to be 4:2:1 in conformity with the synthesis of 99% of Ti_3SiC_2 from Ti/Si/TiC (2:2:3) elemental powders [78]. At sintering temperature of 1350 °C, more than 92% pure Ti_3SiC_2 was achieved with density of 99%. The microstructure of Ti_3SiC_2 comprised of fine ($d \leq 10\mu m$), coarse ($d \geq 50\mu m$), and duplex ($10\mu m \leq d \leq 50\mu m$) grains. The size and volume fraction of coarse grains increased gradually with sintering temperature.

1.6.5 Ti/$TiSi_2$/TiC powder mixture*:*

Another powder mixture of Ti/$TiSi_2$/TiC with two different molar ratios of 1:1:4 and 1:1:3 was reported for the synthesis of Ti_3SiC_2. When sintering was conducted at 1300°C for 15 min highest purity (95%) Ti_3SiC_2 was observed for compositions of Ti/$TiSi_2$/TiC (1:1:3). Auxiliary TiC and $TiSi_2$ phases co-existed in the fabricated products at this processing condition [79]. The amount of appurtenant phases could be further reduced by adding more titanium in initial powder or by increasing sintering time. The density of terminal product was higher than 99% above temperature of 1225°C.

The purity of Ti_3SiC_2 depends on starting powder mixture. Zhang et al. [85] compared the content of secondary TiC, main auxiliary phase, for five different initial powders sintered at different temperatures. It can be concluded that the sample with lowest content of impurity TiC is synthesized from Ti/Si/TiC powder. This is because in Ti/Si/TiC starting powder, Ti-Si liquid phase is formed due to inclusion of Si and this phase stimulates diffusion controlled reaction process compared to other initial powder [86]. Cost is another constraint for industrial application of Ti_3SiC_2 and results indicate that Ti/Si/TiC has relatively lower price in comparison with other four powders [85]. So, in terms of cost and purity of Ti_3SiC_2, Ti/Si/TiC seems to be best initial composition.

1.6.6 Addition of Aluminum:

Sun et al. reported that, addition of small amount of Al in the initial powder can decrease sintering temperature and pressure for same purity of Ti_3SiC_2 [87]. As Al has lowest melting point (660°C) among the elements used in starting powder mixture, it acts as a melting pool during sintering and accelerate diffusion of both Ti and Si atoms for Ti_3SiC_2 formation. Zhu et al. [81-83] sintered Ti_3SiC_2 with two kinds of starting compositions: (a) extra amount of Si; Ti/Si/C (3:1.2:2), and (b) replacing Si with Al; Ti/Si/Al/C (3:1:0.2:2) to investigate the optimum starting composition for Ti_3SiC_2 formation with less amount of adjuvant phases. From XRD analysis of sintered samples, both TiC and Ti_3SiC_2 peaks were observed in composition with extra amount of Si. On the other hand, single phase Ti_3SiC_2 existed in composition with excess Al. For the comparison, 0.2% Al was added in (i) Ti/Si/C (3:1:2) and (ii) TiC/Ti/Si (2:1:1) starting powders. After sintering, lower content of Ti_3SiC_2 was found in composition without any TiC (i). In case of mixture (i), the reactions involved in Ti_3SiC_2 formation produce more heat than mixture (ii) resulting in evaporation of higher fraction of Si and thus the higher content of auxiliary TiC.

1.6.7 Effect of Mechanical Alloying:

Low temperature synthesis of Ti_3SiC_2 by mechanical alloying (MA) and SPS was also reported by Liang et al [84]. The purity of Ti_3SiC_2 reached 98% at sintering temperature of 900°C which is 300°C lower than that reported earlier [70-84]. During MA, larger surface area and grain boundaries with defects and internal strains act as diffusion routes for atoms and thus improve the sinterability of powder. At the same time, significant amount of Ti_3SiC_2 formed during MA incites formation of high purity bulk Ti_3SiC_2 by acting as active nuclei during subsequent sintering process.

Bulk high purity Ti_3SiC_2 (nearly 98%) were successfully synthesized by using hot isostatic pressing method from Ti/Si/C, Ti/SiC/C, and Ti/Si/TiC powder mixtures [88-92]. However, these sintering processes are required to be conducted at relatively higher temperatures (1400°C-1600°C) for longer times (4-24 h). Because of higher temperatures, volume fraction of coarse grains of Ti_3SiC_2 increases. In contrast, the SPS process results in higher purity Ti_3SiC_2 at relatively lower sintering temperature and shorter time. This is expected to lower the cost of processing along with improvements in densification and mechanical properties.

1.7: Ti_3SiC_2 based composites:

Ti_3SiC_2 is relatively soft (Vickers hardness of 4-6 GPa) and has low oxidation resistance as oxidation kinematics changes to linear from parabolic above 1000 °C due to stress buildup on the outer layer [93]. Because of the lower hardness and layered structure polycrystalline Ti_3SiC_2 demonstrates high friction coefficient and wear losses. Ti_3SiC_2 is a promising material for many high temperature application including automobile engines cylinder materials and electrical connections. An ideal material for this applications require materials that exhibit excellent wear and oxidation resistance and has low contact resistance over wide range of temperature. Hard secondary phases have been incorporated into Ti_3SiC_2 matrix to conquer constrains of using it in

high temperature mechanical applications. Similarly, Because of its unique damage tolerance characteristic and machinability, Ti_3SiC_2 could also be employed as binder material for hard ceramics. Recently Ti_3SiC_2 was being used as the joining materials for SiC based ceramics [94] and C/C composites [95]. Good interference bonding and high shear strength was reported in presence of Ti_3SiC_2 on the interface.

1.7.1 Ti_3SiC_2-TiC Composites:

Composites involving Ti_3SiC_2 and their corresponding binary carbides have been synthesized and characterized on the recent publications. According to Ti-Si-C phase diagram both TiC and SiC is thermodynamic stable with Ti_3SiC_2 [96]. Ti_3SiC_2–SiC composites have been studied more rigorously in recent times because of their higher hardness and wear resistance [97, 98]. Presence of SiC was reported to improve oxidation resistance of composites at higher temperature [99]. Though damage tolerance, hardness and thermal shock resistance of the composites have increased, strength and fracture toughness was reported to decrease because of the thermal expansion mismatch between Ti_3SiC_2 and SiC [100]. The thermal expansion coefficients of SiC and Ti_3SiC_2 are, respectively, $5.12x10^{-6}$/K [101], $8.6x10^{-6}$/K (Ti_3SiC_2, a-direction) and $9.7x10^{-6}$/K(Ti_3SiC_2, c-direction) [71].

On the other hand, TiC has very high hardness in the range of 28-35 GPa, High temperature sustainability (melts at 3067 °C), high E value (410-510 GPa) and good erosion resistance. Most importantly, thermal expansion coefficient of TiC and Ti_3SiC_2 are reportedly $7.4x10^{-6}$/K [99], $8.6x10^{-6}$/K (Ti_3SiC_2, a-direction) and $9.7x10^{-6}$/K(Ti_3SiC_2, c-direction) [102], respectively. As there is very small difference in thermal expansion coefficient between TiC and Ti_3SiC_2, TiC is more suitable reinforcement for Ti_3SiC_2.

1.8 Previous work on Ti_3SiC_2 based composites:

1.8.1 Ti_3SiC_2-TiC composites:

Hu et al. [103] first reported densification of Ti_3SiC_2-TiC(30% Vol.) and Ti_3SiC_2-SiC(30% Vol.) composites from Ti, SiC and C powder through HIP at 1500-1600 °C for 8 h or holding time. The strength of Ti_3SiC_2-SiC composites was lower than monolithic Ti_3SiC_2 because of thermal expansion mismatch between Ti_3SiC_2 and SiC. Processing of Ti_3SiC_2-TiC composite was carried out through combination of mechanical alloying and hot pressing and was compared with hot pressing [104]. More uniform microstructure was achieved on MA-HP process than by HP process. Uniform dispersion of Ti_3SiC_2 phases improved the damage tolerance of brittle TiC by crack arrest mechanism in case of MA-HP sample. Tada et al. [105] fabricated Ti_3SiC_2-TiC composites through traveling zone sintering method, in which sintering temperature could be precisely controlled at any point of the mold. Fabrication of Ti_3SiC_2-TiC composites through Spark Plasma Sintering has been reported only by handful of authors. To attain monolithic Ti_3SiC_2 many of the papers have reported synthesis of Ti_3SiC_2-TiC composites but as none of them were intended to do so thus they were not recognized as Ti_3SiC_2-TiC composite processing. Zhang et al. [106] fabricated TiC/Ti_3SiC_2 composites with 0-40 vol.% TiC from Ti, C, Si, Al reactants using SPS at 1280°C (with heating rate of 100°C/min, soaking time of 10 min and pressure of 70 MPa). The microstructure of the final sample consisted of coarse grains of Ti_3SiC_2 (2-10μm) and fine grains of TiC (about 1 μm). The grain size tends to decrease with the increase in TiC content. The Vickers hardness was increased with TiC content, and reached about 13GPa for Ti_3SiC_2/40 vol.% TiC. The toughness and flexural strength also increased with up to 30 vol.% of TiC compared to monolithic Ti_3SiC_2, but decreased for higher vol.% of TiC. The reasons behind this abrupt behavior are the formation of TiC cluster, lower density, and transition of fracture mode from intergranular to transgranular. As TiC has relatively lower thermal conductivity compared to Ti_3SiC_2, the thermal conductivity of Ti_3SiC_2/TiC composites decreased

with the increased amount of TiC. The Ti_3SiC_2-90 vol.% TiC composite samples were also densified using Ti/Si/TiC powder mixture with SPS at 1250-1400°C (heating rate of 100°C/min, 15 min and 50 MPa) [107]. The relative density of the prepared samples with higher TiC percentage was lower. The composite samples with 10% TiC showed best densification effect. From the SEM micrographs (fig. 1.8) at higher volume content of TiC non homogenous microstructure with TiC agglomeration was observed.

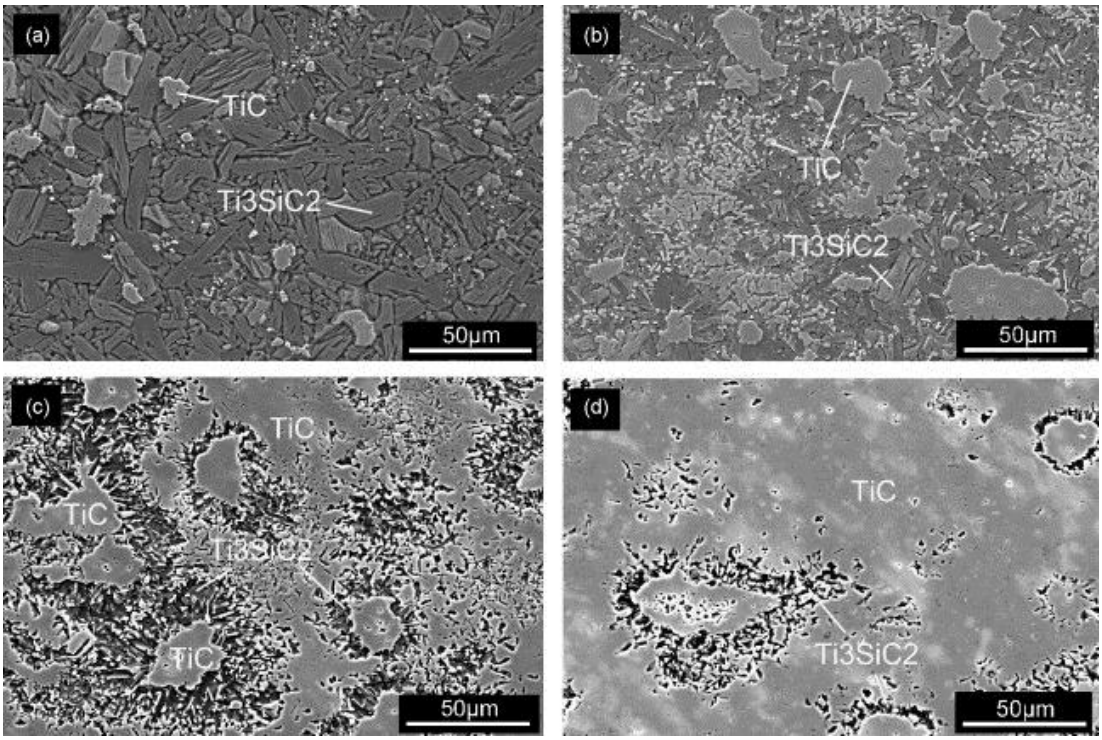

Fig. 1.8 SEM micrographs of samples containing (a) 0 vol.% TiC (b) 20 vol.% TiC (c) 60 vol.% TiC and (d) 80 vol.% TiC [107].

Vickers hardness increased almost linearly with TiC content to a value of 20.1±1.4GPa for 90 vol.% TiC. The flexural strength increased gradually with TiC content up to 50 vol.%, and then decreased at high end of TiC volume fraction due to change in fracture mode from intergranular to transgranular. Konoplyuk et al. [108] also synthesized Ti_3SiC_2-TiC composites from TiH_2/SiC/Si/C reactants at different molar ratios. Processed composites exhibited higher bending

(400-600 GPa) and compression strength (1500 MPa) over single phase Ti_3SiC_2 provided by presence of hard TiC phase.

1.8.2 Ti_3SiC_2-SiC composites:

The properties such as hardness and wear resistance of Ti_3SiC_2 could be further improved by reinforcing it with SiC. Furthermore, SiC is thermodynamically stable with Ti_3SiC_2 [109-110]. Zhang et al. [111] investigated SPS to synthesize Ti_3SiC_2-20 vol.% SiC nanocomposites from Ti/Si/C/Al powder in a temperature range of 900-1300°C with soaking time of 6 min, pressure of 70 MPa, and heating rate of 100-200°C/min. In the temperature range of 1150-1300°C, the composite attained critical grain size of 5 μm for Ti_3SiC_2 and 100 nm for SiC resulting in improvements in flexural strength and Vickers hardness at room temperature. The SiC in the nanocomposite does not form directly from the initial powder but from intermediate TiC_x and $Ti_5Si_3C_y$. The same authors also successfully prepared nanosized SiC reinforced Ti_3SiC_2 composites with 0-40 vol.% SiC (1280°C; 70 MPa; 10 min of soaking time) [112]. The Ti_3SiC_2-SiC formed from Ti, Si, C, Al powders according to the following reaction:

$$3(1-x)Ti+Si+(2-x)C \rightarrow (1-x)Ti_3SiC_2 + xSiC \quad \ldots\ldots\ldots\ldots (1.1)$$

Al was added as a sintering aid. The microstructure of the samples (fig. 1.9) showed that nanosized SiC particles were dispersed uniformly up to 30 vol.% of SiC. Some SiC clusters were formed with 40 vol.%. In general, the mechanical and physical properties, including Vickers hardness, fracture toughness, thermal conductivity, and electrical resistivity of the composites, improved with increment in SiC content. The Ti_3SiC_2-40 vol.% SiC exhibited lower fracture toughness compared to Ti_3SiC_2/30% vol. due to lower density and cluster formation of SiC in the composite. The flexural strength of the composites was lower than monolithic Ti_3SiC_2, but the decrease is less than previously reported values [103, 113]. This improvement was attributed to

the formation of nanosized SiC particles in the composites which is quite difficult to form in HIP process because of its higher sintering temperature and longer sintering time.

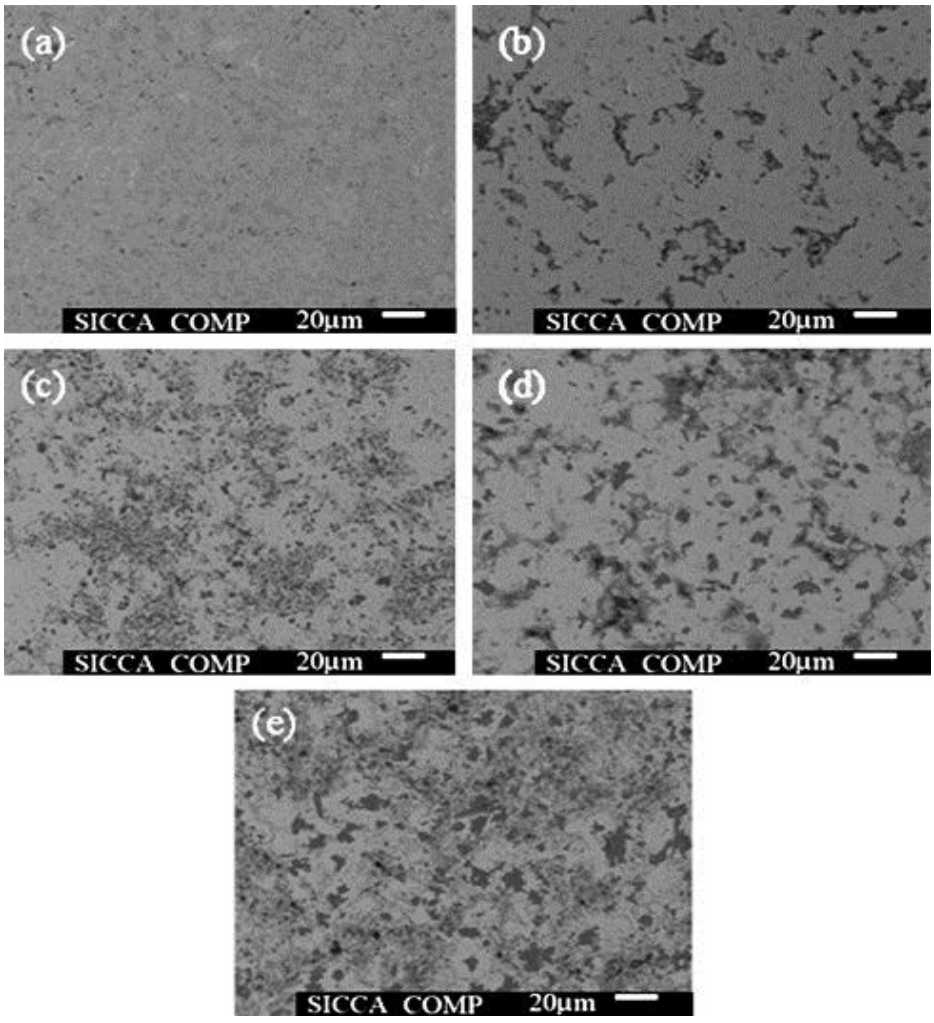

Fig. 1.9: Backscattered electron images with (a) 0% vol.% (b) 10% vol.% (c) 20% vol.% (d) 30% vol.% (e) 0% vol.% of SiC [112].

1.8.3 Ti_3SiC_2- Al_2O_3 composites:

Al_2O_3 reinforcement in Ti_3SiC_2 also contributes to improved hardness, wear resistance, and mechanical performance compared to monolithicTi_3SiC_2/10%vol. The Ti_3SiC_2/Al_2O_3 composites were SPS sintered from Ti, TiC, Si, and Al_2O_3 starting powders in temperature range of 1200-1400°C with holding time of 5-15 min and pressure of 40 MPa [114]. The optimized sintering

temperature of stability of MAX phase was about 1300°C. At temperature higher than 1350°C, the decomposition of Ti_3SiC_2 takes place and the amount of Ti_3SiC_2 decreases. For samples processed with optimized SPS parameters, the flexural strength and fracture toughness were about 600 MPa and 7.4 $MPa.m^{1/2}$, respectively. Wang et al. [115] reported mechanical properties of composites with different percentage of Al_2O_3 vol. content (sintered in the temperature range of 1200-1400°C with 40MPa pressure and 5-15 min soaking time). The Vickers hardness of the composites reached its maximum value at about 20% vol. content of Al_2O_3. Addition of Al_2O_3 greater than 10% vol. resulted in slight decrease in flexural strength and fracture toughness due to Al_2O_3 agglomeration. Luo et al. [116] also synthesized Ti_3SiC_2/Al_2O_3 composites and reported that Vickers hardness of the composite increases, and fracture toughness and bending strength decreases with Al_2O_3 content.

1.8.4 3Y-TZP- Ti_3SiC_2 composites:

Ti_3SiC_2/3Y-TZP (3 mol.% yttria-stabilized tetragonal zirconia polycrystal) composites with up to 50% Ti_3SiC_2 as reinforcement were synthesized using SPS [117]. The Vickers hardness and bending strength decreased with increasing Ti_3SiC_2 content; whereas, fracture toughness increased compared to monolithic 3Y-TZP. Presence of Ti_3SiC_2 in the composites contributes to crack deflection, crack bridging, and transformation toughening important for improving fracture toughness.

1.9 Objective and Scope of Work:

The intent of this study was multi-fold. Processing of single phase Ti_3SiC_2 at lower temperature by proper amount of Al addition with Ti/SiC/C (3:1:1) was the first objective. The second goal was to develop Spark Plasma Sintering (SPS) technique for processing of Ti_3SiC_2-TiC composites (0-30 vol.% of TiC) from Ti/Si/TiC/Al powder mixture.

The objectives of this work include:

- Phase evaluation, microstructure analysis and tribological characterization of monolithic Ti_3SiC_2 sintered in the range of 1050-1450 °C.
- Investigate the reaction mechanism involving synthesis of Ti_3SiC_2 from constituent phases present and to analyze possibility of $Ti_3(Si_{1-x}Al_x)C_2$ solid solution formation in presence of Al.
- Analyze existing sprinkled literature results on phase stability of Ti_3SiC_2 and compare them with experimental results.
- Identify the dependence of starting composition in processing of Ti_3SiC_2 through SPS from three sets of powder mixtures, Ti/SiC/C, TiC/Ti/SiC and TiC/Ti/Si.
- Measure experimental volume content of constituent phases on Ti_3SiC_2–TiC composites and to compare it with designed value from initial composition.
- Study microstructure, densification and hardness of synthesized Ti_3SiC_2–TiC composites.
- Investigate detailed tribological characterization of the composites at room temperature to understand the effect of TiC on tribological behavior of Ti_3SiC_2 matrix composites.

CHAPTER II

EXPERIMENTAL DETAILS

2.1 Starting Powders:

This work was conducted by using commercially available powders of titanium (<44 μm, 99.5%, Alfa Aesar, Ward Hill, MA, USA), silicon Carbide (2-10 μm, 99%, American Elements, Los Angeles, CA, USA), silicon (1.5 μm, 99%, Atlantic Equipment Engineers, Bergenfield, NJ USA), graphite (< 44 μm, 99.99%, Alfa Aesar), aluminium (2~10 μm, 98%, Alfa Aesar), titanium carbide (2 μm, 99.5%, Alfa Aesar).

For synthesizing monolithic Ti_3SiC_2 starting powders of Ti, SiC, C and Al was weighted according to molar ratio of 3:1:1:0.15. 3Ti-SiC-C-0.15Al, 2Ti-SiC-TiC-0.15Al and Ti-Si-2TiC-0.15Al were mixed together to understand the effect of starting composition on processing of monolithic Ti_3SiC_2.

TiC, Si, Ti and Al powders were weighted to yield a final composition with appropriate stoichiometry as shown on table 2.2. The samples were named based on the theoretical percentage of the TiC reinforcement added on the sample. Samples with no TiC reinforcement is named as TSC assuming the only phase present on the sample will be titanium silicon carbide. (Ti_3SiC_2).

Table 2.1 The volume content of TiC in the designed composites

Sample	Ti_3SiC_2 (Vol. %)	TiC (Vol. %)
TSC	100	0
TC10	90	10
TC20	80	20
TC30	70	30

For preparation of single phase Ti_3SiC_2 and Ti_3SiC_2-TiC composites Ti, Si, and TiC powders were mixed according to the following compositions.

$$Ti + Si + xTiC = Ti_3SiC_2 + (x-2)\ TiC \quad \text{.....(2.1)}$$

Al is added to reduce the amount of auxiliary TiC on the sintered samples.

Table 2.2 Weight percentage of the powder mixture to obtain desired volume content of TiC.

Sample	Weight percentage (wt.%)				Theoretical TiC (vol.%)
	Ti	Si	TiC	Al	
TSC	23.82	13.97	59.60	2.61	0%
TC10	21.31	12.50	63.85	2.34	10%
TC20	18.83	11.05	68.05	2.07	20%
TC30	16.38	9.61	72.20	1.81	30%

2.2 Experimental procedure:

2.2.1 Mechanical Milling:

Mechanical milling was accomplished in a high energy planetary ball mill (Fritsch planetary micro mill, 'pulverisette 7' premium line) as shown on fig. 2.1. In conventional planetary milling machine grinding bowls are arranged eccentrically on the sun disk. This grinding jar rotates through an ark around the sun and simultaneously also revolves around their own axis. Energy created in this process is significantly higher than traditional ball milling. In this planetary ball milling machine grindings bowls are clamped to the sun disk which limits the rotational speed because of the production of high amount of centrifugal force during milling. In 'pulverisette 7' model of ball milling machine Fritish sunk the grinding jar into the sun disks and because of that jars center of gravity are on the same plane of the sun disks which significantly reduces the amount of centrifugal force. The rotation speed of these machines could be as high as 1100 rpm and generates 150% higher energy resulting reduction in grinding time and ultra-fine powders. This special planetary milling machine has been demonstrated to enable the creation of nano-particles. Self-lock technology is included with the system which automatically check the lock of the milling jars before starting and shut off operation in case of any imbalance.

Powders with appropriate stoichiometry were dry milled in Tungsten carbide containers bearing tungsten carbide balls (5mm in diameter). The powders were milled for 1h with milling speed of 500 rpm where ball to powder ratio was set at 8:1. Ball milling parameters were chosen to prevent high temperature generation inside the jar as high temperature will cause the melting of constituent powders. After every 3 min of milling time, 25 min of cooling time was provided to maintain lower temperature.

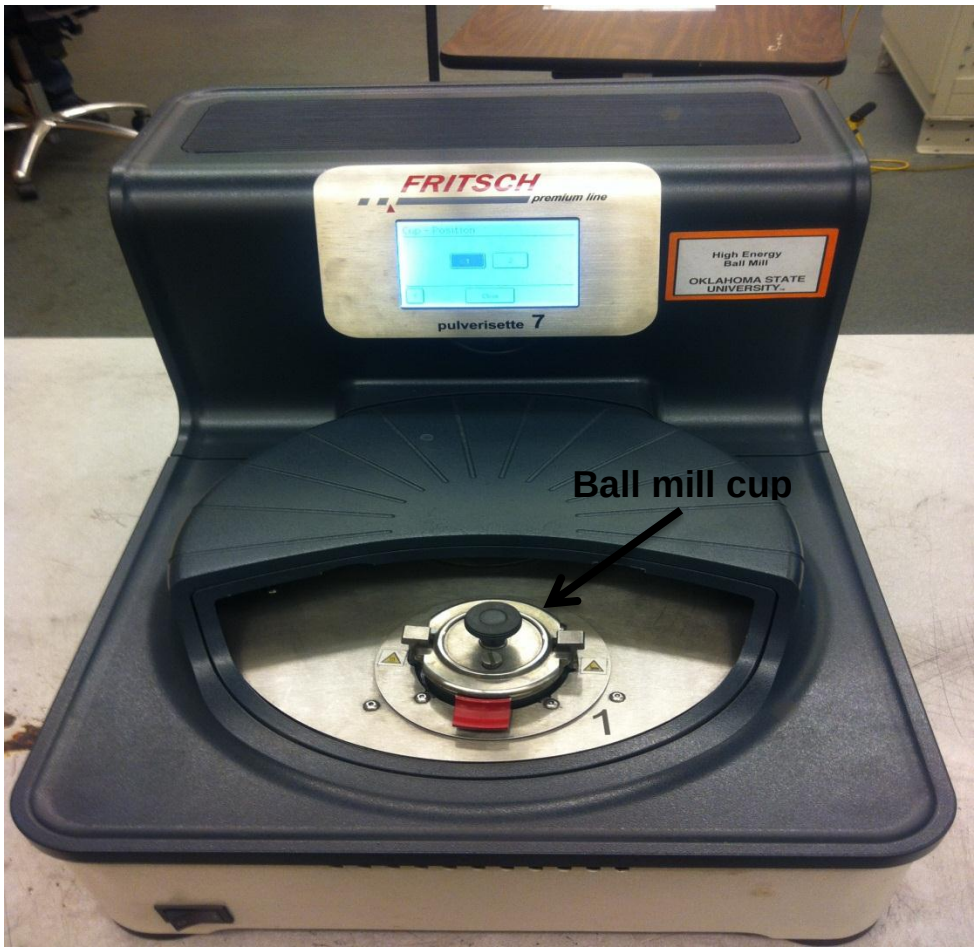

Fig. 2.1 "pulverisette 7" high energy ball milling equipment.

2.2.2 Spark Plasma Sintering:

Processing of Ti_3SiC_2 and Ti_3SiC_2-TiC composites was done by SPS model 10-3 manufactured by Thermal Technologies LLC (Santa Rosa, CA, USA). This SPS model can provide a maximum of 10 tons of force and 3000 amps of 5 Volts DC power supply. The system of SPS consists with 3 main parts, named as power supply unit, furnace and cooling water and vacuum control unit as shown on fig. 2.2. The whole SPS process is regulated by controlling the pulsed DC current from the power supply unit. Power supply comprised of three 3 individual 1000 amps unit thus no downtime is necessary if one unit fails. Power supply can be programmed from straight DC or

pulsing with on time ranging from 4 to 900 ms and off time 0 to 9 ms. It has the ability to change the pulse pattern during the run to attain maximum benefit in terms of densification. This advanced power supply unit provides unparalleled adjustability and can achieve heat rates greater than 600°C per minute. This unit is capable of reaching a temperature of 2500°C in less than 5 minutes. SPS furnace is water cooled chamber designed with punch electrodes which are also water cooled. A high vacuum of 10^{-2} Torr can be achieved by vacuum pump which is necessary to maintain purity of the samples. By means of air/argon/nitrogen gas atmosphere control mechanism cooling rate can be effectively controlled inside the furnace. Digital servo valve controlled hydraulic system enables ultra-fine precession force control and starting pressure could be set as low as 3 MPa. Multiple thermocouple chords are set on the furnace to measure the ram and mold temperature. Sintering temperature is constantly monitored and recorded either by thermocouple (< 1000 °C) or by A single-color optical pyrometer (Raytek, RAYMM1MHVF1V) focused on a hole drilled on the surface of the die. The pyrometer can be adjusted on the X, Y and Z axis. Displacement, temperature and pressure profiles are monitored and recorded by an on or off line PC system for further analysis of the densification mechanism. Various interlock safety system units are also included with the system to ensure safe operation.

Known quantity of powders to be sintered is placed in cylindrical die and the die, punch and spacer assembly is placed inside the heating furnace as shown on fig. 2.3. In the die, the powders were lined with graphite sheet to alleviate easy removal of the sample after sintering. Graphite die is wrapped with graphite cloth to minimize radiation losses. Pyrometer (figure 2.4) is focused on the small hole drilled through halfway of the thickness of the die to ensure accurate temperature measurement. The electrodes, dies, punches and spacer are made of electrically conducting materials (graphite, copper, ceramics, stainless steel etc.) to ensure electrical circuit closing.

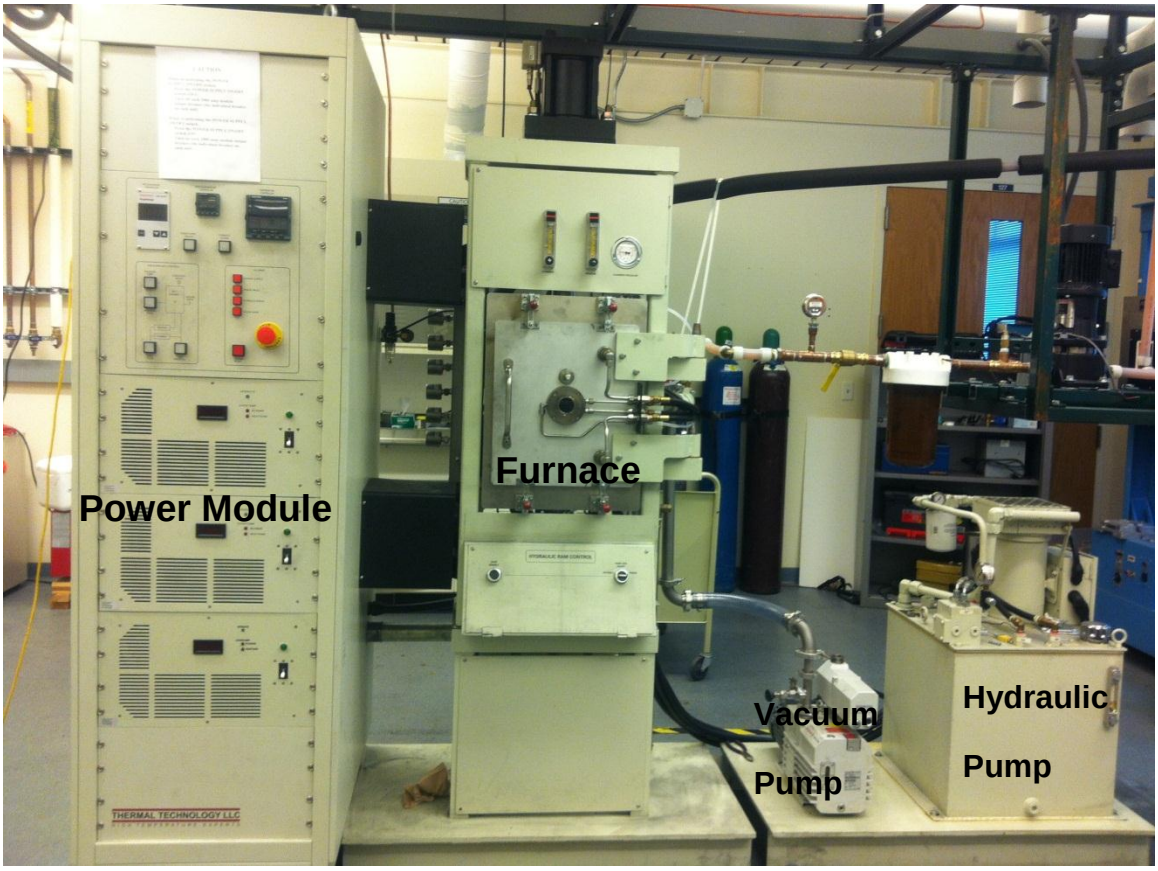

Fig. 2.2 Spark Plasma Sintering setup.

Dies and punches made of graphite are mostly used in SPS process because of their good thermo-electrical properties at higher temperature. Use of graphite limits the applied pressure to a maximum of 100 MPa therefore; graphite dies are commonly used in high temperature and moderate pressure sintering. Mechanical pressure, Heating rate, temperature and cooling rate required for the sintering is set through PC system and could be varied in different densification stages.

To sinter monolithic Ti_3SiC_2 and Ti_3SiC_2-TiC, 3.5 g. of ball milled powders lined with graphite sheet were compacted loosely into a graphite die of 20 mm in diameter and sintered under a medium vacuum of $1*10^{-1}$ Torr.

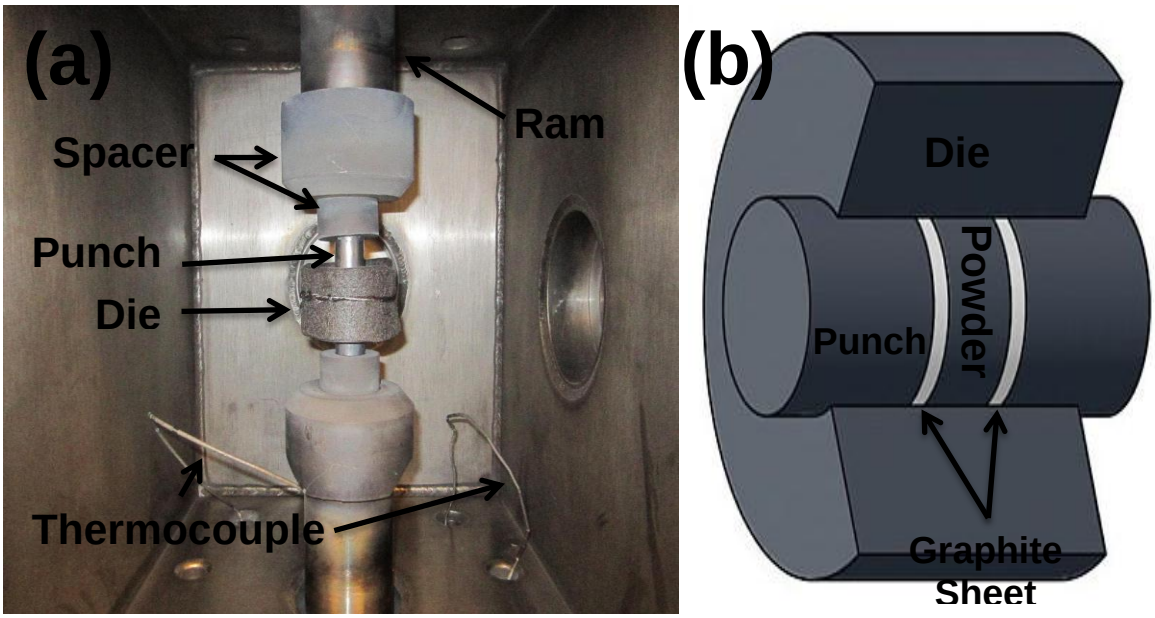

Fig. 2.3 (a) Die-Punch assembly inside the heating chamber (b) X-section of Die-punch assembly.

Fig. 2.4 Raytek Single color optical pyrometer

To sinter monolithic Ti_3SiC_2 and to understand the effect of temperature, SPS was done in the range of 1050-1450°C with 50 MPa uniaxial pressure, 15 min soaking time, and 100 °C/min heating rate. To evaluate the effect of initial powder 3Ti-SiC-C-0.15Al, 2Ti-SiC-TiC-0.15Al and Ti-Si-2TiC-0.15Al powder mixture were sintered at 1150 °C with 50 MPa pressure and 15 min of soaking time. Ti_3SiC_2-TiC composites were sintered from TiC/Ti/Si/Al powders at 1250 °C with 15 min of dwell time and 50 MPa of pressure.

2.2.3 Sample preparation:

The samples obtained from SPS were separated from die and punch assembly using hydraulic press (fig. 2.5 (a)) and then grinded with 400, 600, 800 and 1200 SiC paper to remove the carbon sheet layer. Then they were polished with 3 μm and 1μm diamond paste to get mirror like finishing. After polishing these samples were cleaned with acetone by ultrasonic cleaner and etched in HNO_3:HF:H_2O (1:1:2) solution for 30s to accomplish phase and microstructural analysis through SEM and EDS.

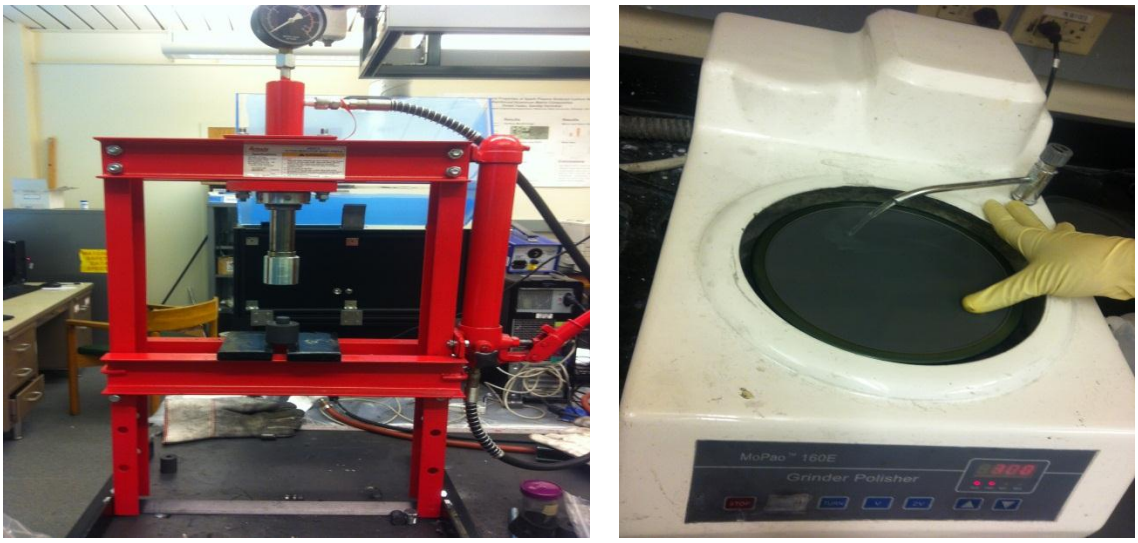

Fig 2.5 (a) Hydraulic press equipment and (b) Polisher.

2.3 Material Characterization:

2.3.1 Relative Density Measurement:

Density of the synthesized Ti_3SiC_2 and Ti_3SiC_2-TiC composites were measured using Archimedes principle employing Mettler Toledo (Delta Range XD204) equipment. The following equation was used to calculate the density of the sintered sample.

$$\rho = \frac{x}{x-y}(\rho_o - \rho_L) + \rho_L \text{.....(2.2)}$$

Where, ρ is the density of the sintered sample, ρ_o is the density of water (0.99804 g/cm^3 at room temperature), ρ_L is the density of air (0.0012 g/cm^3 at 25 °C) weight of samples in air, x and y are weight of samples in air and water, respectively. Relative density was calculated using following equation:

$$Relative\ Density = \frac{Density\ of\ sintered\ samples}{Theoretical\ Density\ calculated\ from\ phases\ present\ on\ XRD} \times 100 \text{.....(2.3)}$$

2.3.2 Phase & Microstructural Analysis:

2.3.2.1 X-Ray Diffraction:

X-ray diffraction (XRD) is a nondestructive technique to identify phase compositions. The recognition of peaks was done by comparing it with the reference diffraction pattern. Relative intensity of the peaks is representative to the number of grains present in that particular orientation. The ball milled powder and sintered sample was scanned from 10° to 90° by Philips Norelco X-ray diffractometer operating with Cu Kα (λ=1.54178 Å) radiation at 45 kV and 40 mA with a step increment of 0.02°/sec. High Score Plus software which is based on ICDD PDF2 database were employed to determine existing phases. Relative Ti_3SiC_2 content was calculated from relative intensity of the XRD peaks.

2.3.2.2 Microstructural Analysis:

Microstructure evaluation and analysis of wear track was studied by Scanning Electron microscopy using FEI Quanta 600 field-emission gun Environmental SEM (JSM-6360, JEOL). Elemental mapping and point Energy dispersion X-ray spectroscopy (EDS) at different point on the micrographs were executed by Evex EDS X-ray microanalysis system to chemically characterize the sintered samples.

2.4 Mechanical Characterization:

2.4.1: Microhardness:

The Vickers hardness of the Specimens was measured by Clark microhardness tester (Novi, MI) at the force of 9.8N with a holding time of 15s. The microhardness was measured on the mirror polished surface of the consolidated samples. Ten (10) readings were taken on each sample and the average value was reported.

2.4.2 Tribological characterization:

The wear tests were conducted on Nanovea tribometer (Irvin, CA) with a pin on disk configuration. 20 mm diameter Spark plasma sintered disc with test surface smoothly polished down to 1 μm surface roughness was slid against counter ball and create a 4 mm diameter wear track on the surface. The samples and balls were ultrasonically cleaned with acetone before testing. The test parameters were: 10 N normal force and sliding velocity of 200 rpm. Tests were carried out at room temperature for 1 hour and after every 10 min interval the weight loss data was being recorded. After every 10 min the counter body (alumina ball) was rotated to a new position so that new area comes into contact with the sample disk. Depth profile of the wear tracks were measured out using non-contact optical 3D Nanovea profilometer (Irvin, CA). Detailed morphological characterization was investigated using SEM. For tribological

characterization of monolithic Ti_3SiC_2 6 mm diameter of Al_2O_3 ball was used and for Ti_3SiC_2-TiC composites similar diameter Si_3N_4 ball was employed. All the other parameters remain same.

Fig. 2.6 Nanovea wear testing equipment.

Fig. 2.7 Nanovea non-contact optical 3D profilometer

CHAPTER III

RESULTS AND DISCUSSION

3.1 Monolithic Ti_3SiC_2:

3.1.1 XRD Analysis of the Powder and Synthesized Samples:

The X-ray diffraction profiles of the powders after mechanical milling and SPS sintered samples in temperature range of (1050-1450 °C) are summarized in fig. 3.1. For the ball milled powder Ti and SiC peaks were clearly visible in the XRD pattern whereas they disappear in the sintered samples. Disappearance of the Ti and SiC peaks after sintering suggests thoroughly completed reaction at this temperature range and soaking time. For the samples sintered at comparatively lower temperature range (1050-1150 °C) only TiC and Ti_5Si_3 peaks were detected. When the powders were sintered to a temperature of 1250 °C, newly formed peaks of Ti_3SiC_2 were found. Although the peaks of TiC can still be observed at this temperature, the intensity of TiC was much lower compared to Ti_3SiC_2. With an increase in sintering temperature (1350-1450 °C) the intensity of the TiC peaks increased again, though relative intensity of Ti_3SiC_2 remained significantly higher than TiC on sintered product.

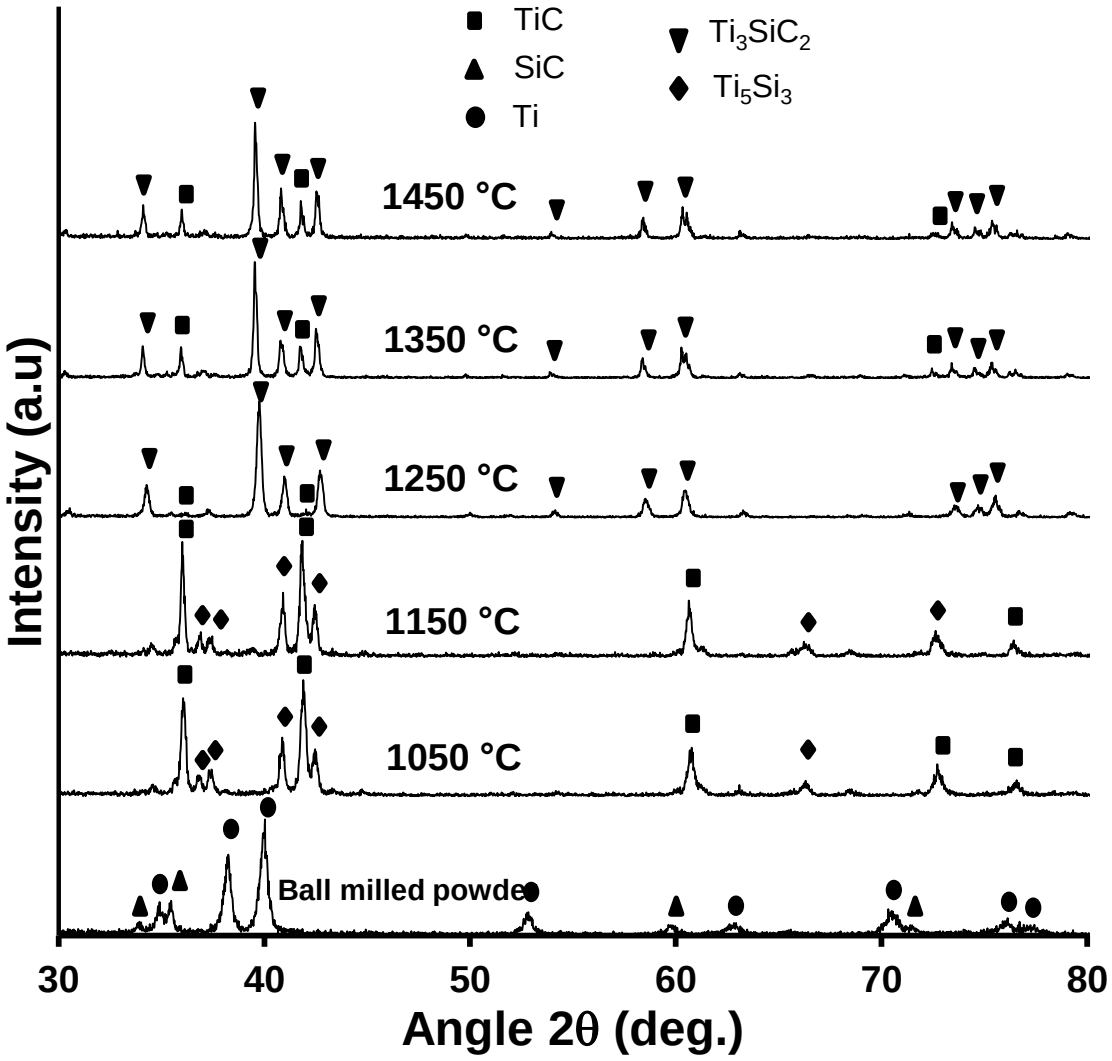

Fig. 3.1 X-ray diffraction patterns of ball milled powder and samples sintered at 1050, 1150, 1250, 1350 and 1450°C.

Quantitative evaluations of the contents of phases present in the synthesized samples were done employing experimentally calibrated standard additive method derived by Zou et al [118]. The intensities of TiC, Ti_5Si_3 and Ti_3SiC_2 are represented by $I_{TC,}$ $I_{TS,}$ I_{TSC} respectively. Diffraction peaks of TiC (111) Ti_5Si_3 (102) and Ti_3SiC_2 (104) were chosen as representative reflections as they did not overlap with any other peaks in XRD patterns.

$$W_{TS} = \frac{I_{TS}}{0.240I_{TSC} + I_{TS} + 0.197I_{TC}} \quad \text{..... (3.1)}$$

$$W_{TC} = \frac{I_{TC}}{1.222I_{TSC} + 5.084I_{TS} + I_{TC}} \quad \text{..... (3.2)}$$

$$W_{TSC} = \frac{I_{TSC}}{I_{TSC} + 4.159I_{TS} + 0.818I_{TC}} \quad \text{..... (3.3)}$$

Wherein, $W_{TS,}$ W_{TC} and W_{TSC} are the weight percentage of Ti_5Si_3, TiC, and Ti_3SiC_2 respectively. Fig. 3.2 shows the variation of weight percentage of phases present on samples sintered at 1050-1450 °C.

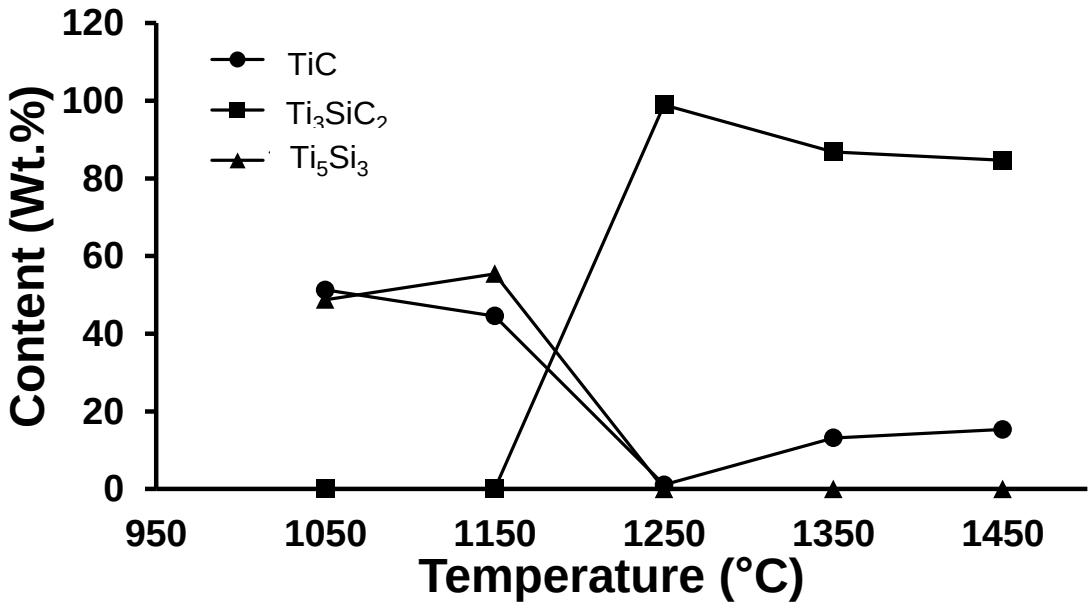

Fig. 3.2 Content of Ti_3SiC_2, Ti_5Si_3 and TiC at samples sintered over temperature range 1050-1450 °C

Samples sintered at 1050 and 1150 °C were composed with Ti_5Si_3 and TiC only and the amount of Ti_5Si_3 was increased with temperature. Ti_3SiC_2 phase first appeared at 1250 °C and content (wt.%) of Ti_3SiC_2 was found to be nearly 98.5% at this temperature. The only auxiliary phase

present at this temperature was TiC, suggesting complete consumption of Ti_5Si_3 in process of Ti_3SiC_2 formation. Above 1250 °C increased amount of auxiliary TiC indicates decomposition of Ti_3SiC_2 into TiC at higher temperature. The optimal sintering temperature for synthesis of single phase Ti_3SiC_2 was found to be 1250 °C and further increase in that sintering temperature enhanced undesirable TiC content.

Upon sintering to a temperature of 1050-1150 °C Ti react with free C and SiC to form TiC and Ti_5Si_3. Presence of TiC and Ti_5Si_3 suggests TiC and Ti_5Si_3 as the intermediate phases for the formation of Ti_3SiC_2 from Ti/SiC/C starting powder which reaffirmed the results of El-Raghy *et al*.[119] and S. Arunajatesan et al. [120]. Absence of Ti_3SiC_2 in the temperature range of 1050-1150 °C suggests minimum required temperature for Ti_3SiC_2 formation is above 1150 °C which is in accordance with Cordoba [121] and Wu et al. [122] observation.

Absence of Ti_5Si_3 on the XRD of the sintered samples at 1250 °C-1450 °C act as the denotation of full Ti_5Si_3 consumption in the conversion to Ti_3SiC_2. Thus nucleation and growth of Ti_3SiC_2 occurred in Ti_5Si_3 crystals rather than TiC is proposed. Nucleation on Ti_5Si_3 requires diffusion of C whereas nucleation on TiC involves diffusion of both Si and C atoms [119, 123]. Low diffusion rate of Si in TiC related system [124] and closer structural relationship between Ti_5Si_3 and Ti_3SiC_2 [125] suggests Ti_3SiC_2 is more unlikely to nucleate on TiC crystals. Another possible reaction mechanism was proposed involving formation of Ti-Si liquid phase which further react with TiC particles to synthesize Ti_3SiC_2 [126-128]. This Ti-Si liquid phase could be either Ti-Ti_5Si_3 [129] or Ti-$TiSi_2$ [130-131] and both formed at a temperature of about 1333 °C [132]. But in our experiment, optimum sintering temperature for getting single phase Ti_3SiC_2 was found to be 1250 °C which is lower than the eutectic temperature of Ti-Si liquid phase (1333 °C). Again, neutron diffraction study of Ti-SiC-C system [122, 133] also failed to provide any obligating evidence of major liquid phase formation. So the reaction involved is largely solid state reaction between TiC and Ti_5Si_3 rather than Ti-Si liquid phase formation. El raghy *et al.* [119] proposed

formation of intermediate phases and their conversion into Ti_3SiC_2 is simultaneous process. But on experimental results only TiC, Ti_5Si_3 phases were detected till 1150 °C suggesting Ti_3SiC_2 starts to form only after complete formation of intermediate TiC, and Ti_5Si_3.

3.1.2 Phase stability of Ti_3SiC_2:

Increment in the amount of auxiliary TiC was detected on samples sintered above 1250 °C. This phenomenon is attributed to the fact that, Ti_3SiC_2 became unstable and decomposed at higher temperature. At high temperature MAX phase materials decomposes instead of melting according to following reaction [5].

$$M_{N+1}X_N + A \longrightarrow M_{N+1}AX_N \quad \ldots\ldots\ldots\ldots\ldots\ldots\ldots\ldots(3.4)$$

Ti_3SiC_2 has sandwich like structure where Ti-C blocks are separated by hexagonal nets of Si and decomposition of Ti_3SiC_2 is initiated by loss of Si. Ti_3SiC_2 was reported to be thermodynamically stable up to 1600 °C in vacuum or Ar atmosphere for 24 h [119].**Error! Bookmark not defined.** But decomposition kinematics of Ti_3SiC_2 is highly dependent on the encompassing medium of Ti_3SiC_2. Presence of C act as driving force for increasing Si segregation and resultantly Ti_3SiC_2 decomposes at a temperature lower than 1600 °C according to the reaction $Ti_3SiC_2 \rightarrow 3TiC_{0.67}(s) + Si(g)$ [134]. In SPS graphite dies and punch act as graphite surrounding medium thus Ti_3SiC_2 decomposed into TiC_x primarily on the surface layer at higher temperature (1350 and 1450 °C). By means of inward diffusion of C, Si planes of Ti_3SiC_2 are replaced by C planes and resultantly form TiC_x layers on surface [135]. Racault et al. [134] suggested Free Si and C on skirting medium formed SiC through the reaction Si (g) + C = SiC. XRD and SEM micrographs of the samples sintered above 1300°C confirmed absence of any SiC on surface layer. Thus the free Si escaped from the surface of the samples rather than forming SiC. This observation also explains the weight loss when Ti_3SiC_2 was being heated in C crucibles above 1300 °C [134].

3.1.3 Effect of Starting Composition:

To explicate the effect of composition three different powder mixtures of 3Ti-SiC-C, 2Ti-SiC-TiC and Ti-Si-2TiC were sintered at 1150 °C with a pressure 50 MPa and 15 min of soaking time. XRD patterns of the synthesized samples are shown in fig. 3.3. From the fig. it can be seen that no Ti_3SiC_2 phase was present for 3Ti-SiC-C at this temperature whereas peaks of Ti_3SiC_2 were detected for 2Ti-SiC-TiC. Intensity of Ti_3SiC_2 peaks were increased for Ti-Si-2TiC composition. Relative content of Ti_3SiC_2 was calculated employing equation (3.3) and were found to be 0%, 13.18% and 39.85% for 3Ti-SiC-C, 2Ti-SiC-TiC and Ti-Si-2TiC compositions respectively. Thus Ti_3SiC_2 could be consolidated at lower temperature from Ti-Si-2TiC and was found to be best composition among these three to start with.

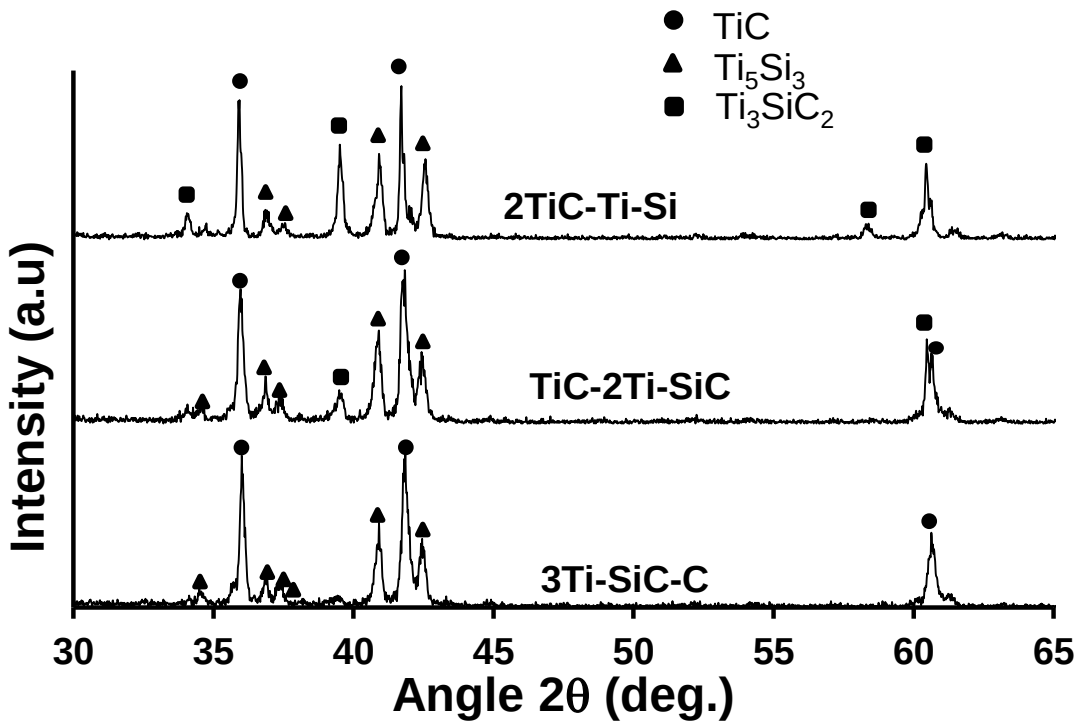

Fig. 3.3 X-Ray diffraction pattern for samples sintered at 1150 °C staring from three different compositions.

In Ti/SiC system intermediate TiC formed first by following reaction as TiC has higher thermodynamic stability [119]:

$$SiC + Ti = TiC + Si. \quad \Delta G^0 = -107 \text{ KJ } (1000 \text{ °C}) \ldots\ldots\ldots\ldots\ldots\ldots \quad (3.5)$$

Released Si then reacts with Ti and other intermediate phase Ti_5Si_3 is formed by following reaction:

$$5Ti + 3Si = Ti_5Si_3. \quad \Delta G^0 = -590 \text{ KJ } (1000 \text{ °C}) \ldots\ldots\ldots\ldots\ldots\ldots\ldots\ldots (3.6)$$

Since Gibbs free energy changes are negative thus both the reactions are thermodynamically favored [125]. From fig. 3.2, desired Ti_3SiC_2 formed when the constitutions of TiC and Ti_5Si_3 phases were completed. Intermediate TiC and Ti_5Si_3 starts to form at almost same temperature and addition of TiC as the starting material favors completion of Ti_5Si_3 constitution at lower temperature. This phenomenon explains why the content of Ti_3SiC_2 is substantially increased when TiC is used in the starting powder. Similarly, addition of Si instead of SiC on starting powder made it easier to form Ti_5Si_3 through reaction (3.6) by skipping reaction (3.5). Thus, Initial composition contained with TiC and Si favors completion of intermediate phases at lower temperature leading to decrease in sintering temperature for Ti_3SiC_2 formation.

3.1.4 Microstructural Analysis:

The SEM microstructure of polished and etched surfaces of SPS sintered Ti_3SiC_2 samples are illustrated in fig. 4. When the sintering temperature was 1050 °C, TiC and Ti_5Si_3 (as shown of fig. 3.4 (a)) were observed in micrographs. HF present in the etching solution promptly dissolves silicides (here Ti_5Si_3) thus Ti_5Si_3 appears corroded on micrographs [120]. At 1250 °C, uniform duplex microstructure of fine equiaxed grains (1-2 μm in diameter) and large plate shape grains (3-5 μm in length and 1-2 μm in width) were observed. EDS analysis was performed at the plate

shape grain (spot 1), bright circular grain (spot 2) and fine equiaxed grain (spot 3) of 1250 °C sample and shown as fig. 3.5.

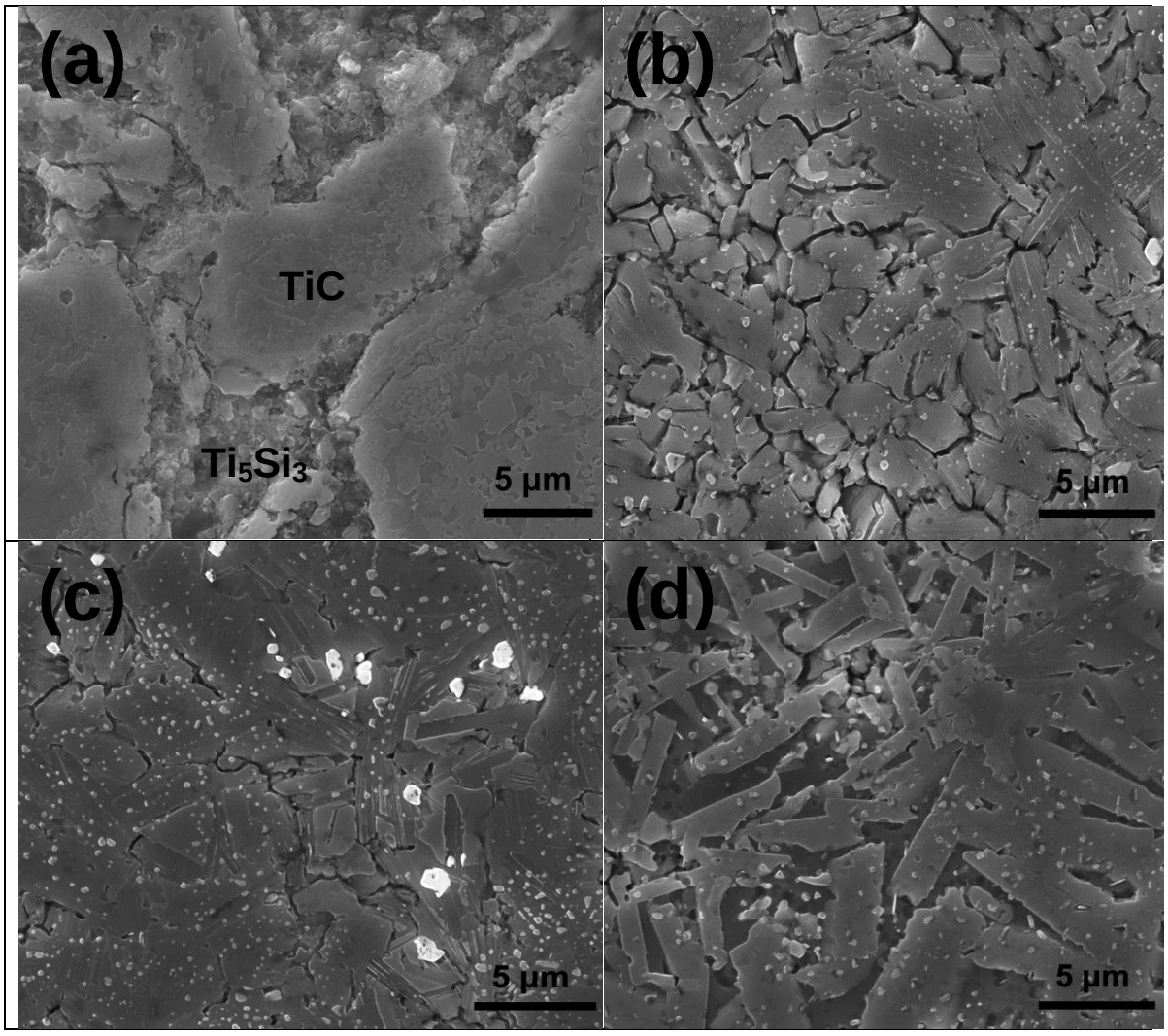

Fig. 3.4 Microstructure of the samples sintered from 3Ti/SiC/C/0.2Al powders at (a) 1050 °C (b) 1250 °C (C) 1350 °C (d) 1450 °C

With the EDS detector used, only Ti, Si, and Al peaks could be detected. From the corresponding peaks of Ti, Si, and Al, the plate shaped grains (point 1) and equiaxed grains (point 3) seem to be Ti_3SiC_2. The XRD analysis also indicated Ti_3SiC_2 as a major phase at this sintering temperature (Fig. 1). Intense peaks of Al and Si were observed for the bright grain (point 2) and it seems to be

a solid solution of Ti_3SiC_2 and Al, $Ti_3(Si_{1-x}Al_x)C_2$. Plate-like grains continued to expand and reached about 5-8 μm in length & 2-4 μm in width at 1350 °C. The size of plate-like grains have reached in a size of 10-20 μm in length & 3-5 μm in width with further increase in sintering temperature to 1450 °C. From the micrographs, it can be concluded that grain size of Ti_3SiC_2 and TiC crystals strongly depends on sintering temperature.

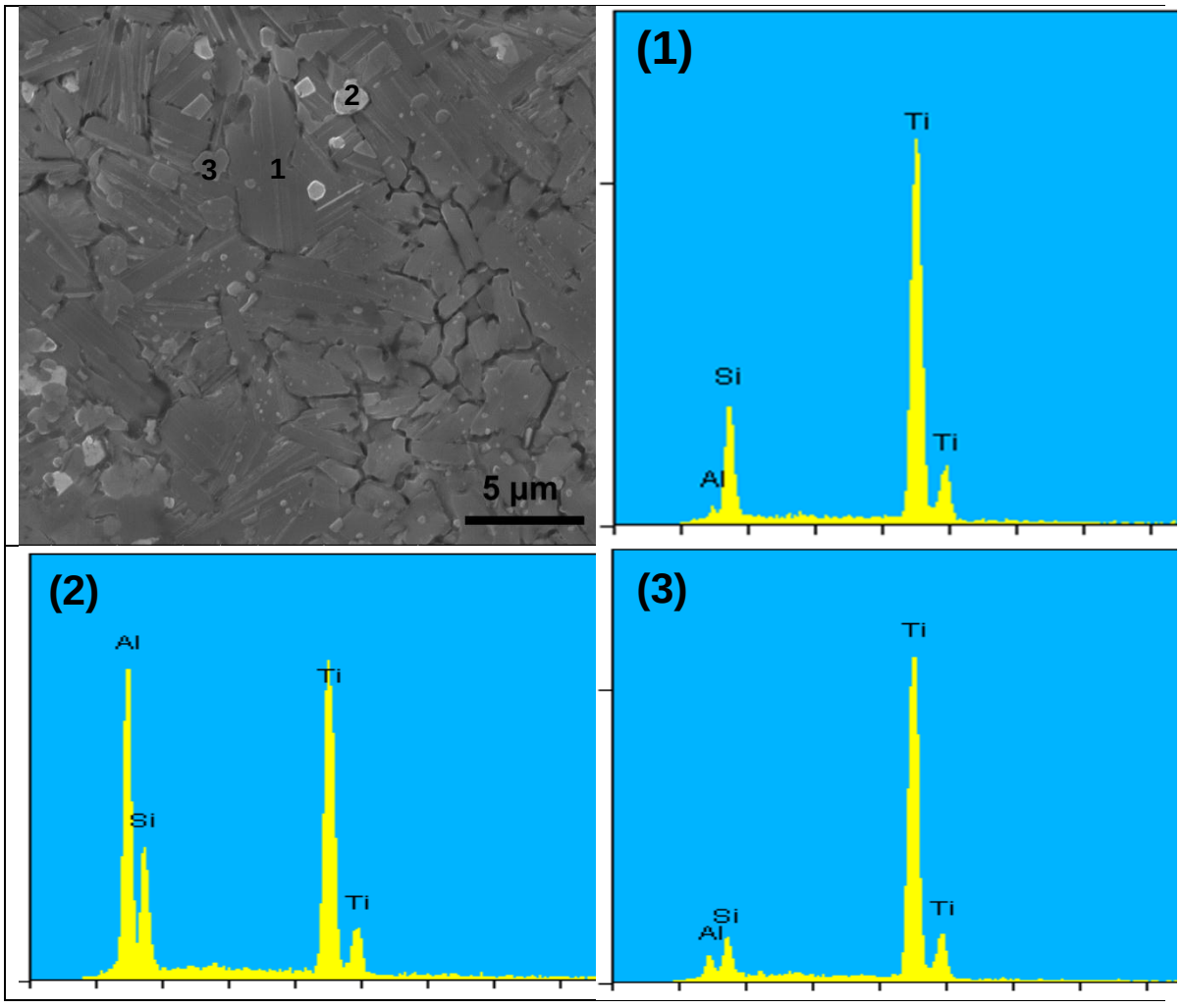

Fig. 3.5 Energy Dispersive Spectra (EDS) at three different points on the sample sintered at 1250 °C.

El-Raghy et al. [119] processed single phase Ti_3SiC_2 (>99%) from Ti-SiC-C starting composition through HIP in the temperature range of 1450-1600 °C. The average grain size of Ti_3SiC_2 in hot pressed sample was found to be 100-200 μm after 4 hr. at 1600 °C. From above results, 98.5% pure Ti_3SiC_2 was sintered at comparatively lower sintering temperature (1250 °C) and shorter holding time (15 min) through SPS. Lower sintering temperature and shorter time required in SPS retards grain coarsening and even the grain size achieved at highest sintering temperature (1450 °C) is nearly 10 times lower compared to HIP and other conventional sintering technique [136]. Because of higher heating rate in SPS, low temperature stages where surface diffusion dominates mass transport can be bypassed which increases the sinterability of powders and retards grain growth in SPS. Application of current in SPS also enhances mass transport by increasing point defect concentration or enhancing defect mobility [61]. Combined effect of these factors allow SPS to sinter at lower temperature and pressure, shorter sintering time with finer and homogeneous microstructure compared to conventional sintering process.

3.1.5 Effect of Al Addition:

Sun et al. [74] synthesized Ti_3SiC_2 applying Ti/SiC/C (3:1:1) powders through SPS and only poor phase purity of Ti_3SiC_2 (50% Ti_3SiC_2 or less) were possible over wide range of temperature and time. With addition of 0.15 mol of Al on stoichiometric Ti/SiC/C (3:1:1) composition, the product sintered at 1250 °C reached a phase purity of 98.5% Ti_3SiC_2 as shown on fig. 3.2. As Al has low melting point (660°C), minor interfacial liquid phase was formed into the system which favors diffusion of Ti and C atoms thus supplements Ti_3SiC_2 formation. In recent publications, it was reported that addition of small amount of Al during the synthesis of Ti_3SiC_2 removes the impurity TiC by forming solid solution of $Ti_3(Si_{1-x}Al_x)C_2$ [137]. To understand the effect of Al addition on synthesis of Ti_3SiC_2 and to analyze the possibility of Solid solution formation, EDS mapping of Al on the sample sintered at 1250 °C was done which is shown on fig. 3.6.

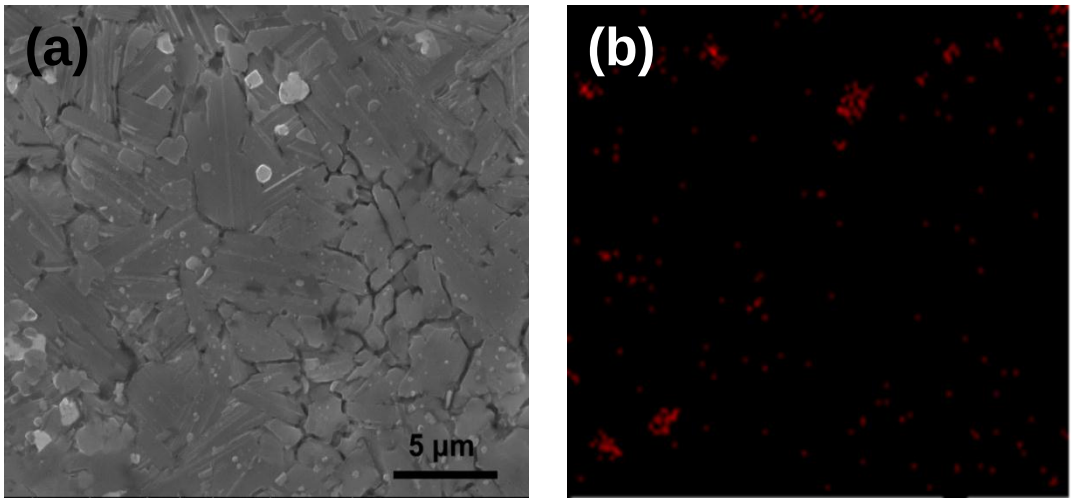

Fig. 3.6 (a) SEM micrograph and (b) Energy Dispersive Spectra (EDS) mapping of Al on the sample sintered at 1250 °C.

From EDS mapping, Distribution of Al (fig. 6(b)) was not uniform and agglomeration of Al was observed on the mapping. These agglomerations of Al represented the corresponding bright white spots on the SEM micrographs. Points EDS of these spots (fig. 5 spot 2) demonstrated presence of both Al and Si along with Ti, suggesting formation of $Ti_3(Si_{1-x}Al_x)C_2$ solid solution. Mechanical properties of $Ti_3(Si_{1-x}Al_x)C_2$ resembled those of Ti_3SiC_2 and high temperature oxidation resistance of Ti_3SiC_2 was significantly improved by solid solution formation [138]. Addition of excess Al in starting composition induces reaction between Ti and Al and aluminum related compounds such as, Ti_3AlC_2 and Ti_3Al formed. No Ti_3AlC_2 or Ti_3Al peaks were detected in the XRD profiles and SEM micrographs precludes the possibility of excess Al addition.

3.1.6 Micro-hardness and Wear test results:

Micro hardness of samples sintered at 1250 °C which contains 98.5% Ti_3SiC_2 was found to be 6.32 ± 0.166 Gpa. For the samples fabricated at 1350 °C and 1450 °C exhibited hardness value of 6.834 ± 0.1214 GPa and 7.05 ± 0.21 GPa respectively. The value reported in the literature for pure Ti_3SiC_2 was nearly 4 GPa [139]. The high hardness value might be associated with lower

indentation load, finer microstructure and the presence of impurity (1.5 % TiC) in the specimen. At lower loads the value represents the hardness of single crystal as indentation is within one grain and Raghy *et al*.[89] reported hardness becomes independent of indentation load and grain size at higher loads (100N). Higher hardness values for samples sintered at 1350 and 1450 °C are colligated with higher percentage of impurity TiC phase present on the samples which is nearly 13% and 15% respectively.

The accumulative wear loss as function of sliding time for samples sintered at 1050 °C, 1250 °C and 1450°C are recorded on fig. 3.7. As samples sintered over temperature range of 1050°C-1150°C and 1350°C-1450°C has almost same phase constituents (fig. 3.2) so only 1050 °C, 1250 °C and 1450°C samples were chosen to do wear test. Samples sintered at 1250 °C demonstrated maximum weight loss and minimum wear loss was observed for 1050 °C sample.

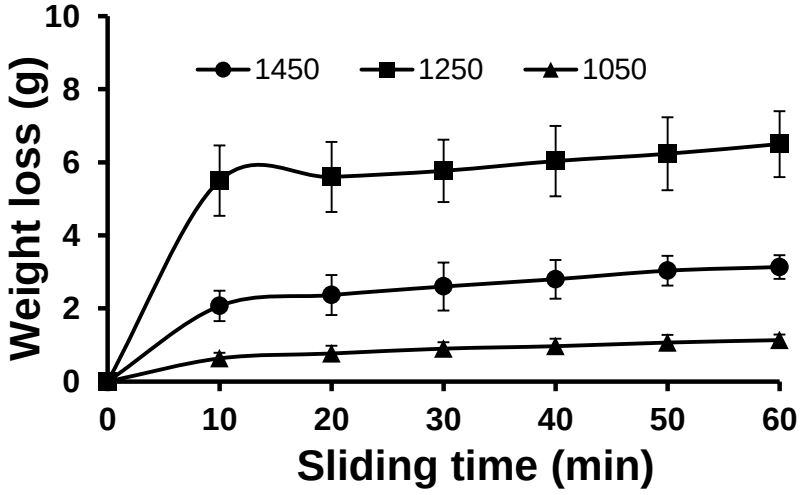

Fig. 3.7 Cumulative weight loss vs. sliding time for samples sintered at 1050 °C, 1250 °C and 1450°C.

The samples sintered at 1250 °C and 1050 °C exhibited highest and lowest wear weight loss, respectively. The samples sintered at 1450 °C showed intermediate values of cumulative weight

loss. This trend can be explained based on the variation of TiC content in the final sintered microstructure. As discussed earlier (Fig. 2), the samples sintered at 1250 °C contained lowest percentage of TiC (~1.5%) while those sintered at 1050 °C sample contained 51.25% TiC. The samples sintered at 1450 °C contained nearly 16% TiC. As TiC has significantly higher hardness (23.5 GPa) compared to Ti_3SiC_2 (6 GPa), the normal load on Ti_3SiC_2 during testing is effectively reduced with the presence of TiC. The harder TiC phase present in the microstructure seems to reduce ploughing or scrapping effect at the contact surfaces resulting in lower weight loss for samples with higher TiC content. The samples sintered at 1250 °C also showed wider wear track with average depth of wear track of about 50-60 µm. The average depths of wear track for samples sintered at 1050 and 1450 °C were about 10 and 20 µm, respectively (Fig. 8).

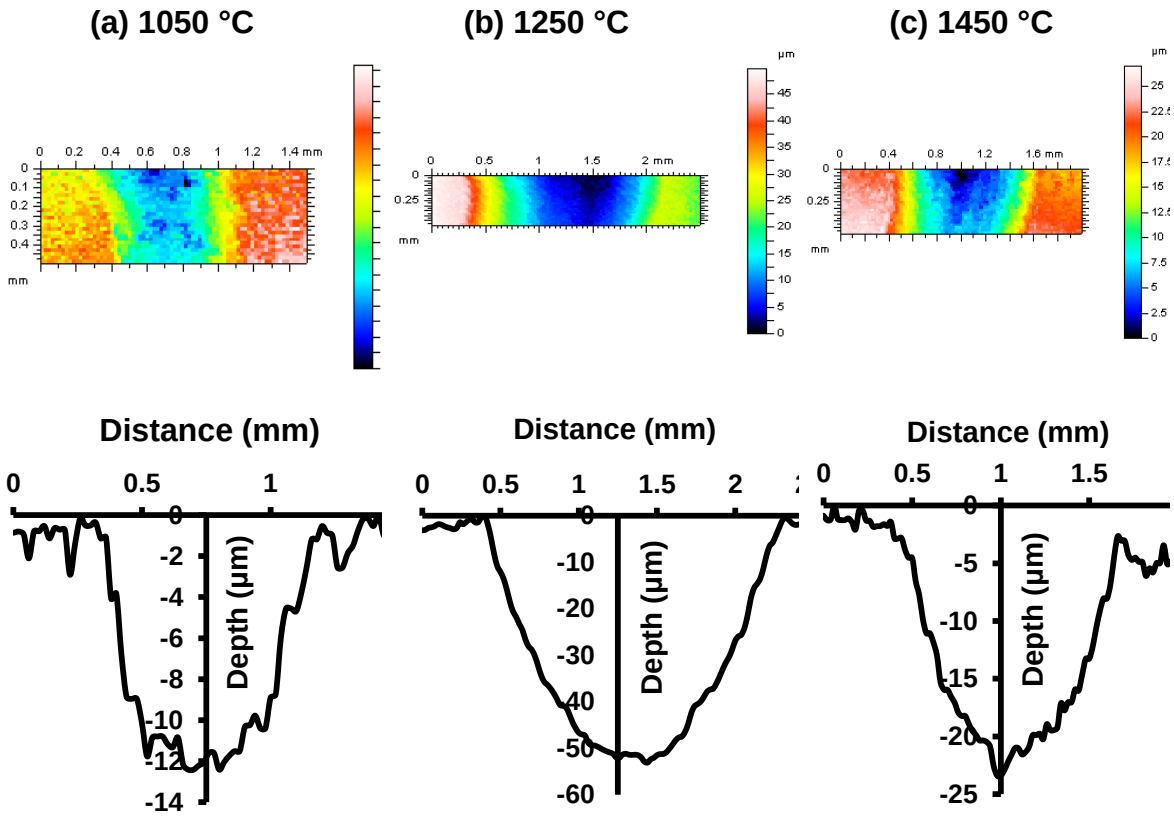

Figure 3.8 Depth profile across wear track for samples sintered at (a) 1050 °C (b) 1250 °C and (c) 1450 °C.

The wear loss over sliding time and the depth profile follows inverse relation between wear loss and corresponding hardness known as Archard's rule. The Response of samples sintered in 1050, 1250 and 1450 °C at 10 N loads as a function of sliding time is shown in fig. 3.9 (a, b, and c).

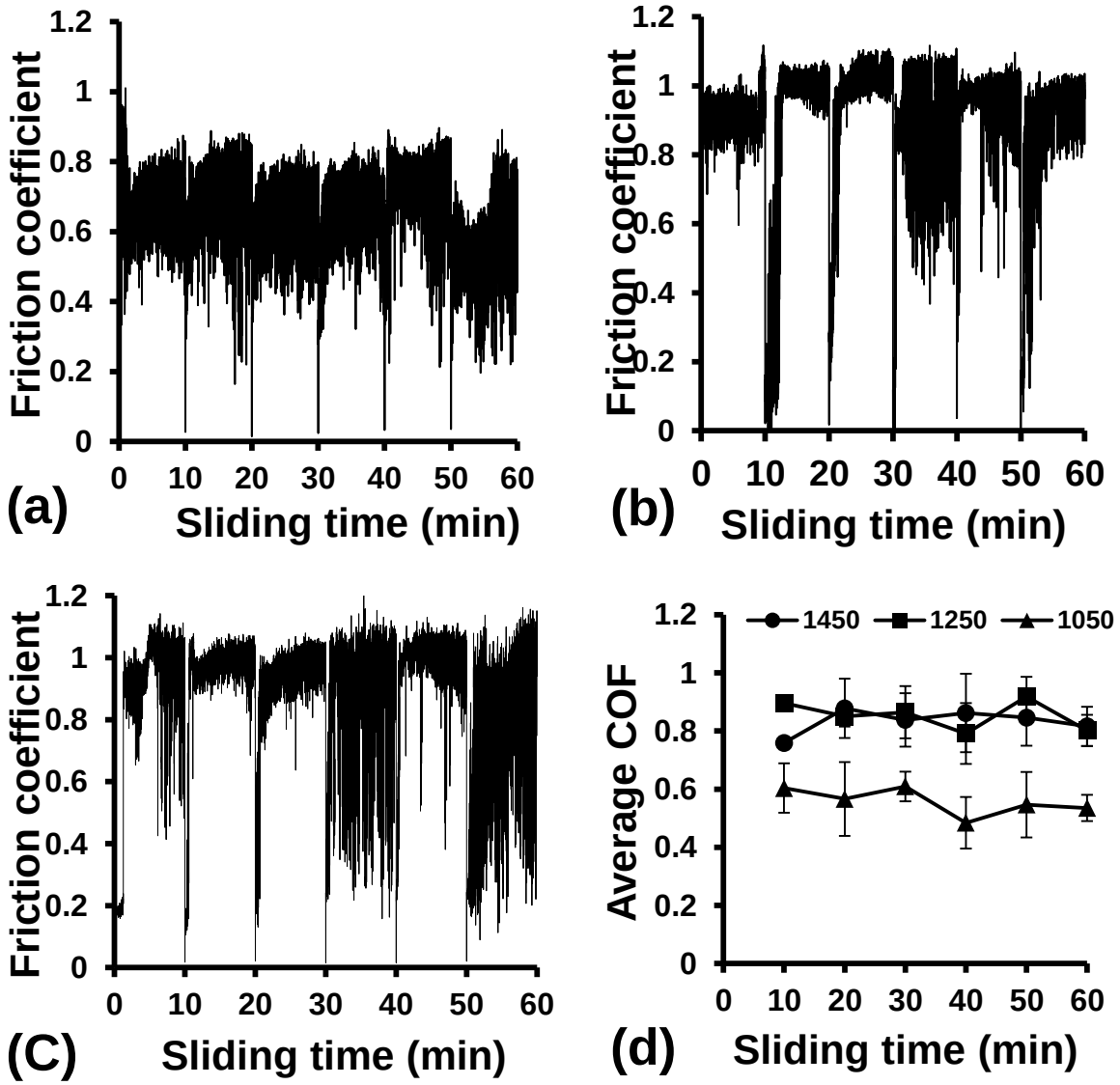

Fig 3.9 Friction coefficient as a function of sliding time for samples sintered at (a) 1050 °C (b) 1250 °C (c) 1450 °C (d) average friction coefficient for specimen sintered at 1050 °C, 1250 °C and 1450°C.

During first 10 min interval, the coefficient of friction increases rapidly and stabilizes to steady state value for each sample. Note that most of the wear weight loss was observed in the first 10 min interval of the wear test. The weight loss seems to initiate with the two-body abrasive wear mechanism in the first interval causing sudden increase in coefficient of friction. After this initial stage, the formed wear debris seems to cause three-body abrasive wear at the contacting surfaces for rest of the wear tests (all test intervals). The average coefficient of friction for the samples sintered at 1250 °C and 1450 °C was about 0.85 (fig. 3.9(d)). The average coefficient of friction was relatively lower (~0.6) for samples sintered at 1050 °C. This can be attributed to the very high amount (~51%) hard TiC phase in these samples.

The SEM micrographs of the worn out surfaces of SPS sintered samples are presented in fig. 3.10. The worn surface surfaces of the samples sintered at 1050 and 1450 °C were relative flatter (see for example, the elevated flatter region on left of Fig. 10(a) and on right of Fig. 10(c)) than those for samples sintered at 1250 °C. However, major cracks separate the elevated flatter surface features from rougher depressed regions covered with fine wear debris. The worn surface from the samples sintered at 1250 °C exhibited numerous flat elevated features and debris-filled depressed regions with micro-cracks leading to debris-filled regions. Ti_3SiC_2 has hexagonal layered structure where the layers are connected with metallic bonding which can't really resist against shear [141]. The lamellar structure of Ti_3SiC_2 makes it susceptible to grain breakup and detachment thus grains were easily decohered from the surface [142]. Grain buckling is common mode of failure for coarse grain structure. Because of the finer grains of Ti_3SiC_2, grain buckling was not observed on any of the SEM micrographs.

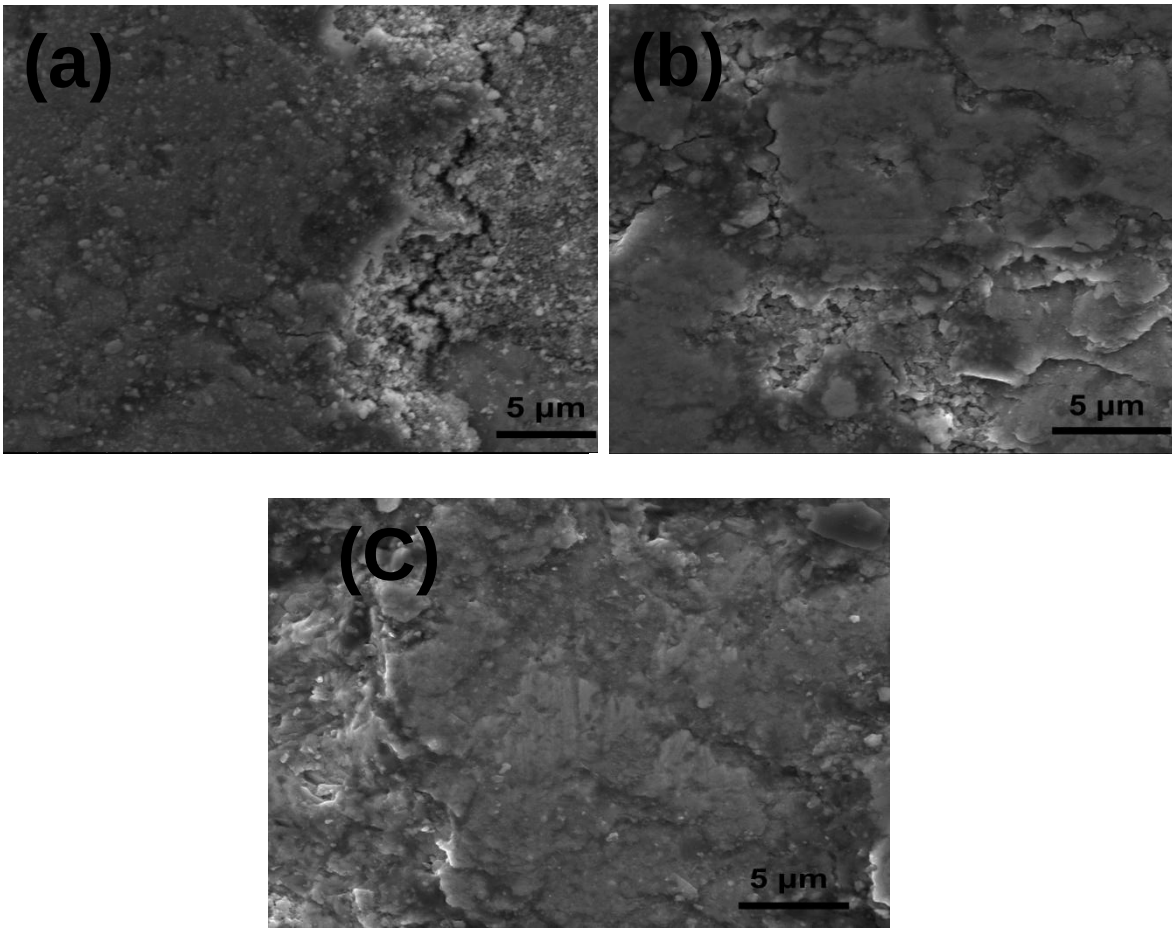

Fig. 3.10: SEM micrograph of the tribosurface for sample disk sintered at (a) 1050 °C (b) 1250 °C and (c) 1450 °C against alumina pin.

3.2 Ti_3SiC_2-TiC composites:

3.2.1 XRD analysis of powders and sintered Ti_3SiC_2 –TiC composites:

Fig 3.11 shows the x-ray diffractograms of starting powders in the 2θ range from 20° to 80° after 1 h of ball milling. The reflection of ball milled powders in all the compositions were indexed as TiC, Si and Ti peaks. The main peak was for TiC, from table 3, TiC was added in 59-72 wt.% on initial powders. The intensity of Ti and Si peaks were diminished from lower to higher percentage of TiC reinforcement added in the composites. From table 2.2, the content of Ti and Si decreased from 23.82 to 16.38 wt.% and 13.97 to 9.61 wt.%, respectively, for 0% to 30% of theoretical TiC reinforcement. Al peak did not appear in the spectrum after ball milling as the amount of Al was to less to detect. Any diffraction peaks of Ti-Si alloy was not found suggesting Si did not react with Ti at this milling condition.

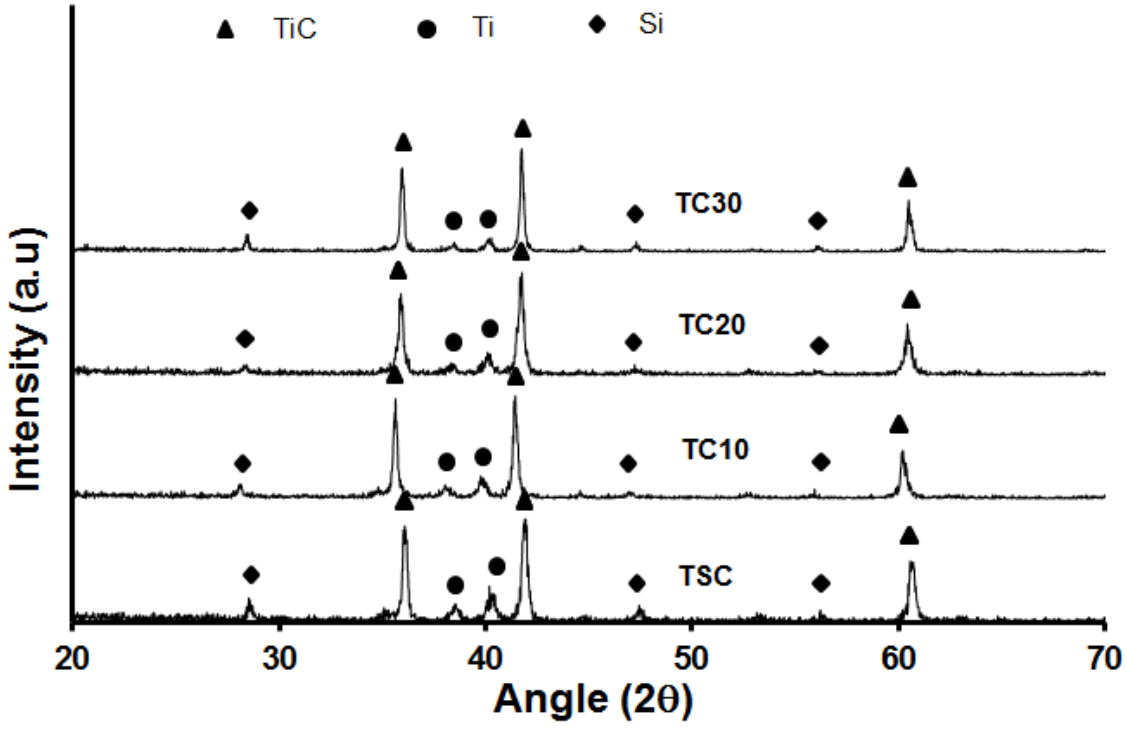

Fig. 3.11 XRD of mechanically milled powders of for 4 different compositions.

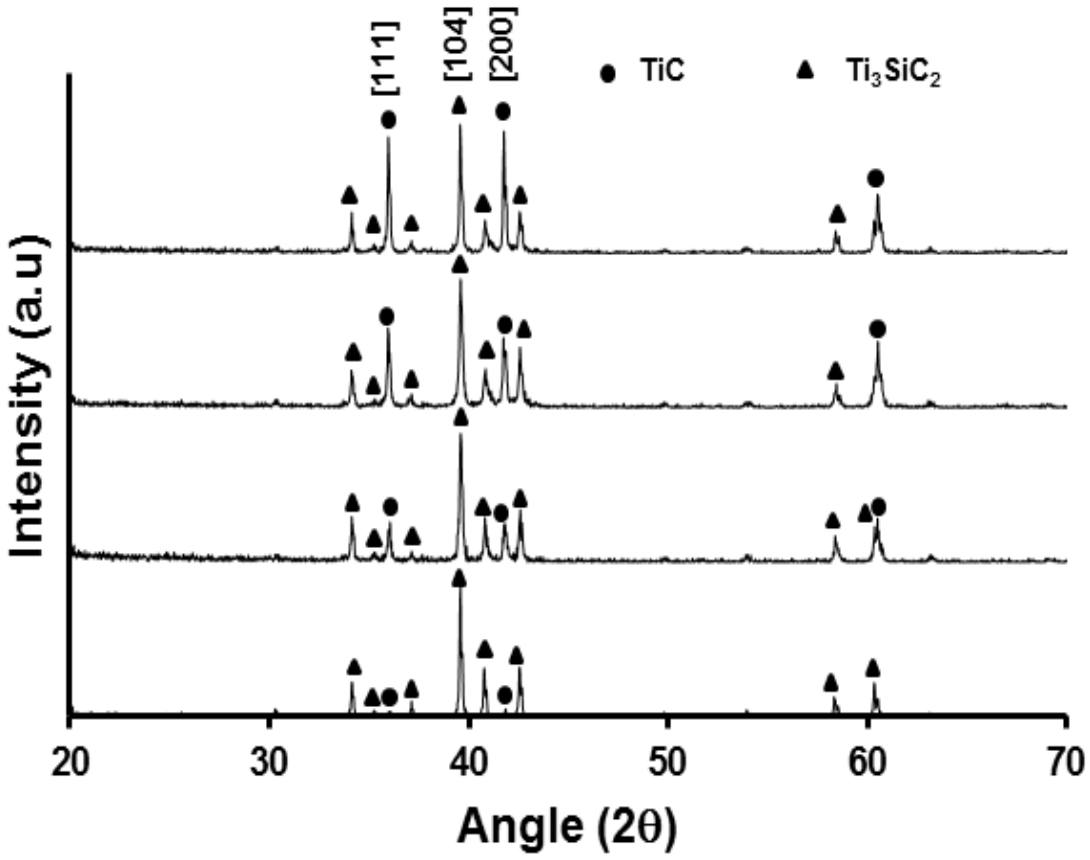

Fig. 3.12 XRD of samples sintered through SPS at 1250 °C for 15 min.

X-ray diffraction profiles of the samples sintered by SPS in the 2θ range from 30° to 70° are summarized in figure 3.12. Ti and Si peaks were disappeared after sintering suggesting complete reaction at these sintering parameters. As illustrated in figure 3.12, newly formed peaks of Ti_3SiC_2 were detected along with the peaks of TiC. Intermediate phases for example, Titanium silicide ($TiSi_2$ and Ti_5Si_3) were absent in all the bulk products. Only peaks of Ti_3SiC_2 and TiC were present indicating completion in the formation of Ti_3SiC_2 at the sintering temperature of 1250 °C. From figure 3.12 it should be noted that, peak from Ti_3SiC_2 (104) plane remains the main peak for all the sintered samples. Peaks of TiC from (111) and (200) plane became stronger with increasing TiC reinforcement in the composites. In case of TSC sample very minuscule peak

of TiC was detected wherein in TC30 sample, peak intensity of TiC has increased to nearly the same intensity of Ti_3SiC_2 peak.

In order to compare the phase composition of the obtained composites to the designed ones, TiC content (vol.%) of the composites based on XRD diffractograms were calculated. Quantitative phase analyses of the composites were done using calibrated standard additive method. Two different set of equations was developed for quantifications of the coexisting phases based on two different TiC peaks at (111) and (200) plane, respectively. Diffraction peaks of TiC (111) at 2θ = 35.89 ° and Ti_3SiC_2 (104) at 2θ = 39.548 ° were chosen as representative reflections by Zou et al. [118] and the equations are as follows.

$$W_{TiC} = \frac{I_{TiC}}{1.222 I_{Ti_3SiC_2} + I_{TiC}} \quad \ldots\ldots\ldots\ldots\ldots\ldots\ldots\ldots\ldots\ldots (3.7)$$

$$W_{Ti_3SiC_2} = \frac{I_{Ti_3SiC_2}}{I_{Ti_3SiC_2} + 0.818 I_{TiC}} \quad \ldots\ldots\ldots\ldots\ldots\ldots\ldots\ldots\ldots\ldots\ldots\ldots\ldots\ldots\ldots\ldots\ldots\ldots (3.8)$$

By employing these two equations wt.% of the phases were calculated. Volume content of TiC was calculated employing following equations taking $\rho_{TiC.}$ = 4.93 g/cm^3 and $\rho_{Ti_3SiC_2}$ = 4.53 g/cm^3.

$$V_{TiC} = \frac{W_{TiC} / \rho_{TiC}}{W_{TiC} / \rho_{TiC} + W_{Ti_3SiC_2} / \rho_{Ti_3SiC_2}} \quad \ldots\ldots\ldots\ldots\ldots\ldots\ldots\ldots\ldots\ldots\ldots\ldots\ldots\ldots\ldots\ldots\ldots\ldots (3.9)$$

Now by taking Diffraction peaks of TiC (2 0 0) at 2θ = 41.74 ° and Ti_3SiC_2 (104) at 2θ = 39.548 ° Relative Volume content of TiC on the samples were directly calculated by employing following equations developed by Zhang et al.[71].

$$V_{TiC} = \frac{I_{TiC} / I_{Ti_3SiC_2}}{1.95 + I_{TiC} / I_{Ti_3SiC_2}} \quad \ldots\ldots\ldots\ldots\ldots\ldots\ldots\ldots\ldots\ldots\ldots\ldots\ldots\ldots\ldots\ldots\ldots\ldots (3.10)$$

TiC amounts present on the sample were calculated by the above two methods are shown were shown in table 3.1 and compared with the theoretical one as shown on figure 3.13.

Table 3.1: Experimental volume fraction calculation of TiC from XRD data.

Sample	TSC	TC10	TC20	TC30
Theoretical	0	10	20	30
Intensity of TiC(111)	4.04	31.13	61.97	90.25
Intensity of TiC(200)	4.9	29.94	54.46	94.915
$I_{TiC(111)} / I_{TiC(200)}$	0.8973	1.03	1.08	0.95
Intensity of Ti_3SiC_2 (104)	100	100	100	100
Experimental Vol.% TiC(111)	2.96	19.02	30.79	40.515
Experimental Vol.% TiC(200)	2.25	13.31	21.83	32.74

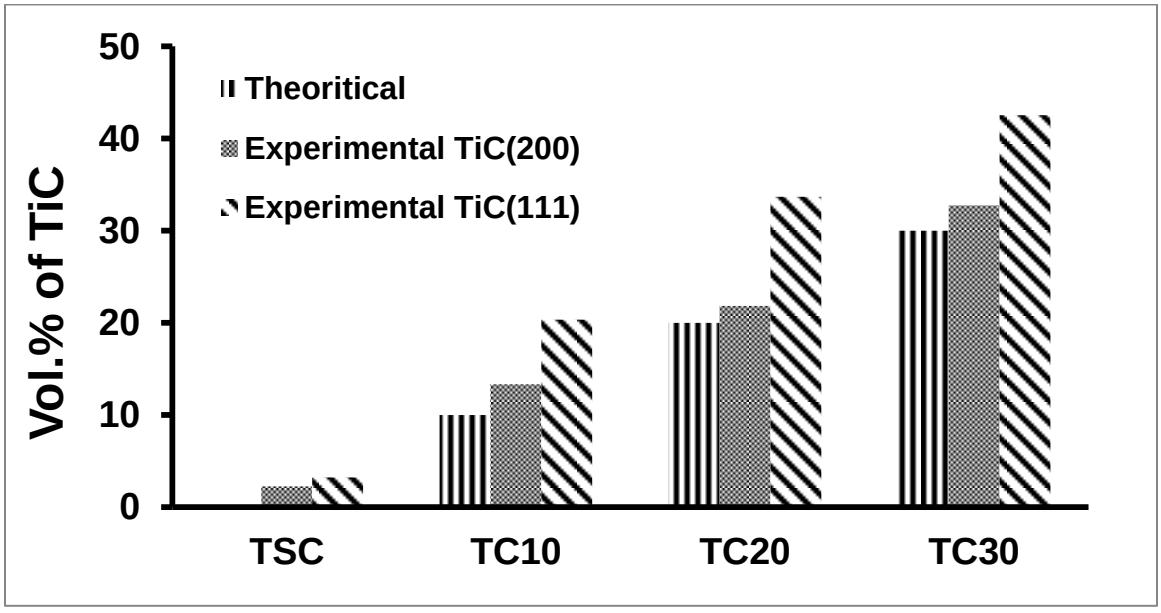

Fig. 3.13: Comparison between theoretical volume fraction and experimental calculated from Ti_3SiC_2 (104), TiC (200) and TiC (111) plane.

Figure 3.13 reveals that designed TiC content and the calculated one using TiC (200) plane reflection are quite close wherein TiC content calculated from (111) reflection always demonstrates nearly 10% higher than the theoretical values. According to JCPDS data the ratio between TiC (111) and TiC (200) peak intensity is 0.93. According to our data, (as shown on table 3.1) the ratio between the intensities of TiC at (111) and (200) plane were pretty close to the reference but calculated values from TiC (111) plane always demonstrated significantly higher TiC phase yield. This discrepancy has not yet been clearly understood and more future work is required on the calibration method for calculating relative percentage.

This result act as a confirmation that, formation of Ti_3SiC_2 was accomplished at the sintering temperature of 1250 °C for 15 min and phase composition of the obtained Ti_3SiC_2-TiC composite can be effectively controlled by adding excess TiC on the stoichiometric composition of Ti/Si/TiC. The sintering temperature and pressure used is this study is significantly lower than reported in the literature for HP process [104]. 30% (vol.) TiC- Ti_3SiC_2 composite was hot pressed from Ti-SiC powders above 1500 °C to obtain fully dense samples. This low temperature sinterablity of the powders is attributed to the combined effect of joule heating, higher heating rate, enhanced mass transfer rate in SPS process. Addition of Al also reduces the synthesis temperature of Ti_3SiC_2 and remove unwanted secondary TiC phase. Minor interfacial liquid phase was formed in presence Al because of the lower melting point (660°C), and this liquid phase favors diffusion of Ti and C atoms supplementing Ti_3SiC_2 formation. Additionally mechanically milled powders demonstrate high sintering activity, promoting low temperature sintering of Ti_3SiC_2 –TiC composites.

3.2.2 Relative density and microstructure:

Theoretical densities of the sintered samples were calculated employing rule of mixture from the densities of the phases present on the microstructure. The theoretical densities for Ti_3SiC_2 and TiC used for the calculation were 4.53 g/m^3 and 4.93 g/m^3, respectively (shown on table 3.2). Relative densities of the Ti_3SiC_2 –TiC composites sintered from different starting compositions are plotted in figure 3.14. The TSC sample (nearly single phase Ti_3SiC_2) has demonstrated best densification at this temperature with relative density of above 99%. The relative density of the composites got decreased with increase in TiC content and reduced to an amount of 95.86% for TC40 composite. Lower density could be attributed to the presence of large fraction of TiC on the green powders. Yang et al. [143] processed Ti_3SiC_2 from Ti-Si-TiC powder mixture and disclose the reaction route in the temperature range of 700-1200 °C. In this temperature range Ti_5Si_3 was found to be the only intermediate phase which forms from the reaction between Ti and Si and no change in intensities of the TiC peak was observed. Unaltered TiC requires higher sintering temperature for full densification. Teber et al. [144] reported SPS processing of TiC in the temperature range of 1350-1800 °C under 80 MPa for 5 min of dwell time. Structure with open porosities was observed at lower temperature (1350 °C) and pore size reduces with temperature increment. Fully dense sample with relative density of 99.4% was sintered at 1800 °C. In our case, sintering temperature and pressure employed is significantly lower in comparison and explains lower densities at higher TiC content composites. By increasing the sintering temperature full densification of the higher TiC contained composites could be achieved. From our previous result, Ti_3SiC_2 starts to decompose into TiC above 1300 °C which will result in higher TiC then designed in the composites. Thus, to effectively control obtained volume content of TiC on Ti_3SiC_2 –TiC composites, temperature was chosen to be 1250 °C. Lower sintering temperature will also ensure smaller grain size leading to better mechanical properties of the Ti_3SiC_2 –TiC composites.

Table 3.2 Relative densities of Ti_3SiC_2 –TiC composites:

Sample	Experimental Vol.%	Theoretical Density	Measured Density	Relative Density
TSC	1.91	4.54	4.51	99.39
TC10	13.31	4.58	4.503	98.25
TC20	21.83	4.62	4.471	96.83
TC30	32.74	4.66	4.468	95.86

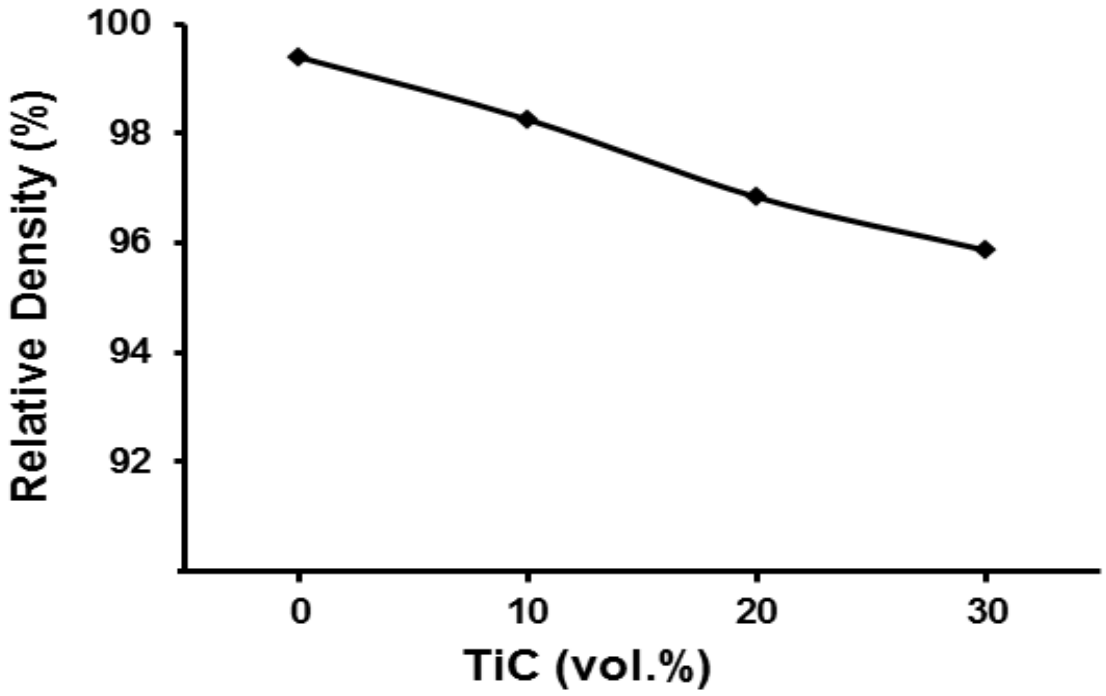

Fig. 3.14 Relative densities of the Ti_3SiC_2–TiC composites with different amount of TiC reinforcement.

The SEM microstructure of polished and etched surfaces of SPS sintered Ti_3SiC_2-TiC composites samples are illustrated in fig. 3.15. The micrographs indicate that three distinct phases with different grain sizes were present. EDS analysis was done to determine phases which indicates

plate shape grains as Ti_3SiC_2, comparatively bigger equiaxed grain as TiC and bright white circles as $Ti_3(Si_{1-x}Al_x)C_2$ solid solution.

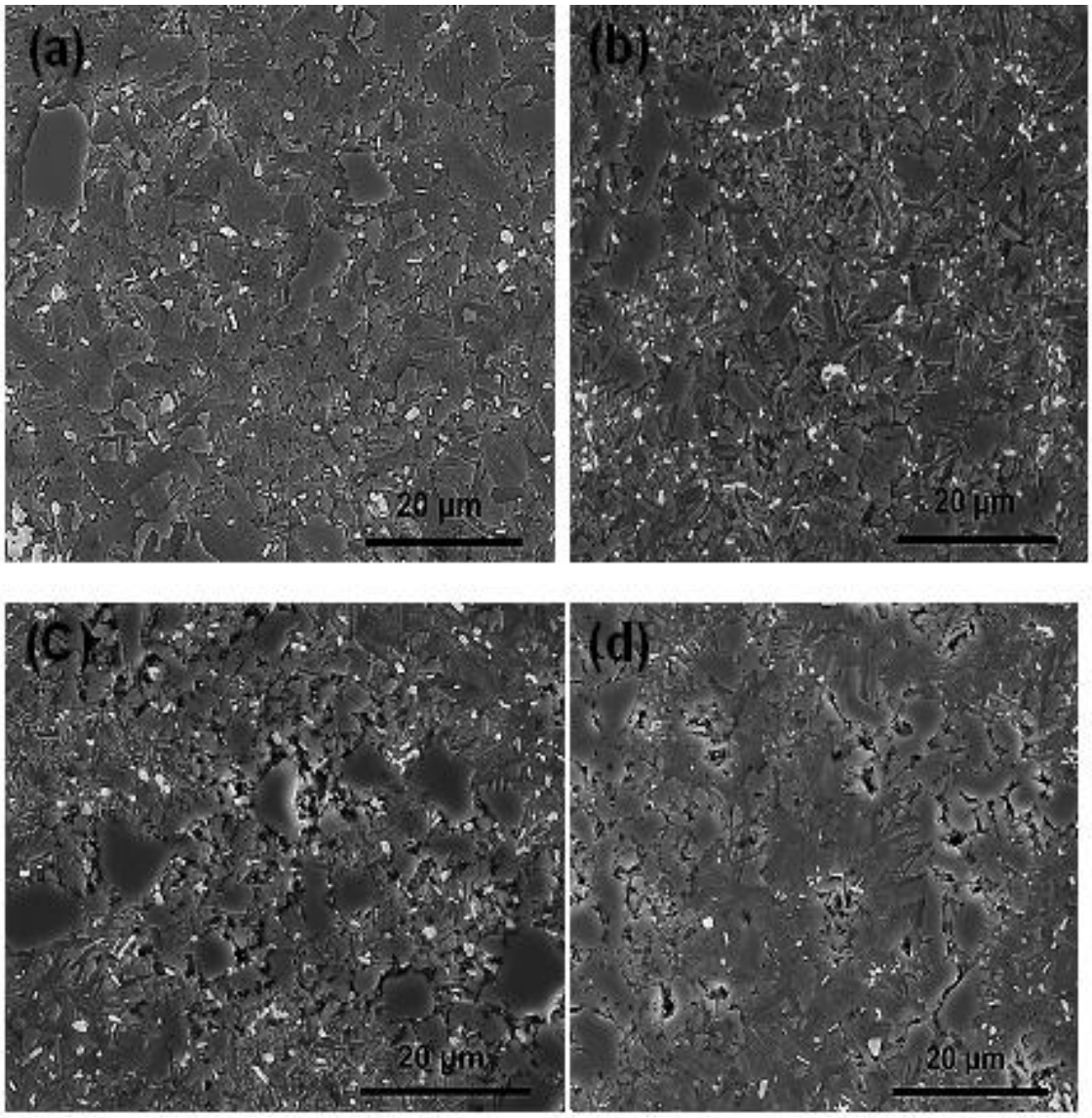

Figure 3.15: SEM microscopy images on the polished and etched surfaces of the sample (a) TSC (b) TC10 (c) TC20 (d) TC30

As we go from TSC to TC30 (0% vol.% to 30 vol.% of TiC) the grain size of Ti_3SiC_2 tends to decrease as presence of hard TiC inhibit coarsening of Ti_3SiC_2 grains. Distribution of the phases in the sintered composites was non-homogeneous and agglomeration of TiC grains was observed.

Comparing fig. 3.15 (b-d) TiC agglomeration has increased with increasing the volume content of TiC on the composites. Excess amount of TiC was added on the starting powder for the formation of Ti_3SiC_2-TiC composites. Yang et al. [143] demonstrated TiC on initial composition only reacts to form Ti_3SiC_2 and in absence of excess Si on the medium they will not be involved in any reaction. Because of that, increase in TiC content on green powders enhances TiC agglomeration in the microstructure. Another factor is the difference in particle size of the powders used in the experiment. Powder size of Ti (-325 mesh, 45 μm) was larger compared to silicon (1.5 μm) and TiC (2 μm). Because of their smaller particle sizes during the milling process agglomeration of mixtures took place enhancing non uniform morphology in the final microstructure. Tian et al. [145] **Error! Bookmark not defined.** sintered Ti_3SiC_2 –TiC composites from three different powder mixtures of Ti/Si/TiC, Ti/Si/C/TiC and Ti/Si/C and reported TiC agglomeration in the samples sintered from Ti/Si/TiC, Ti/Si/C/TiC. This result act as a confirmation that, use of TiC powder in starting material will lead to non-uniform distribution of phases in the sintered sample. The non-uniform morphology of Ti_3SiC_2-TiC composites will result in thermal stress development because of the thermal expansion mismatch between Ti_3SiC_2 and TiC; and will lower the strength of the composite.

EDS elemental maps from the sample with 0% theoretical volume content are presented on figure 3.16. The EDS employed was unable to detect C thus, only Ti, Si and Al mapping were done. From the mapping, Distribution of Ti and Si (fig. 3.16 (c) and (d)) are pretty uniform and deficiency in Si (black spots on fig. 16 (c)) represents TiC phase formation. Distribution of Al (fig. 6(b)) was not uniform and agglomeration of Al was observed on the mapping. These agglomerations of Al represented the corresponding bright white spots on the SEM micrographs. Points EDS of the spot (black spot on fig. 3.17) demonstrated presence of both Al and Si peak along with Ti, suggesting formation of $Ti_3(Si_{1-x}Al_x)C_2$ solid solution. In previous literature on Ti_3SiC_2 –TiC composites experimental volume fraction of TiC was found to be lower than

predicted from stoichiometric calculation which is quite unusual [106-146]. Formation of partial solid solution could explain this discrepancy between obtained and designed TiC content.

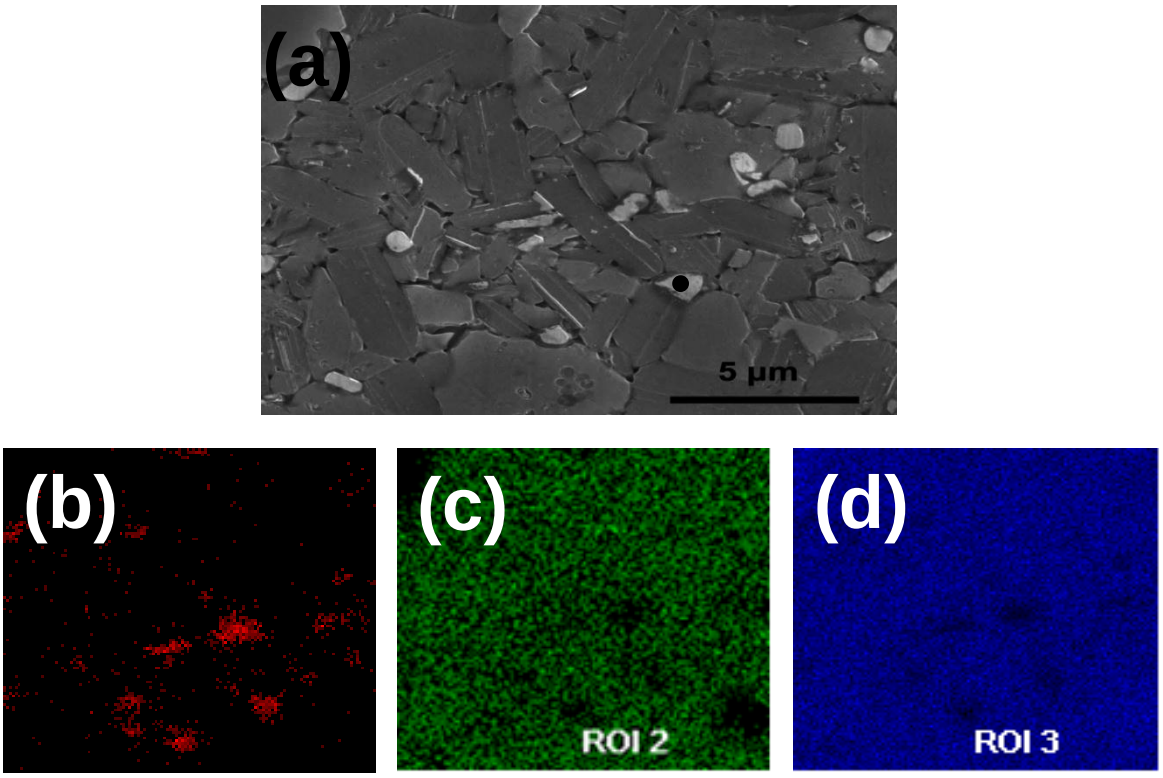

Fig. 3.16 (a) SEM micrograph and EDS mapping of (b) Al, (c) Si and (d) Ti on TSC.

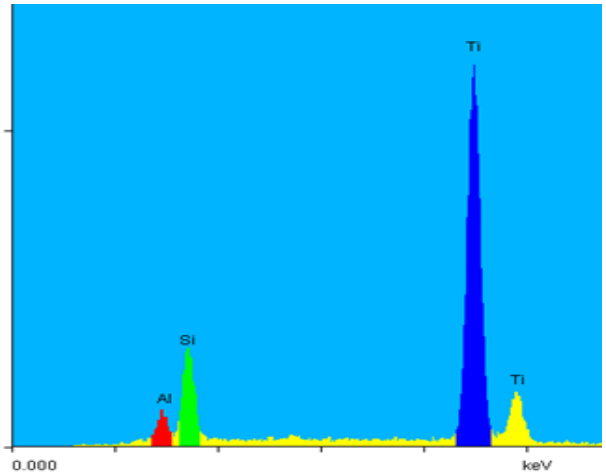

Fig. 3.17 Point Energy Dispersive Spectra (EDS) at bright white spot on TSC sample.

3.2.3 Vickers Hardness:

Vickers hardness of the processed composites were measured and plotted against volume fraction of TiC (figure. 3.17). Vickers hardness values for the composite have increased almost linearly with increasing TiC content (vol.%). TiC has nearly 6-7 times higher hardness than monolithic Ti_3SiC_2 and presence of hard TiC particles limit deformation and prohibit crack propagation in Ti_3SiC_2 –TiC composites. For nearly single phase Ti_3SiC_2 (sample TSC) microhardness was found to be 5.96 ± 0.19 Gpa which is higher to that of reported for monolithic Ti_3SiC_2 [139]. Raghy et al [89] reported indentation load effect on hardness and found that hardness values decrease with increasing load and attain asymptotic value above 100N. Thus, higher hardness values for TSC sample are associated with lower indentation load as in lower loads the indentation often confines into a single crystal measuring single crystal hardness instead of bulk. Maximum Vickers hardness of 9.32±0.37 GPa was observed in sample containing 30% (vol.) of TiC. Hardness values obtained in that study are consistent with previous work on TiC reinforced composites by Tian et al. [107, 146] and Ho-Duc et al. [103] but is lowered by nearly 2 GPa than reported by Zhang et al.[106].

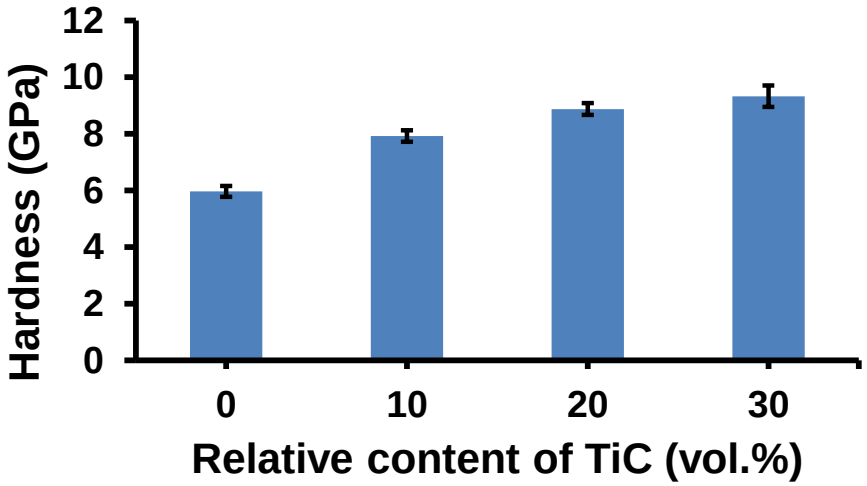

Fig. 3.18 Vickers hardness of Ti_3SiC_2 –TiC composites at different TiC content.

It should be noted from figure 3.18 that standard deviation in the measured hardness values for TC30 sample (~0.37 GPa) is higher compared to other 3 samples (~0.2 GPa). From microstructure (fig. 3.15(d)) larger TiC agglomeration was coexisted with Ti_3SiC_2 in TC30 sample. Because of the lower indentation load and TiC agglomeration, indents centered into a region (Ti_3SiC_2 or TiC) confined into that area and measured values are reflections of the hardness of that particular phase instead of the whole composite. This phenomenon explains high scatter values in the samples with higher TiC agglomeration.

Increase in Vickers hardness at different TiC volume fraction (V_f) follows linearity (as shown in fig. 3.19). Least square fit of the obtained results is expressed in following formula.

$$\text{VHN (GPa)} = 6.3643 + 0.1104\ V_f \qquad R^2 = 0.9133$$

This relationship is only valid for Ti_3SiC_2 –TiC composites from 0% to 30% TiC reinforcement and indentation load of 9.8 N.

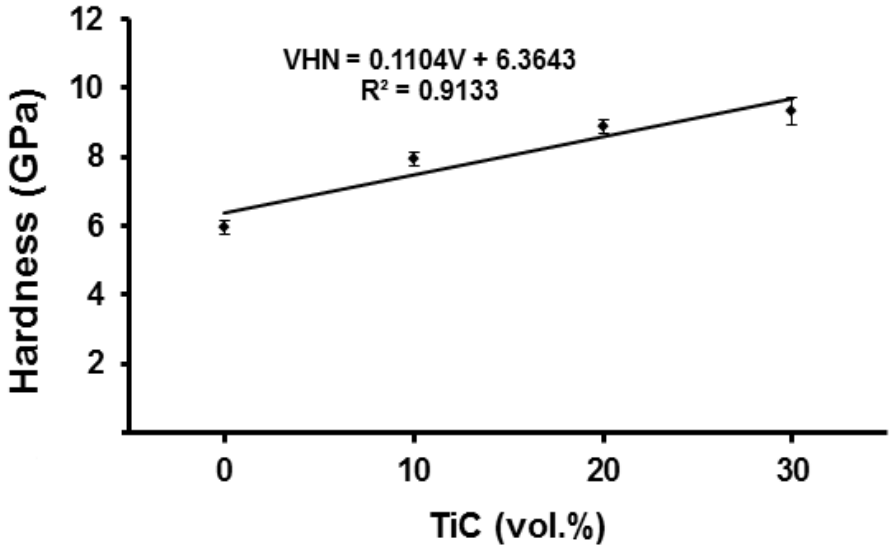

Fig. 3.19 Vickers hardness of Ti_3SiC_2 –TiC composites vs. TiC volume content.

3.2.4 Tribological Characterization of Composites:

The accumulative wear loss as function of sliding time during ball-on-disc wear test for composites sintered at 1250 °C are recorded on fig. 3.20. TSC Samples demonstrated maximum weight loss and from quantitative analysis TSC contains nearly 98% of Ti_3SiC_2. Wear loss significantly decreases in Ti_3SiC_2–TiC composites containing 10-30 (vol.%) of TiC content (fig. 3. 20) suggesting wear resistance is greatly enhanced by incorporating TiC particles into Ti_3SiC_2 matrix. Area and depth profiles across the wear track are presented on figure 3.21 and 3.22 respectively. Average width and depth of the wear track in TSC sample was maximum (1.5 mm and 38 μm, respectively); wherein, TC10 sample demonstrated minimum wear loss with width of 1.25 mm and depth of 10 μm. Wear depth in the TC20 and TC30 sample lies in between which were 18 μm and 30 μm respectively.

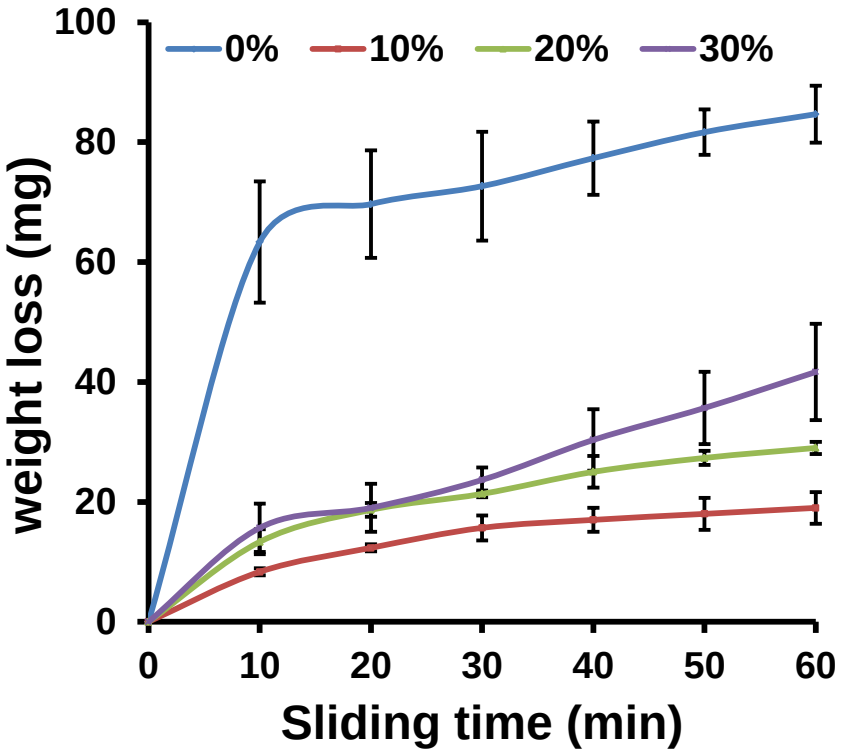

Fig. 3.20 Cumulative weight loss against sliding time for Ti_3SiC_2–TiC composites.

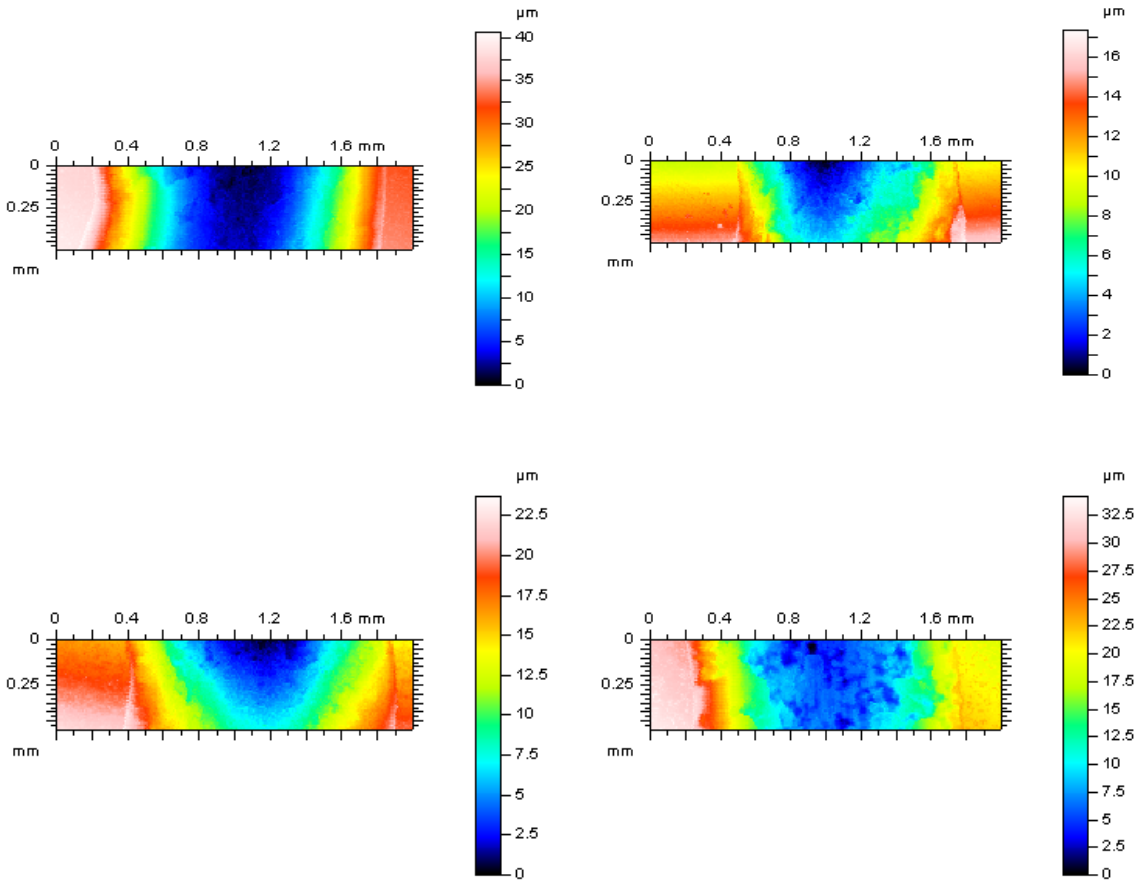

Fig. 3.21 Area Profile across the wear track of the composites (a) TSC, (b) TC10, (c) TC20 and (d) TC30.

SEM micrographs of the worn surface for TSC sample, exhibited grain fracture, pull out and detachment because of the low hardness of Ti_3SiC_2 resulting rough worn surface related to higher coefficient of friction and wear loss (fig. 3.23 (a) and (b)). Wan et al. [146] showed the pulled particles were adhered to the counterpart surface suggesting adhesive wear as the active wear mechanism on TSC sample. Hardness of the soft Ti_3SiC_2 has increased by addition of TiC (fig. 3.18). Hard TiC particles will endure the scrapping effect on the composite and will effectively reduce the effective load on the soft matrix by acting as load bearing components. Because of that, adhesive wear mechanism between Ti_3SiC_2 and counterpart transforms into abrasive wear in

case of Ti_3SiC_2/TiC composites. Improved wear resistance was also reported in case of Ti_3SiC_2/SiC [146], Ti_3SiC_2/(TiC+TiB_2) [147], and Ti_3SiC_2/Al_2O_3 [148] composites by the same mechanism. Hu et al. [148] demonstrated by FEM analysis that Presence of hard reinforcing particle (Al_2O_3) can effectively decentralize the shear stress under the counterpart and improve wear resistance of the composites. Thus by inhibiting plastic deformation, decreasing normal load on soft matrix and decentralizing shear stress under sliding ball, TiC particles improve the wear resistance of Ti_3SiC_2 matrix.

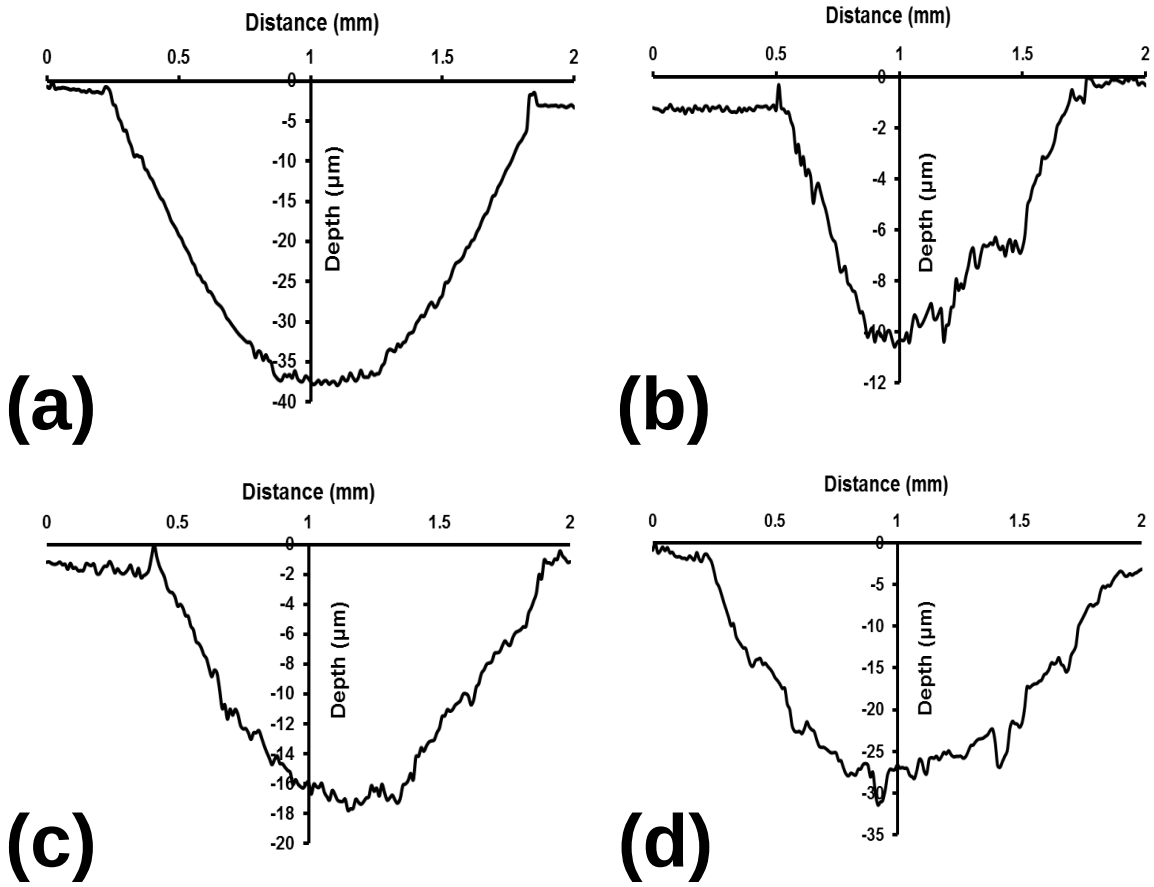

Fig. 3.22: Depth Profile across the wear track of the composites (a) TSC, (b) TC10, (c) TC20 and (d) TC30

In case of SiC [146] and Al_2O_3 [148] reinforcement wear loss of the composites decrease with increased amount of reinforcement. But In this study, the wear resistance of the composites did not increase monotonically with increase in amount of TiC reinforcement. Minimum wear loss was observed in 10% TiC reinforced sample (TC10) and it increases with increasing TiC reinforcement; wherein, TC40 demonstrated minimum wear resistance. The causation could be traced to the higher reinforcement-matrix interfacial area. This interfacial area is the weakest point to start crack and resultantly grains can be easily pulled out by the counterpart. Similar behavior was reported in SiC reinforced magnesium where after reaching a certain amount of reinforcement the wear resistance started to decrease [149]. The other determining factor in the wear mechanism of the composites is the homogenous distribution of reinforcing particles. Vencl et al. reported microstructure with uniformly dispersed relatively smaller grain size particles results in maximum wear resistance in Ti-Si alloy [150]. Thus presence of clustered TiC on the microstructure had degrading effect on improving wear resistance of the material [149, 151]. From the SEM microscope images (fig. 3.15) with increasing TiC volume content, non-uniformity in the microstructure with bigger TiC clusters arises. Thus, higher interfacial area between matrix and reinforcing particle and enhancement in non-homogeneity in the microstructure explains degradation in wear resistance at higher (vol.%) of TiC (20% and 30%).

The variation of friction coefficient of the Ti_3SiC_2–TiC composites at 10 N load against Si_3N_4 as a function of sliding time is shown in figure 3.23. For all the samples, μ was found to be 0.2 at the initial stage of the sliding and this stage was followed by a second stage where μ abruptly increased to 0.5~0.7. At the initial stage of sliding because of the smooth surface of the sliding sample low COF was obtained. After initial stage removal of the surface materials started and formed debris entrapped between the contact surfaces caused third body abrasion which was two body abrasions at the beginning. Real contact area between ball and sliding surfaces increases because of that third body abrasion hence, the coefficient of friction [140].

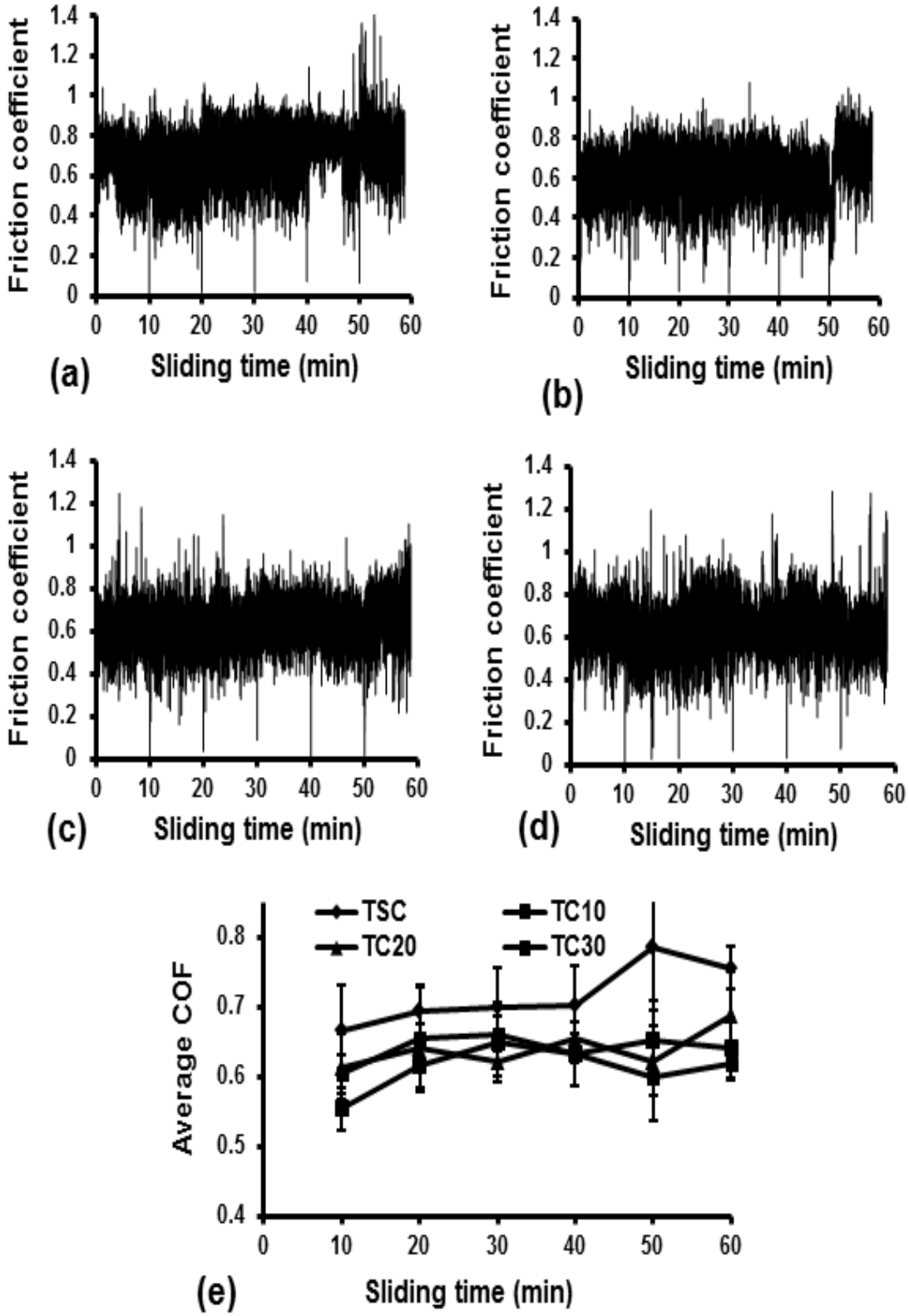

Fig. 3.23 Friction coefficient vs. sliding time (a)TSC (b)TC10 (c) TC20 (d) TC30 (e) Avg. COF.

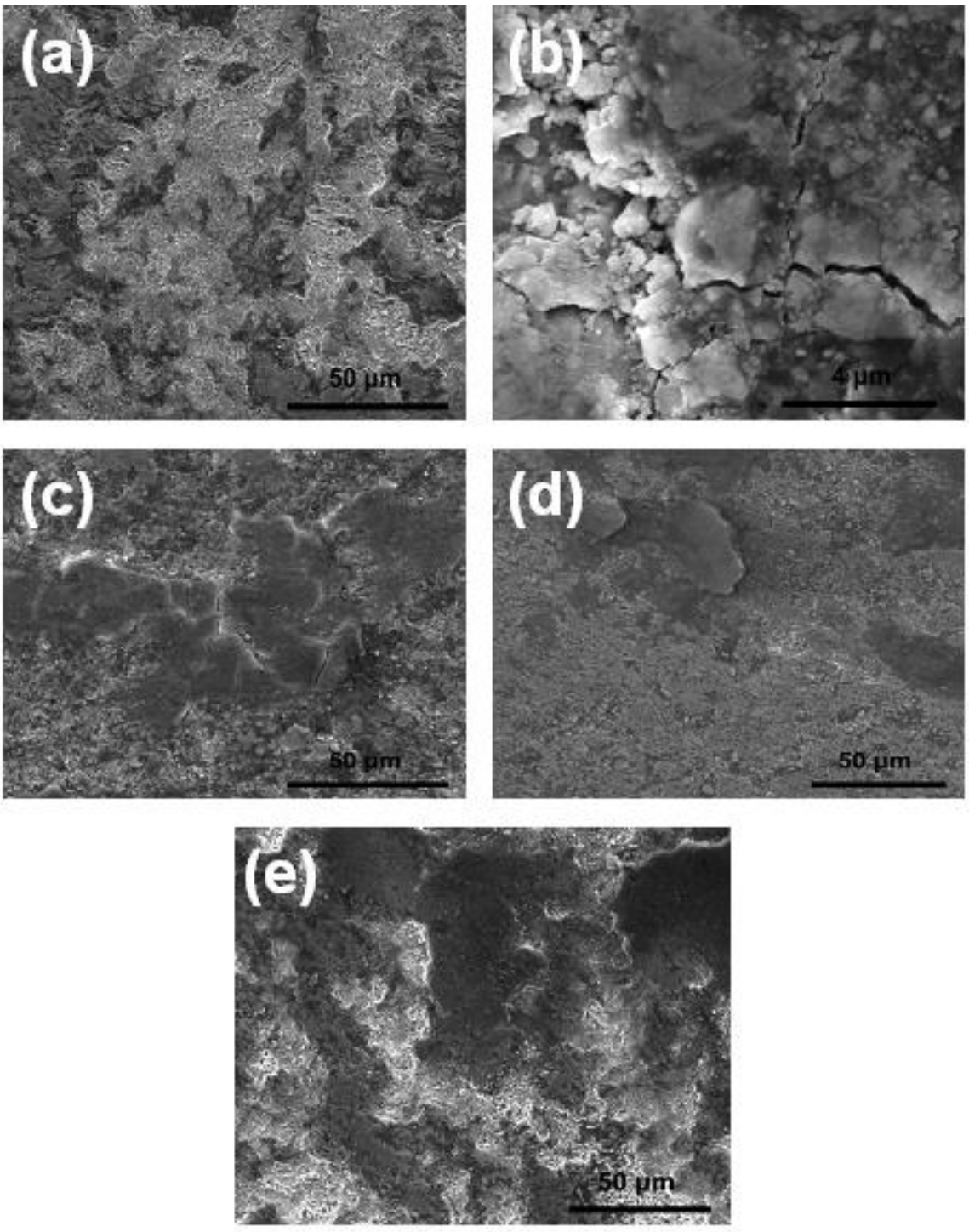

Fig. 3.24 SEM micrographs of the worn tracks of TSC ((a) low magnification and (b) high magnification), (c) TC10, (d) TC20 and (e) TC30 tested under load of 10N for 60 min.

From the plot of average friction coefficient against sliding time (fig 3.23(e)), COF for TSC sample was in the range of 0.7~0.75. TC composites (TC10, TC20 and TC30) represent lower COF compared to TSC and COF was kept at 0.6-0.65 range. Addition of hard TiC particles decrease accumulative strain and strain energy and decentralize shear stress at the contact point resultantly, low COF were observed in case of Ti_3SiC_2/TiC composites.

SEM micrographs of the worn surfaces of Ti_3SiC_2 and Ti_3SiC_2-TiC composites are shown in fig. 3.24. For TSC (fig. 3.24(a) and (b)), irregular worn surface with severely fractured and pulled out grains along with micro-cracks was observed. Metallic bonding between the layers of Ti_3SiC_2 are really weak against shear and this weak metallic bonding along with weak grain boundaries leads to easy pullout of the grains in Ti_3SiC_2 [141, 142]. For Ti_3SiC_2/TiC composites relatively flatter extruded surface was formed on the worn tracks. Similar wear tracks pattern was observed in SiC reinforced Ti_3SiC_2 composites and was attributed to the presence of hard SiC particles which resist the deformation of soft Ti_3SiC_2 matrix by forming extruded flat regions [146].

CHAPTER IV

CONCLUSION

Nearly single phase dense Ti_3SiC_2 was consolidated *in-situ* from 3Ti/SiC/C/0.15Al powder mixture using spark plasma sintering at 1250 °C. At lower sintering temperatures, formation of intermediate phases TiC and Ti_5Si_3 was observed. The formation of Ti_3SiC_2 seems to initiate after complete constitution of intermediate phases. The stability of Ti_3SiC_2 decreases in presence of surrounding carbon medium at temperature above 1300 °C leading to decomposition of Ti_3SiC_2, forming auxiliary TiC phase. The starting powder compositions (2Ti/SiC/TiC and Ti/Si/2TiC) with higher amount of TiC (one of the intermediate phases) lead to Ti_3SiC_2 formation at lower temperature compared to that with conventional 3Ti/SiC/C powder composition. The samples with higher percentage of TiC, both as an intermediate phase or the product of Ti_3SiC_2 decomposition, exhibited higher microhardness and better wear resistance compared to near single phase Ti_3SiC_2.

Ti_3SiC_2-TiC composites with TiC volume content varying from 0 to 30% have been successfully processed through SPS from different composition of TiC/Si/Ti/Al powder mixture at 1250 °C and 50 MPa of pressure. From XRD analysis the experimental volume fraction of TiC was found to be close to the theoretical one and density of synthesized sample decreases at higher vol.% of TiC. SEM micrographs showed TiC agglomeration on the microstructure and attributed to the use of TiC in the initial powders. Hardness of the composites increased with TiC addition and

maximum hardness of 9.32±0.37 GPa was demonstrated by TC30 sample. Wear loss and friction coefficient of the composites decreases with addition of TiC among which TC10 showed best wear resistance characteristic. Inhomogeneous microstructure, higher matrix reinforcement interfacial area and porosity leads to increase in wear loss on samples containing higher TiC reinforcement.

CHAPTER V

FUTURE WORK

- Detailed study of the mechanical behavior of Ti_3SiC_2 based composites.
- Perform high temperature tribological characterization of monolithic Ti_3SiC_2 and Ti_3SiC_2-TiC composites.
- Conduct Oxidation behavior of monolithic Ti_3SiC_2 and their composites at higher temperature.
- Processing of Ti_3SiC_2 coatings for high temperature application through SPS.
- Study synthesis of Ti_3SiC_2 based solid solutions.
- Investigate bonding of ceramic materials using Ti_3SiC_2 as binder.
- Corrosion resistance of Ti_3SiC_2 and TiC/SiC/Al_2O_3 reinforced composites.

REFERENCES

[1] M. W. Barsoum and T. El-Raghy, "The MAX Phases: Unique new Carbide and Nitride Materials", Am. Sci., (2001) 89 [4] 334–343.

[2] W. Jeitschko, H. Nowotny, and F. Benesovsky, "Carbides of Formula Ti_2MC", Journal of the Less-Common Metals, (1964) 7 133-138.

[3] H. Nowotny, "Struktuchemie Einiger Verbindungen der Ubergangsmetalle mit den elementen C, Si, Ge, Sn.", Prog. Solid St. Chem., (1970) 2.

[4] M. W. Barsoum and T. ElRaghy, "Synthesis and Characterization of a Remarkable Ceramic: Ti_3SiC_2", J. Am. Ceram. Soc., (1996) 79 [7] 1953–1956.

[5] M. W. Barsoum, "The MN+1AXN Phases: A New Class of Solids; Thermodynamically Stable Nanolaminates", Prog. Solid State Chem., (2000) 28 [1–4] 201–281.

[6] M. W. Barsoum, M. C. Flemings, E. J. Kramer, S. Mahajan, Veyssiere "P. Physical properties of the MAX phases.", In: Encyclopedia of materials science and technology; (2006).

[7] M.W. Barsoum, D. Brodkin and T. El-Raghy, "Layered machinable ceramics for high temperature applications", Scripta Met Mater (1997) 36 535.

[8] M.W. Barsoum and T. El-Raghy, "Room temperature ductile carbides", Metall Mater Trans (1999) 30A, p. 363.

[9] JP Palmquist, S Li, POA Persson, J Emmerlich, O Wilhelmsson, H Högberg, MI Katsnelson, B Johansson, R Ahuja, O Eriksson, L Hultman and U Jansson: "$M_{n+1}AX_n$ phases in the Ti-Si-C system studied by thin-film synthesis and ab initio calculations " Phys. Rev. B, 2004, 70B, 165401.

[10] Z. J. Lin, MJ Zhuo, YC Zhou, MS Li and JY Wang: "Microstructures and Theoretical Bulk Modulus of Layered Ternary Tantalum Aluminum Carbides" J. Am. Ceram. Soc., 2006, 89, 3765–3769.

[11] J Zhang, B Liu, JY Wang and YC Zhou: "Low temperature instability of Ti2SnC: a combined TEM, DSC and XRD investigations"J. Mater. Res., 2009, 24, 39–49.

[12] W. Jeitschko, H. Nowotny and F. Benesovsky: "Die Kristallstruktur von Ti_3SiC_2—ein neuer Komplexcarbid-Typ "Mon-tash. fur Chem., 1967, 98, 329.

[13] Y.C. Zhou and Z.M. Sun: "Crystallographic relations between Ti_3SiC_2 and TiC" Mater. Res. Innovat., 2000, 3, 286.

[14] Y. Zhou and Z. Sun, ''Electronic Structure and Bonding Properties in Layered Ternary Carbide Ti_3SiC_2,'' J. Phys. Cond. Matter, 12, 457–62 (2000).

[15] M. W. Barsoum, T. El-Raghy, C. J. Rawn, W. D. Porter, H. Wang, E. A. Payzant, and C. R. Hubbard (unpublished)

[16] AmerM, Barsoum MW, El-Raghy T,Weiss I, LeClair S, Liptak D. 1998. Raman spectrum of Ti_3SiC_2. J. Appl. Phys. 84:5817–19

[17] Radovic M, Ganguly A, Barsoum MW, Zhen T, Finkel P, et al. 2006. On the elastic properties and mechanical damping of Ti_3SiC_2, Ti_3GeC_2, $Ti3Si_{0.5}Al_{0.5}C_2$ and Ti_2AlC in the 300–1573 K temperature range. Acta Mater. 54:2757–67

[18] Onodera A, Hirano H, Yuasa T, Gao NF,Miyamoto Y. 1999. Static compression of Ti_3SiC_2 to 61 GPa. Appl. Phys. Lett. 74:3782–84

[19] P. Finkel, M.W. Bawsoum and T.El-Raghy, "Low temperature dependence of the elastic properties of Ti_3SiC_2," J. Appl. Phys., 1999, 85, 7123.

[20] Y.C. Zhou and Z.M. Sun, "Micros scale plastic deformation of ploycrystallune Ti_3SiC_2 under room temperature compression", J. Eur. Ceram. Soc., 2001, 21, 1007.

[21] M.W. Barsoum, T. El-Raghy, C.J. Rawn, W.D. Porter, A. Payzant and C.Hubbard, ""Thermal Properties of Ti_3SiC_2" J. Phys. Chem.Solids., 1999, 60, 429.

[22] Barsoum MW, El-Raghy T. Room temperature ductile carbides. Met Mat Trans A 1999;30A:363. [23] Farber L, Levin I, Barsoum MW. HRTEM study of low angle boundary in plastically deformed Ti_3SiC_2. Phil Mag Lett 1999;79:4103.

[24] Barsoum MW, Farber L, El-Raghy T. Dislocations, kink bands and room temperature plasticity of Ti_3SiC_2. Met Mat Trans 1999;30A:1727.

[25] Barsoum MW, Radovic M, Finkel P, El-Raghy T. Ti_3SiC_2 and Ice. Appl Phys Lettrs 2001;79:479.

[26] El-Raghy, T., Zavaliangos, A., Barsoum, M. W. & Kalidindi, S. R. Damage Mechanisms Around Hardness Indentations in Ti_3SiC_2. J. Am. Ceram. Soc. 80, 513-516 (1997).

[27] A. Murugaiah, M.W. Barsoum, S.R. Kalidindi, and T. Zhen, "Spherical nanoindentations and kink bands in Ti_3SiC_2" J. Mater. Res., Vol. 19, No. 4, Apr 2004

[28] S. Basu, A Zhou, M. W. Barsoum, "On spherical nanoindentations, kinking nonlinear elasticity of mica single crystals and their geological implications" J. of Structural Geology, Volume 31, Issue 8, (2009), 791-801

[29] M.W. Barsoum, T. Zhen, S. Kalidindi, M. Radovic, and A. Murugaiah, Fully reversible dislocation-based compression deformation of Ti3SiC2 to 1 GPa, Nat. Mater. 2, 107 (2003).

[30] T. Goto and T. Hirai,., Chemically Vapor Deposited Ti_3SiC_2, Mat. Res. Bull 1987:22; 2295.

[31] J. Nickl, K. K. Schweitzer & P. Luxenberg, J. Less Common Metals, 1972:26;283.

[32] Barsoum MW, El-Raghy T, Rawn CJ, Porter W D, Wang H, Payzant E A and Hubbard C R, "Thermal properties of Ti_3SiC_2" J. Phys. and Chem. of Solids. 1999:60;429.

[33] A. M. Cruise, “principles of space instrument design”, (Cambridge university press, Cambridge, 1998).

[34] Suilin Shi, Lingzhen Zhang, and Junshou Li, “Ti_3SiC_2 material: An application for electromagnetic interference shielding” Appl. Phys. Lett. 93, 172903 (2008).

[35] M. Utili, M Agostini, G. Coccoluto, E. Lorenzini, “Ti_3SiC_2 as a candidate material for lead cooled fast reactor”, Nuclear Engineering and Design (2010),

[36] E. N. Hoffman, D. W. Vinson, R. L. Sindelar, D. J. Tallman, G. Kohse, M. W. Barsoum, “MAX phase carbides and nitrides: properties for future nuclear power plant in-core application and neutron transmutation analysis”, Nuclear Engineering and Design 244 (2012) 17-24.

[37] J. J. Nickl, K.K. Schweitzer, and P. Luxenberg, Gaphasenabscheidung im Systeme Ti-C-Si. J. Less Common Metals”, (1972) 26.

[38] C. Racault, F. Langlais, and R. Naslain, “Solid-state synthesis and characterization of the ternary phase Ti_3SiC_2”, J. Mater. Sci. , (1994) 29 3384.

[39] J. Emmerlich, H. Hogberg, S. Sasvari, P. O. A. Persson, L. Hultman, J. P. Palmquist,, U. Jansson, J.M. Molina-Aldareguia, and Z. Czigany, “Growth of Ti_3SiC_2 thin films by elemental target magnetron sputtering.”, J. Appl. Phys., 2004. 96[9] 4817.

[40] H. Hogberg, L. Hultman, J. Emmerlich, T. Joelsson, P. Eklund, J. M. Molina-Aldareguia, J. P. Palmquist, O. Wilhelmsson, and U. Jansson, “Growth and characterization of MAX-phase thin films.”, Surf. Coat. Tech., (2005) 193 [1-3] 6.

[41] S. Arunajatesan, and A. H. Carim, “Synthesis of Titanium Silicon Carbide.”, J. Am. Ceram. Soc., 1995. 78[3] 667.

[42] J. Lis, and R. Pampuch, “Reaction sintering phenomena of self-propagating hightemperature synthesis-derived ceramic powders in the Ti-Si-C system.”, Solid State Ionics, 1997. 101-103 [1-2] 59.

[43] J. J. Hu, Bultman, J.E., Patton, S., and Zabinski, J.S., "Pulsed Laser Deposition and Properties of Mn+1AXn Phase Formulated Ti_3SiC_2 Thin Films", Tribology Lett., 2004. 16 [1-2] 113.

[44] S. B. Li,, and H.X. Zhai,, "Synthesis and Reaction Mechanism of Ti_3SiC_2 by Mechanical Alloying of Elemental Ti, Si and C Powders.", J. Am. Ceram. Soc.,. (2005) 88 [8] 2092-2098.

[45] S. B. Li, Zhai, H.X., Zhou, Y., and Zhang, Z.L., "Synthesis of Ti_3SiC_2 powders by mechanically activated sintering of elemental powders of Ti, Si and C.", Mater. Sci. Eng. A, 2005. 407 [1-2] 315.

[46] J. F. Li, T. Matsuki, and R. Watanabe, "Combustion Reaction During Mechanical Alloying Synthesis of Ti_3SiC_2 Ceramics from 3Ti/Si/2C Powder Mixture.", J. Am. Ceram. Soc., 2005. 88(5) 1318.

[47] J. Lis, Y. Miyamoto, R. Pampuch, and K. Tanihata, "Ti_3SiC_2-based Materials Prepared by HIP-SHS Techniques", Mater. Lett., (1995) 22 [3–4] 163–168.

[48] M. W. Barsoum, G. Yaroschuk, S. Tyagi, "Fabrication and Characterization of M_2SnC (M=Ti, Zr,Hf and Nb).", Scripta Materialia. (1997) 37 [10] 1583.

[49] A. T. Procopio, T. El-Raghy and M. W. Barsoum, "Synthesis of Ti_4AlN_3 and phase equilibria in the Ti-Al-N system.", Met. Mat. Trans. A, (2000) 31 [2] 373

[50] M. W. Barsoum and T. El-Raghy, "A Progress Report on Ti_3SiC_2, Ti_3GeC_2, and the H-phases, M2BX", J. Mater. Synth. Process., (1997) 5 [3] 197–216.

[51] G. F. TAYLOR, US Patent No. 1,896,854, 1933.

[52] G. F. TAYLOR, US Patent No. 1,896,853, 1933.

[53] K. Inoue, US Patent, No. 3 241 956 (1966).

[54] K. Inoue, US Patent, No. 3 250 892 (1966).

[55] M. Omori, "Sintering, Consolidation, Reaction and Crystal Growth by the Spark Plasma System (SPS)", Mater. Sci. Eng. A, (2000) 287 [2] 183–188.

[56] D. M. Hulbert, A. Anders, J. Andersson, E. J. Lavernia, and A. K. Mukherjee, "A Discussion on the Absence of Plasma in Spark Plasma Sintering", Scr. Mater. (2009) 60 [10] 835–838.

[57] D.M. Hulbert, A. Anders, D.V. Dudina, J. Andersson, D. Jiang and C. Unuvar et al., "The absence of plasma in spark plasma sintering", J Appl Phys (2008), 104 33305.

[58] R. Orru, R. Licheri, A. M. Locci, A. Cincotti, and G. Cao, "Consolidation/Synthesis of Materials by Electric Current Activated/Assisted Sintering," Mater. Sci. Eng. R, (2009) 63 [4–6] 127–287.

[59] M. Tokita, Mechanism of spark plasma sintering, Proceedings of NEDO International Symposium on Functionally Graded Materials, Tokyo, Japan, (1999) pp. 23–33.

[60] R . M. GERMAN , Sintering Theory and Practice, (Wiley, New York, 1996) p. 482.

[61] Z. A. Munir, U. Anselmi-Tamburini, and M. Ohyanagi, "The Effect of Electric Field and Pressure on the Synthesis and Consolidation of Materials: A Review of the Spark Plasma Sintering Method", J. Mater. Sci., (2006) 41 [3] 763–777.

[62] U. Anselmi-Tamburini, S. Gennari, J. E. Garay, and Z. A. Munir, "Fundamental Investigations on the Spark Plasma Sintering/Synthesis Process—II. Modeling of Current and Temperature Distributions", Mater. Sci. Eng. A, (2005) 394 [1–2] 139–148.

[63] Z. J. Shen, M. Johnsson, Z. Zhao, M. Nygren, "Spark Plasma Sintering of Alumina" J. Am. Ceram. Soc. 2002, 85, 1921.

[64] H. U. Kessel, J. Hennicke, R. Kirchner, T. Kessel, "Rapid sintering of novel materials by fast/sps – further development to the point of an industrial production process with high cost efficiency", FCT Systeme GmbH.

[65] V. Yadav, S. P. Harimkar, Microstructure and properties of spark plasma sintered carbon nanotube reinforced aluminum matrix composites, Advanced Engineering Materials, 13, 1128-1134 (2011).

[66] G.B. Yadhukulakrishnan, A. Rehman, S. Karumuri, M. Stackpoole, A.K. Kalkan, R.P. Singh, S. P. Harimkar, Spark plasma sintering of silicon carbide and multi-walled carbon

nanotube reinforced zirconium diboride ceramic composites, Materials Science and Engineering A, In Print (2012).

[67] J. Galy, Private Communication 2007.

[68] Salvatore Grasso, Chunfeng Hu, Giovanni Maizza, and Yoshio Sakka, "Spark Plasma Sintering of Diamond Binderless WC Composites", J. Am. Ceram. Soc., 1–6 (2011)

[69] K Nanda, W Masaaki, Y Akira, K Akira, K Kazuya, "SparkPlasma Sintering of binderless n-WC and n-WC- X (X=Nb, Re, Ta, Ti, B, Si)", Transaction of JWRI, vol. 39 (2010),

[70] Z. F. Zhang, Z. M. Sun, H. Hashimoto, and T. Abe, "Application of Pulse Discharge Sintering (PDS) Technique to Rapid Synthesis of Ti_3SiC_2 from Ti/Si/C Powders", J. Eur. Ceram. Soc., (2002) 22 [16] 2957–2961.

[71] Z. F. Zhang, Z. M. Sun, and H. Hashimoto, "Rapid Synthesis of Ternary Carbide Ti_3SiC_2 Through Pulse-Discharge Sintering Technique from Ti/Si/TiC Powders", Met. Mat. Trans. A, (2002) 33 [11] 3321–3328.

[72] S. Yang , Z. M. Sun, H. Hashimoto, "Formation of Ti_3SiC_2 from Ti-Si-TiC powders by pulse discharge sintering (PDS) technique", Mat Res Innovat (2003) 7 225–230.

[73] N.F Gao, J.T Lib, D Zhangc and Y Miyamotoa, "Rapid synthesis of dense Ti3SiC2 by spark plasma sintering", J. Eur. Ceram. Soc. (2002) 22 2365.

[74] Z M Sun, H Hashimoto, Z F Zhang, S L Yang and S Tada, "Synthesis and Characterization of a Metallic Ceramic Material– Ti_3SiC_2", Materials Transactions, (2006) 47 [1] 170-174.

[75] Z. F. Zhang, Z. M. Sun, H. Hashimoto, and T. Abe, "Effects of Sintering Temperature and Si Content on the Purity of Ti_3SiC_2 Synthesized from Ti/Si/TiC Powders", J. Alloys Compd., (2003) 352 [1–2] 283–289.

[76] Z. F. Zhang, Z. M. Sun, and H. Hashimoto, "Low Temperature Synthesis of Ti_3SiC_2 from Ti/SiC/C Powders," Mater. Sci. Technol., (2004) 20 [10] 1252–1256.

[77] Z. M. Sun, Z. F. Zhang, H. Hashimoto, and T. Abe, "Ternary Compound Ti_3SiC_2: Part I. Pulse Discharge Sintering Synthesis," Mater. Trans., (2002) 43 [3] 428–431.

[78] Z. F. Zhang, Z. M. Sun, H. Hashimoto, and T. Abe, "A New Synthesis Reaction of Ti_3SiC_2 Through Pulse Discharge Sintering Ti/SiC/TiC Powder," Scr. Mater., (2001) 45 [12] 1461–1467.

[79] Z. F. Zhang, Z. M. Sun, H. Hashimoto, and T. Abe, "A New Synthesis Reaction of Ti_3SiC_2 from Ti/TiSi2/TiC Powder Mixtures Through Pulse Discharge Sintering (PDS) Technique," Mater. Res. Innovations, (2002) 5 [3–4] 185–189

[80] Y. Zou, Z. M. Sun, S. Tada, and H. Hashimoto, "Synthesis Reactions for Ti_3SiC_2 through Pulse Discharge Sintering TiH2/Si/TiC Powder Mixture," Mater. Res. Bull., (2008) 43 [4] 968–975.

[81] J. Zhu, B. Mei, X. Xu and J. Liu, "Effect of aluminum on the reaction synthesis of ternary carbide Ti_3SiC_2," Scripta Mater. (2003) 49 693.

[82] W.B. Zhu, B.C. Mei and J.Q. Zhu, "Fabrication of high-purity ternary carbide Ti_3SiC_2 by spark plasma sintering technique," Mater. Lett., (2005) 59 1547.

[83] J. Zhu and B. Mei, "Fabrication of high-purity Ti_3SiC_2 by spark plasma sintering (SPS) of elemental powders," J. Mater. Sci. Lett. (2003) 22 889.

[84] B.Y. Lianga, S.Z. Jinb and M.Z. Wanga, "Low-temperature fabrication of high purity Ti_3SiC_2," J. Alloy Compd. (2008) 460 440-443.

[85] Z.F. Zhang, Z.M. Sun and H. Hashimoto, "Fabrication and mechanical properties of ternary compound Ti_3SiC_2: application of pulse discharge sintering technique," Adv. Eng. Mater. (2002) 4 864.

[86] T.B. Massalski, J.L. Murray, L.H. Bennet, H. Baker and L. Kacprzaki, Binary Alloy Phase Diagrams, American Society for Metals, Materials Park, OH (1986).

[87] Z.M. Sun, Z. Yong and T. Shuji et al., "Effect of Al addition on pressureless reactive sintering of Ti_3SiC_2," Scripta Mater. (2006) 55 [11] 1011–1014.

[88] M. W. BARSOUM and T EL-RAGHY, Synthesis and characterization of a remarkable ceramic: Ti_3SiC_2 [J], J Am Ceram Soc (1996) 79 [7] 1953–1956.

[89] T. El-Raghy and M.W. Barsoum, Processing and Mechanical Properties of Ti_3SiC_2. Part I: Reaction Path and Microstructure Evolution. J. Amer. Cer. Soc. (1999) 82 2849–2854.

[90] N.F. Gao, Y. Miyamoto and K. Tanihata. "Dense Ti_3SiC_2 prepared by reactive HIP," J. Mater. Sci. (1999) 34 4385–4392

[91] J.T. Li and Y. Miyamoto."Fabrication of Monolithic Ti_3SiC_2 Ceramic Through Reactive Sintering of Ti/Si/2TiC", J. Mater. Synth. Proc. (1999) 7 91–96.

[92] J.F. Li, F. Sato and R. Watanabe. "Synthesis of Ti_3SiC_2 polycrystals by hot-isostatic pressing of the elemental powders", J. Mater. Sci. Lett. (1999) 18 1595.

[93] M.W. Barsoum, L.H. Ho-doc, M. Radovic, T. El-Raghy, Long time oxidation study of Ti_3SiC_2, Ti_3SiC_2/SiC and Ti_3SiC_2/TiC composites in air, J. Electrochem. Soc. 150 (4) (2003) B166–B175.

[94] H Donga, S Li, Y Tengb, W Mac, "Joining of SiC ceramic-based materials with ternary carbide Ti_3SiC_2 " Materials Science and Engineering B 176 (2011) 60–64

[95] F. T. Lan, K. Z. Li, H. J. Li, Y. G. He, X. T. Shen, W. F. Cao, "Joining of carbon/carbon composites for nuclear applications", J Mater Sci (2009) 44:3747–3750.

[96] W.J.J Wakelkamp, F.J van Loo, R Metselaar "Phase Relations in the Ti-Si-C System" J. Eur. Cer. Soc., 8 (1991), p. 135

[97] J. Zhanga, L. Wanga, L. Shia, W. Jianga, and L. Chena, "Rapid fabrication of Ti_3SiC_2–SiC nanocomposite using the spark plasma sintering-reactive synthesis (SPS-RS) method," Scripta Materialia Volume (2007) 56 [3] 241-244.

[98] J. Zhanga, T. Wua, L. Wanga, W. Jianga, and L. Chena, "Microstructure and properties of Ti_3SiC_2/SiC nanocomposites fabricated by spark plasma sintering," Composites Science and Technology, (2008) 68 [2] 499-505

[99] D. T. Wan, Y. C. Zhou, Y. W. Bao, and C. K. Yan, ''In-Situ Reaction Synthesis and Characterization of Ti_3Si 9Al0C_2/SiC Composites,'' Ceram. Int.,(2006); 32;883-90.

[100] L. H. Ho-Duc, T. El-Raghy and M.W. Barsoum, Synthesis and characterization of 0.3 V_f TiC– Ti_3SiC_2 and 0.3 V_f SiC– Ti_3SiC_2 composites, J Alloys Compd., (2003) 350 303–312.

[101] H.O. Pierson, Handbook of Refractory Carbides and Nitrides. 1996, Westwood, NJ: Noyes Publications.

[102] Barsoum, M.W., El-Raghy, T., and Radovic, M., Ti3SiC2: "A Layered Machinable Ductile Carbide", Interceram, (2000) 49, 226-233

[103] L. H. Ho-Duc, T. El-Raghy and M.W. Barsoum, Synthesis and characterization of 0.3 V_fTiC– Ti_3SiC_2 and 0.3 V_fSiC– Ti_3SiC_2 composites, J Alloys Compd., (2003) 350 303–312.

[104] H. Hashimoto, Z.M. Sun, "Preparation of TiC- Ti_3SiC_2 composites by mechanical alloying and hot pressing" Mater. Trans., 49 (2008), pp. 1572–1578

[105] S. Tada, K. Murase, H. Hashimoto, and Z. M. Sun, "Fabrication of Functionally Graded Ti_3SiC_2–TiC Binary-Phase Material," Mater. Trans., 48 [2] 139–142 (2007).

[106] J. F. Zhang, L. J. Wang, W. Jiang and L.D. Chen, "Effect of TiC content on the microstructure and properties of Ti_3SiC_2–TiC composites in situ fabricated by spark plasma sintering," Mater. Sci. Eng. A (2008) 487 137–143

[107] W. Tian, Z. M. Sun, Hitoshi Hashimotoa and YuLei Dua, "Synthesis, microstructure and mechanical properties of Ti_3SiC_2–TiC composites pulse discharge sintered from Ti/Si/TiC powder mixture", Materials Science and Engineering, (2009) 526 [1-2] 16-21

[108] S. Konoplyuk, T. Abe, T. Uchimoto, T. Takagi, "Synthesis of Ti_3SiC_2/TiC composites from TiH2/SiC/TiC powders", Materials Letters, (2005) 59 2342-2346.

[109] W. J. J. Wakelkamp, F. J. Vanloo and R. Metselaar, Phase relations in the Ti–Si–C system, J Eur Ceram Soc., (1991) 8 135–139.

[110] Y. Du, J. C. Schuster, H. J. Seifert and F. Aldinger, "Experimental investigation and thermodynamic calculation of the titanium–silicon–carbon system", J Am Ceram Soc., (2000) 83 197–203.

[111] J. Zhanga, L. Wanga, L. Shia, W. Jianga, and L. Chena, "Rapid fabrication of Ti_3SiC_2–SiC nanocomposite using the spark plasma sintering-reactive synthesis (SPS-RS) method," Scripta Materialia Volume (2007) 56 [3] 241-244.

[112] J. Zhanga, T. Wua, L. Wanga, W. Jianga, and L. Chena, "Microstructure and properties of Ti_3SiC_2/SiC nanocomposites fabricated by spark plasma sintering," Composites Science and Technology, (2008) 68 [2] 499-505

[113] D. T. Wan, Y. C. Zhou, Y.W. Bao and C.K. Yan, In situ reaction synthesis and characterization of $Ti_3Si(Al)C_2$/SiC composites, Ceram Inter., (2006) 32 883–890.

[114] H. J. Wang, , Z. H. Jina and Y. Miyamotob, "Ti_3SiC_2/Al2O3 composites prepared by SPS", Ceramics International, (2003) 29 [5] 539-542

[115] H. J. Wang, , a, Z. H. Jina and Y. Miyamotob, "Effect of Al_2O_3 on mechanical properties of Ti_3SiC_2/Al_2O_3 composite," Ceramics International, (2002) 28 [8] 931-934

[116] Y.M. Luo, S.Q. Li, J. Chen, R.G. Wang, J.Q. Li and W. Pan, Effect of composition on properties of alumina/titanium silicon carbide composites, J. Am. Ceram. Soc., (2002) 85 3099–3401.

[117] W. Pan, and S. L. Shia, "Microstructure and mechanical properties of Ti_3SiC_2/3Y-TZP composites by spark plasma sintering," Journal of the European Ceramic Society, (2007) 27 [1] 413-417

[118] Y Zou, Z M Sun, S Tada, H Hashimoto. "Effect of Al addition on low temperature synthesis of Ti_3SiC_2 powder", J of Alloys and Compounds (2008), 461 579-584

[119] T. El-Raghy and M.W. Barsoum, Processing and Mechanical Properties of Ti_3SiC_2. Part I: Reaction Path and Microstructure Evolution. J. Amer. Cer. Soc. (1999) 82 2849–2854.

[120] S. Arunajatesan, A. H. Carim, "Synthesis of Titanium Silicon Carbide", Journal of the American Ceramic Society Volume 78, Issue 3, pages 667–672, March 1995

[121] J. M. Córdoba, María J. Sayagués, María, "Synthesis of Ti_3SiC_2 Powders: Reaction Mechanism", J. Am. Ceram. Soc., 90 [3] 825–830 (2007)

[122] E. Wu and E. H. Kisi, “In situ neutron powder diffraction study of Ti_3SiC_2 analysis”, J. Am. Ceram. Soc., 84 [10] 2281–88 (2001)

[123] K. Tang, C. Wang, Y. Huang, Q. Zan, and X. Xu, ‘‘A Study on the Reaction Mechanism and Growth of Ti_3SiC_2 Synthesized by Hot-Pressing,’’ Mater. Sci. Eng. A, 328, 206–12 (2002).

[124] M. Eizenberg, R. Brener, and S. P. Murarka, "Thermal Stability of the Aluminum/ Titanium Carbide/Silicon Contact System," J. Appl. Phys., 55, 3799 (1984).

[125] I. Barin, Thermochemical Data of Pure Substances, 3rd ed., Weinheim, New York, 1995.

[126] R. Pampuch, M. Raczka, and J. Lis, "The Role of Liquid Phase in Solid Combustion Synthesis of Ti_3SiC_2," Int. J. Mater. Prod. Technol., 10 [3-6] 316-24 (1995).

[127] F. Sato, J. F. Li, and Watanabe, R., Reaction synthesis of Ti_3SiC_2 from mixture of elemental powders. Mater. Trans., JIM, 2000, 41, 605–609.

[128] Z.F. Zhang, Z.M. Sun*, H. Hashimoto, T. Abe, “Application of pulse discharge sintering (PDS) technique to rapid synthesis of Ti_3SiC_2 from Ti/Si/C powders”, Journal of the European Ceramic Society 22 (2002) 2957–2961

[129] Y Zoua, Z Sun, H Hashimotoa and L Cheng, “Reaction mechanism in Ti–SiC–C powder mixture during pulse discharge sintering”, Ceramics International, Volume 36, Issue 3, April 2010, Pages 1027-1031

[130] Z. F. Zhang, Z. M. Sun and H. Hashimoto, “Low temperature synthesis of Ti_3SiC_2 from Ti/SiC/C powders” , Materials Science and Technology October 2004 Vol. 20, 1252-1256

[131] Z. F. zhang, Z. M. Sun and H. Hashimoto, “Rapid synthesis of ternary carbide Ti_3SiC_2 through pulse-discharge sintering technique from Ti/Si/TiC powders” Metall. Mater. Trans. A, 2002, 33A, 3321 – 3328.

[132] j. T. Li and Y. Miyamoto, "Fabrication of Monolithic Ti_3SiC_2 Ceramic Through Reactive Sintering of Ti/Si/2TiC," J. Mater. Synth. Process., 7, 91 (1999).

[133] RILEY, D. Kisi, E. Hansen, T. & Hewat, A.(2002). Self-propagating high-temperature synthesis of Ti_3SiC_2: I, ultra-high-speed neutron diffraction study of the reaction mechanism. Journal of the American Ceramic Society, 85, 2417-2424.

[134] C. Racault, F. Langlais, R. Naslain, "Solid-state synthesis and characterization of the ternary phase Ti3SiC2", journal of materials science 29(1994) 3384-3392.

[135] T. El-Raghy and M. W. Barsoum, "Diffusion kinetics of the carburization and silicidation of Ti_3SiC_2", Am Institute of Physics (1998) 83 [1] 112-119.

[136] N. F. Gao, Y. Miyamoto and K. Tanihata. "Dense Ti_3SiC_2 prepared by reactive HIP," J. Mater. Sci. (1999) 34 4385–4392

[137] J. Zhu, B. Mei, X. Xu and J. Liu, "Synthesis of single-phase polycrystalline Ti_3SiC_2 and Ti3AlC2 by hot pressing with the assistance of metallic Al or Si", Mater. Lett. (2004) 58 588.

[138] Y.C. Zhou, H.B. Zhang, M.Y. Liu, J.Y. Wang, Y.W. Bao, "Preparation of TiC free Ti_3SiC_2 with improved oxidation resistance by substitution of Si with Al", Mater. Res. Innovat., (2004), 8(2), 97–102

[139] T El-Raghy, M W Barsoum, A Zavaliangos, S R Kalidindi, "Processing and mechanical properties of Ti_3SiC_2: II, effect of grain size and deformation temperature", J of the American Ceramic Society (1999), 82, 10, 2855-2860

[140] T El-Raghy, P Blau, M. W. Barsoum,"Effect of grain size and wear behavior of Ti_3SiC_2", Wear (2000), 238, 125-130

[141] S. Ren, J Meng, J Lu and S Yang, "Tribological behavior of Ti_3SiC_2 sliding against nickel based Alloys at elevated temperature", Tribo Lett (2008), 31, 129, 137.

[142] Z. Zhang, Z. Sun, H. Zhang and H. Hashimoto, Micron-scale deformation and damage mechanisms of Ti_3SiC_2 crystals induced by indentation. Adv. Eng. Mater., 6 12 (2004), 980–983.

[143] S yang, Z M SUN, H hashimoto, "Reaction in Ti_3SiC_2 powder synthesis from a Ti-Si-TiC powder mixture", J of Alloys and comounds 368 (2004) 312-317

[144] A. Teber, F. Schonstein, F. Tetard, M. Abdellaoui, N. jouini, “Effect of SPS process sintering on the microstructure and mechanical properties of nanocrystalline TiC for tools application”, Int. j. of Refractory metals and hard materials 30 (2012) 64-70.

[145] W Tian, Z Sun, H Hashimoto, Y Du, “Microstructural evolution and mechanical properties of Ti_3SiC_2-TiC composites” j. of alloys and composunds 502(2010) 49-53.

[146] D.T. Wan, C.F.Hu, Y. W. Bao, Y. C. Zhou, “Effect of SiC particles on the friction and wear behavior of $Ti_3Si(Al)C_2$- based composite”, Wear 262 (2007) 826-832.

[147] J. Yang, W Gu, L. M. Pan, K. Song, X. Chen, T. Qiu, “Friction and Wear properties of in sity (TiB_2+TiC)/ Ti_3SiC_2 composites”, wear 271 (2011) 2940-2946.

[148] C hu, Y Zhou, Y Bao, D Wan, “Tribological properties of polycrystalline Ti_3SiC_2 and Al_2O_3 reinforced Ti_3SiC_2 composite”, J. Am. Ceram. Soc. 89[11] 3456-3461 (2006)

[149] P. Abachi ∗, A. Masoudi, K. Purazrang, “Dry sliding wear behavior of SiCP/QE22 magnesium alloy matrix composites”, Materials Science and Engineering A 435–436 (2006) 653–657

[150] A. Vencl, I. Bobi, Z. Mi¡skovi, “Effect of thixocasting and heat treatment on the tribological properties of hypoeutectic Al–Si alloy”, Wear 264 (2008) 616-623.

[151] K.H. Zum Gahr, Met. Prog, 116 (1979), 46.

VITA

Nidul Chandra Ghosh

Candidate for the Degree of

Master of Science

Thesis: SYNTHESIS AND TRIBOLOGICAL CHARACTERIZATION OF *IN-SITU* SPARK PLASMA SINTERED TI_3SIC_2 AND Ti_3SiC_2-TiC COMPOSITES.

Major Field: Mechanical and Aerospace Engineering

Biographical:

Education:

Completed the requirements for the Master of Science in Mechanical and Aerospace Engineering at Oklahoma State University, Stillwater, Oklahoma in July, 2012.

Completed the requirements for the Bachelor of Science in Mechanical Engineering at Bangladesh University of Science and Technology (BUET), Dhaka, Bangladesh in 2009.

Experience:

- 1 year and six months of experience of working as Graduate Research Assistant in material processing and characterization in OSU.
- Over two years of experience of working as Graduate Teaching Assistant for Machine Design, Mechanical Metallurgy and Material Science courses in BUET and OSU.
- Authored 2 conference papers in International Conference in Mechanical Engineering, Dhaka, Bangladesh and International Conference in Applied Engineering and Technology, Singapore.
- Published one book chapter named as "Consolidation of MAX phases by Spark Plasma Sintering: A review", Woodhead Publishing Limited, In press.

Professional Memberships:
Phi Kappa Phi membership, Golden key and ASME.

Name: Nidul Chandra Ghosh Date of Degree: December, 2012

Institution: Oklahoma State University Location: Stillwater, Oklahoma

Title of Study: SYNTHESIS AND TRIBOLOGICAL CHARACTERIZATION OF *IN-SITU* SPARK PLASMA SINTERED Ti_3SiC_2 AND Ti_3SiC_2-TiC COMPOSITES.

Pages in Study: 95 Candidate for the Degree of Master of Science

Major Field: Mechanical and Aerospace Engineering

Scope and Method of Study:

The $M_{n+1}AX_n$ phases (where M is a transition metal, A is an A group (mostly IIIA and IVA) element, and, X is C and/or N and n=1 to 3) are polycrystalline nanolaminates of ternary carbides and nitrides, and exhibit unique combinational properties of metallic materials and ceramics because of their layered crystal structure. Ti_3SiC_2 is one of the representative members of the MAX phase family. In this research work spark plasma sintering of Ti_3SiC_2 and TiC reinforced Ti_3SiC_2 composites highlighting the effect of sintering parameters on constituting phases, microstructures and wear behavior is reported.

Findings and Conclusions:

In-situ synthesis of dense near-single phase Ti_3SiC_2 ceramics from 3Ti/SiC/C/0.15Al starting powder using spark plasma sintering (SPS) at 1250 °C (uniaxial pressure of 50 MPa and soaking time of 15 min) is reported in this research work. Systematic investigation of effect of sintering temperature, in the range of 1050-1450 °C, on the phase development and wear behavior is presented. Also, the effect of starting powder composition on phase development after SPS sintering at 1150 °C is investigated using three distinct compositions (3Ti/SiC/C, 2Ti/SiC/TiC, and Ti/Si/2TiC). The reaction mechanisms leading to formation of Ti_3SiC_2 and the possibility of formation of $Ti_3(Si_{1-x}Al_x)C_2$ solid solution during SPS sintering are critically analyzed.

SPS has been successfully employed for *in-situ* processing of Ti_3SiC_2-TiC composites with TiC content varying from 0 to 30 vol.% using TiC/Si/Ti/Al powder mixture at 1250 °C for 15 min and with 50 MPa of pressure. Experimental phase content of TiC on the sintered composites are calculated from X-ray diffraction results and compared to the theoretical TiC vol.% present on starting powder. From the results, the phase composition of the composites could be easily tailored by mastering initial compositions. The effect of TiC content on relative density, microhardness, and phase distribution of the consolidated composites is discussed. The triboligical response of Ti_3SiC_2-TiC composites against Si_3N_4 ball have been evaluated at room temperature using pin-on-disk rotating tribometer.

ADVISER'S APPROVAL: Sandip P. Harimkar